GSFC RST CMO
August 10, 2023
Released

RST-SYS-REQ-0020, Revision D

Roman Space Telescope (RST), Code 448

Science Requirements Document

Roman Space Telescope Reviewed – Not Subject to Export Control

Goddard Space Flight Center
Greenbelt, Maryland

National Aeronautics and
Space Administration

Science Requirements Document

Review/Signature/Approval Page

Prepared by:

Jeffrey Kruk

Approved by:

David Content

Electronic Approval available on-line at: https://ipdtdms.gsfc.nasa.gov

Preface

This document is a Roman Space Telescope (RST) Configuration Management (CM)-controlled document.

Note: Prior to May 20, 2020, the project name was Wide Field Infrared Survey Telescope (WFIRST).

For the purposes of configuration management, the prefixes "WFIRST" and "RST" are completely interchangeable. For example, RST-MGMT-PROC-0024 is the same as WFIRST-MGMT-PROC-0024.

Changes to this document require prior approval of the applicable Configuration Control Board (CCB) Chairperson or designee. Proposed changes shall be submitted to the RST CM Office (CMO), along with supportive material justifying the proposed change.

In this document, a requirement is identified by "shall," a good practice by "should," permission by "may" or "can," expectation by "will," and descriptive material by "is."

Questions or comments concerning this document should be addressed to:

RST Configuration Management Office
Mail Stop 448
Goddard Space Flight Center
Greenbelt, Maryland 20771

Change History Log

Revision	Effective Date	Description of Changes (Reference the CCR & CCB/ERB Approval Date)
Revision -	March 30, 2018	Initial Release per WFIRST-CIR-05074
Revision A	October 29, 2018	Changes per WFIRST-CCR-06312 and WFIRST-CCR-06709
Revision B	October 29, 2019	Updated document in preparation for PDR per WFIRST-CCR-0013 and WFIRST-CCR-0091
Revision C	April 19, 2021	**Summary:** Updates per CCR-0324 were incorporated in DOORs per the changes listed in the "FROM/TO 11-17-2020 excel document" posted to the CCR and CCR-0321 for the MRD. These changes included updating requirements, removing child links, adding links, updating figure 6 and adding a new requirement. **New Requirement:** • SRD-177 **New Child Requirement:** • MRD-506 for SRD-88 **Updated Figure:** • Figure 6
Revision D	July 6, 2023	This version incorporates RST-CCR-0696. This was approved by the Project CCB Chair on the effective date shown. Summary of changes (may not be all-encompassing): Updates per **CCR-0696** were incorporated in DOORs per the changes listed in the FROM-TO "SRD_VV_update_D2.xlsx" excel export. • These changes include updating requirements, verif method, verification description, verification event, delete verification level and verification details, add children

Deviations/Waivers Record

Section # / Rqmt.	Deviation / Waiver #	CCR #	Date Approved	Title	Mission

Table of TBCs/TBDs/TBRs/TBSs

Identifier	SRD: RST-SYS-REQ-0020	Rationale	Number of TBx's	Item No.	Location	TBX Summary	TBX Assignee	TBX Due Date	TBX Event

Table of Contents

List of Figures

List of Tables

1 INTRODUCTION

1.1 Purpose

The Roman Space Telescope (RST) is a mission responding to the 2010 National Research Council New Worlds, New Horizons (NWNH) Astronomy and Astrophysics Decadal Survey top priority recommendation in the large space mission category. The science program includes two dedicated investigations to tackle outstanding questions in dark energy research and exoplanet exploration, and includes a substantial General Observer program to enable targeted investigations of astrophysical phenomena to advance other goals from the Decadal Survey. A coronagraph instrument is included in the payload for purposes of advancing the present state of the art of coronagraph technology. There is no formal scientific observing plan for the coronagraph, but if its performance is scientifically interesting it may be made available for scientific investigations.

1.2 Scope

The purpose of this document is to define the scientific requirements for the RST mission that flow down from the Science Objectives and the Level 1 requirements contained in the RST Program Plan controlled at NASA Headquarters. It provides the detailed context and rationale which link the scientific objectives to the Level 1 requirements and to the Level 2 science requirements contained here. It also provides the rationale for the requirements contained in the Mission Requirements Document (MRD), which flow from the science requirements.

We base these requirements on current theoretical understanding and the results from studies using both ground-based and space-based facilities. There is an uncertainty in many of the astrophysical properties, e.g. the H-alpha luminosity function and the microlensing event rate, which drive these scientific requirements, so the requirements are necessarily derived from theoretical predictions and extrapolations from known objects. In these cases we outline the basis of the predictions and the expected uncertainties.

1.3 Related Documentation

The latest versions of all documents below should be used. RST documents can be obtained from URL: https://ipdtdms.gsfc.nasa.gov.

1.3.1 Applicable Documents

The following documents are referenced within this document and are directly applicable or contain policies or other directive matters that are binding for the contents of this document. In the event of conflict between an Applicable Document and the content of this document, the RST Project Configuration Change Board has the final authority for conflict resolution.

Document Number	Title
RST-MGMT-REQ-0044	RST Program Level Requirements Appendix

1.3.2 Reference Documents

The following documents are referenced herein and amplify or clarify the information presented in this document. These documents are not binding on the content of this document.

Document Number	Title
RST-SCI-DESC-0080	Figure of Merit Computations for the HLS Reference Survey
RST-SCI-PLAN-0006	Wide-Field Instrument Calibration Plan

2 SCIENCE BACKGROUND

2.1 Dark Energy and Fundamental Cosmology

The accelerating expansion of the universe is the most surprising cosmological discovery in many decades, with profound consequences for our understanding of fundamental physics and the mechanisms that govern the evolution of the cosmos. The goal of the RST dark energy science program is to answer the two top-level questions in the field of cosmology:

> Is cosmic acceleration caused by a new energy component or by the breakdown of General Relativity (GR) on cosmological scales?
>
> If the cause is a new energy component, is its energy density constant in space and time, or has it evolved over the history of the universe?

A constant energy component, a.k.a. a "cosmological constant," could arise from the gravitational effects of the quantum vacuum. An evolving energy component would imply a new type of dynamical field. Gravitational explanations could come from changing the action in Einstein's GR equation, or from still more radical modifications such as extra spatial dimensions. Any of these possibilities has profound consequences for our basic understanding of physics and cosmology. The future of the universe will be determined largely by whatever force or property of space is causing the acceleration.

Following common practice, we will use "dark energy" as a generic term that is intended to encompass modified gravity explanations of cosmic acceleration as well as new energy components. If the origin is indeed a new energy component, then current measurements imply that it represents about 75% of the total mass-energy of the cosmos. Dark energy is the gravitationally dominant component of the universe, yet we do not know what it is.

Dark energy affects the universe in two significant ways. First, the *expansion history* (or geometry) of the universe is determined by the energy density of dark energy over cosmic time. Second, the *growth of cosmic structures,* from the density perturbations we see in maps of the Cosmic Microwave Background (CMB) to the galaxies and galaxy clusters we see today, is governed by the attractive gravity of matter and the repulsive effect of dark energy, which inhibits the structure growth. Within the confines of General Relativity, measurements of the expansion history and growth of structure will give consistent results. Discrepancies between these two types of measurements might indicate a breakdown of General Relativity. Only by measuring both the expansion history and the growth of structure at high precision over a wide redshift range can we distinguish among the three broad classes of explanations for the acceleration outlined above.

RST has been designed to measure each of these with multiple independent techniques. As described in NWNH, RST "will employ three distinct techniques—measurements of weak gravitational lensing, supernova distances, and baryon acoustic oscillations—to determine the effect of dark energy on the evolution of the universe". In addition to these three methods, RST adds a fourth method, redshift-space distortion (RSD), which provides an alternative measure of the growth of structure based on the same data set employed for BAO. These four methods provide complementary physical information and allow cross-checks for verifying the accuracy of the measurements.

For each method, the combination of near-IR sensitivity, wide field of view, high angular resolution, and stable observing platform afforded by RST offers unique advantages not attainable from the ground. RST is designed to produce dark energy data sets of great statistical power, with thousands of supernovae, tens of millions of galaxy redshifts, and hundreds of millions of galaxy shape measurements. Equally important, it is designed to produce data sets that allow excellent control of systematic uncertainties, so that the full statistical power of its measurements can be applied to testing the tenets of cosmological models.

2.1.1 Type Ia Supernovae

Type Ia supernovae (SNe) are believed to be the explosive disintegrations of a white dwarf star in a binary system that accretes material until thermonuclear runaway ensues. It has been determined empirically that SNIa provide excellent standardizable candles. For a known supernova luminosity L_{SN}, and measured flux F, the relation $F = L_{SN}/4\pi D_L^2$ can be used to calculate the luminosity distance D_L directly. Spectral features in the supernova light may be used to identify the redshift, thereby providing a primary observable of the effect of dark energy: the distance-redshift relation D(z).

The acceleration of the Universe was initially discovered using Type Ia supernova observations at redshifts of $z \leq 0.9$. More recently, SNe beyond $z = 1$ observed from the Hubble Space Telescope (HST) have been employed to observe the transition from an initially matter-dominated Universe to the present dark energy dominance. The SN technique currently shows a dark-energy signal with strong statistical significance and has advanced several generations beyond the original detection. State-of-the-art studies derive cosmological constraints from joint analyses of multiple surveys that collectively span a wide redshift range. (Refer to Figure 1).

Supernova cosmology is a mature method with well-developed study of systematics. This allows a RST mission to be designed that specifically targets the systematics to bring them below the statistical uncertainties. These include the effects of dust reddening, a variation of the luminosity with the rest-frame duration of the event (referred to as the Phillips relation or width-luminosity relation), and variations in luminosity that depend on other properties of the SN or its host galaxy. It has been shown that the variations in luminosity are correlated with other, distance-independent, features of the supernova light curve, spectrum, or host galaxy. Thus Type Ia SNe are standardizable, to a high, degree of precision. This standardization process is empirical; RST will rely on having high-signal-to-noise, well-sampled multi-band SN photometry, and sufficient numbers of events, to allow creation of statistically powerful subsamples that can be compared to assess and control systematic errors.

RST offers critical advantages over present and future ground-based supernova surveys. First, the stability and sharp PSF of space-based imaging allow accurate, well-calibrated photometry over the enormous dynamic range in luminosity spanned by the survey. Second, for the redshifts below $z < 0.4$, RST (as contrasted to ground-based surveys) extends into the rest-frame IR, where Type Ia supernovae have more uniform peak luminosities (improving statistical performance and reducing evolutionary systematics) and where the impact of dust extinction is much smaller than at optical wavelengths.

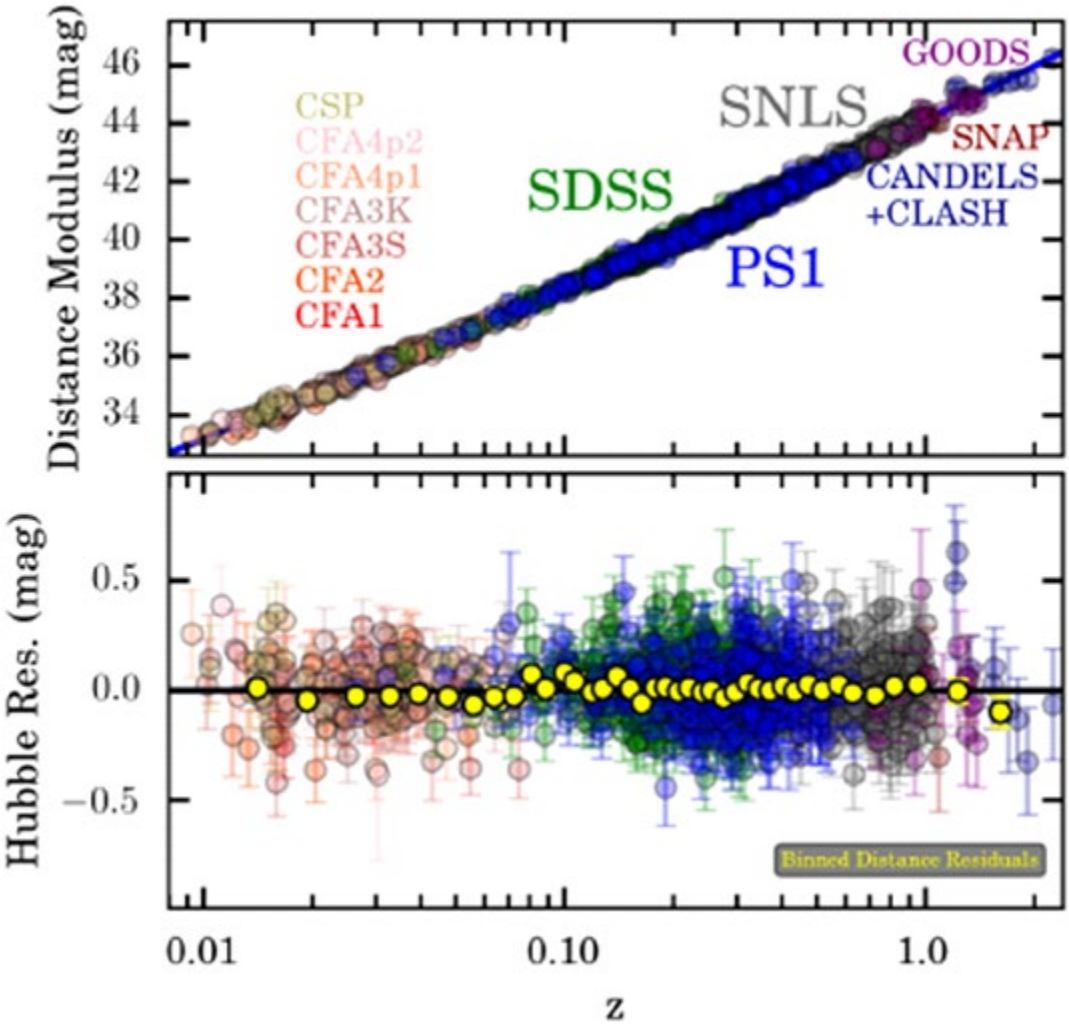

Figure 1 Distance-redshift Relation for SN Ia Observations

The distance-redshift relation (Hubble diagram) for SN Ia observations from a compilation of ground-based and HST surveys. The top panel plots distance modulus, μ = apparent magnitude - absolute magnitude, as a function of redshift. The bottom panel plots the residual of these distance moduli from the predictions of a ΛCDM cosmological model; points with error bars show individual supernovae and yellow points show average residuals in narrow redshift bins. (Taken from Scolnic et al. 2017).

2.1.2 Baryon Acoustic Oscillations

For the first 380,000 years after the Big Bang, nearly all hydrogen in the universe was ionized, and scattering of photons off free electrons produced tight coupling between the cosmic background radiation and baryonic matter. Pressure waves propagated in this hot plasma at roughly 60% of the speed of light. After the plasma cooled and formed neutral atoms, the photons streamed freely through the universe, and we see them today as the cosmic microwave background (CMB). The CMB shows temperature fluctuations that trace underlying variations in the densities of dark matter and baryons. All of the structure in the Universe observed today was

seeded by these primordial density variations. After the final interaction of photons with electrons, the pressure waves (acoustic oscillations) stalled, leaving their signature both on the CMB (verified by the observed acoustic peaks in the CMB power spectrum) and on the matter distribution. A characteristic scale – set by the distance that acoustic waves could propagate before the recombination epoch – was imprinted on the clustering of matter, and subsequently on the clustering of galaxies and intergalactic gas.

The baryon acoustic oscillations (BAO) method uses this imprinted scale as a standard ruler to measure the angular diameter distance $D_A(z)$ and the Hubble parameter $H(z)$, from clustering in the transverse and line-of-sight directions, respectively, to determine the expansion history of the Universe.

The use of BAO to probe dark energy requires accurate, spectroscopic galaxy redshifts and positions over large regions of the sky. Redshift measurement is a straightforward task, and the challenge is to execute these measurements for many millions of objects over large areas with well understood uniformity. Measurements of the distance-redshift relation from supernovae and BAO allow cross-checks of methods based on different physical principles, and the two approaches are complementary in several ways. Supernovae measure relative distances because the absolute luminosity of Type Ia supernovae is not known *a priori*. The BAO distance scale can be computed from first principles, given matter and radiation densities that are well constrained by CMB data. BAO measurements become less precise at low redshift because cosmological volume elements are smaller and cosmic variance errors in clustering measurements are correspondingly larger. Supernovae allow high-precision relative measurements at redshifts up to $z \sim 2$ even in fairly narrow redshift bins. One can differentiate the distance-redshift relation to infer the expansion rate as a function of redshift, but radial BAO measurements determine $H(z)$ directly and can achieve tight constraints on this quantity at moderate and high redshifts. In an overlapping redshift range between $z = 1$ and 1.7 the supernova and BAO techniques are both expected to give comparable accuracies, although their detailed redshift dependencies still provide complementary information, offering the chance for comparison and combination of the two techniques.

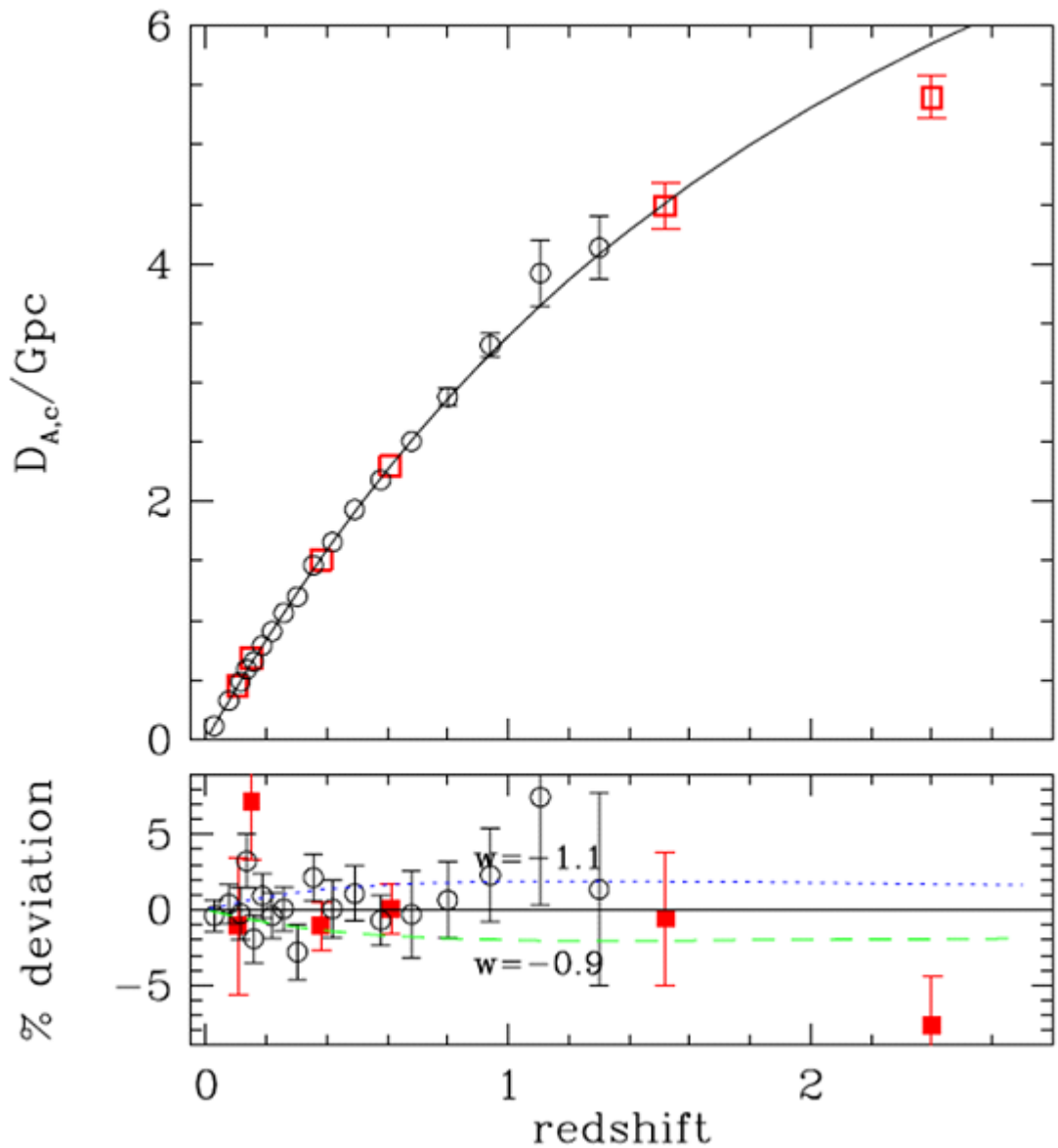

Figure 2 Recent BAO and Supernova Distance Measurements

Recent BAO and supernova distance measurements, compiled by Weinberg & White (2017), compared to the distance-redshift relation predicted for a ΛCDM cosmological model with parameters constrained by Planck CMB observations. In the top panel, circles show binned supernova measurements from the Joint Lightcurve Analysis of Betoule et al. (2014), while squares show BAO measurements from the 6dFGS, SDSS-II, BOSS, and eBOSS surveys. For visual clarity, error bars are plotted only at $z > 0.7$. The lower panel shows residuals relative to the model, and the predictions of dark energy models with w = -0.9 or w = -1.1 (vs. w = -1.0 for ΛCDM) normalized to produce nearly identical CMB fluctuations.

Our current understanding of the BAO method suggests that it will be statistics-limited even for the largest foreseeable surveys. Small corrections are required for the effects of non-linear

gravitational evolution and non-linear galaxy bias, but these can be computed at the required level of accuracy using analytic and numerical techniques. The great challenge for BAO cosmology is to map large volumes with the sampling density required to faithfully trace structure on BAO scales. Ground-based galaxy redshift surveys should be able to do this out to redshift z=1 or slightly beyond. For the vast comoving volume available at z=1-2, the most promising approach is space-based, slitless NIR spectroscopy, measuring the redshifts of star-forming galaxies via the strong Hα emission line. This approach is completely impractical from the ground because of the much higher NIR sky background. Our projections for the RST galaxy redshift survey (also referred-to as the High-Latitude Spectroscopic Survey), discussed below in Section 3.3, predict that the Reference Survey would provide D_A measurements with 2.0-3.0% precision and H(z) measurements with 3.8-5.1% precision in each of nine $\Delta z = 0.1$ redshift bins between z = 1 and z = 1.9, plus measurements with aggregate precision of 2.6% (D_A) and 4.0% (H) from [OIII] emitters at z = 1.94-2.85. It is evident from Figure 2 that these measurements will provide an enormous advance over current knowledge on the behavior of dark energy at z > 1.

2.1.3 Redshift Space Distortions (RSD)

The spectroscopic galaxy redshift survey conducted for BAO also probes the growth of structure. Because galaxy distances are inferred from their redshifts, which are affected by the velocities of individual galaxies (peculiar velocities) as well as cosmological expansion, these peculiar velocities lead to systematic differences between redshift-space and real-space measurements. The effects are a combination of large-scale coherent flows induced by the gravity of large-scale structure, and a small-scale random peculiar velocity of each galaxy. This redshift-space distortion (RSD) can be measured statistically via the anisotropy of clustering in a galaxy redshift survey, as illustrated in Figure 3. The large-scale flows compress the contours of the galaxy redshift-space two-point correlation function along the line of sight, with the degree of compression determined by the growth rate of cosmic large-scale structure and the bias factor between galaxy and matter distributions. The small-scale random motion of galaxies leads to a smearing in the radial direction, known as the "Finger of God" effect. Thus the measured 3D galaxy distribution on large scales from the sky positions and redshifts of galaxies provides a direct measurement of the cosmic large structure growth rate. Consistency of RSD and weak lensing measurements provides another test of general relativity, as many alternative gravity theories predict discrepancies between masses inferred from light-bending and galaxy motions.

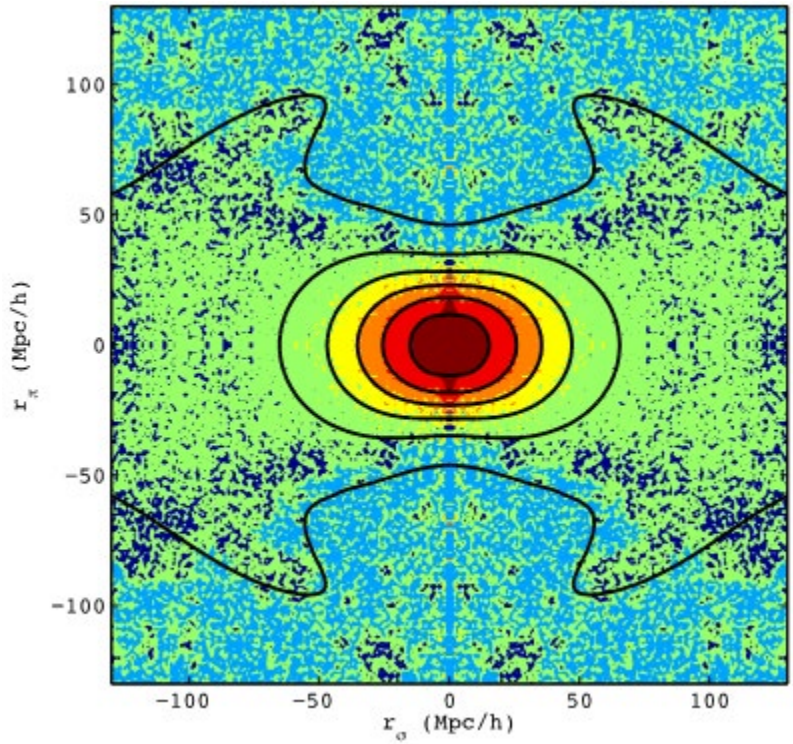

Figure 3 Redshift-Space Distortion of Galaxy

Redshift-space distortion of galaxy clustering in the Baryon Oscillation Spectroscopic Survey (BOSS), from Reid et al. (2012). Colors show the amplitude of the measured galaxy 2-point correlation function in bins of transverse (r_σ) and line-of-sight (r_π) separation, displaying the characteristic flattening of structures along the line of sight and the elongated "fingers of God" appearing as a vertical stripe at small r_σ. Contours show model predictions for best-fitting cosmological parameters; the unusual structure of the outermost contour reflects the impact of BAO.

Reasonable statistical forecasts suggest that RSD measurements can provide tight statistical constraints on structure growth and the expansion history, substantially strengthening the results derived from BAO alone (*e.g.*, White, Song, & Percival 2009; Wang et al. 2010). The critical uncertainty in these forecasts is the level of theoretical systematics in modeling RSD and scale-dependent galaxy bias in the mildly non-linear regime. In Section 3.3.1 we characterize the level of these systematics via an effective value of k_{max}, a maximum wavenumber to which measurements of the full 3-d galaxy power spectrum can be used to infer cosmological parameters without incurring systematic errors that degrade the statistical uncertainty of the RST measurements.

2.1.4 Weak Gravitational Lensing

When light from galaxies propagates across the Universe, fluctuations in the intervening gravitational potential cause subtle distortions and magnification of the images of these distant sources. Weak lensing directly probes the clustering of matter between the observer and the lensed source galaxies, so it measures the growth of structure without uncertainties associated with galaxy bias. The weak lensing signal also depends on distances to the sources and the

lensing matter distribution, so it provides expansion history constraints to compare with SN and BAO measurements. The distance constraints can discriminate a cosmological constant from evolving dark energy, while consistency with growth measurements tests general relativity and modified gravity theories of cosmic acceleration. Alternatively, taking advantage of the complementary expansion history from the SN and BAO measurements makes it possible to more strongly constrain the growth measurements, for a more stringent test of general relativity and modified gravity theories.

RST will detect WL by measuring the coherent distortion ("shear") of the images of distant galaxies. Because galaxies come in a variety of intrinsic shapes, it is not possible to tell whether a single galaxy is gravitationally distorted. But lensing causes galaxies on similar lines of sight to align, so averaging large samples of galaxies can effectively map the lensing distortions. Weak lensing has been quantified by surveys of increasing statistical power over the last decade using both ground and space-based telescopes (see Figure 4). However, away from massive clusters the typical distortion of source galaxy shapes is only about 1%. Measuring the lensing signal with high precision, in the face of intrinsic ellipticity variations that are ~0.4 rms, requires enormous galaxy samples and exquisite control of systematic errors. Space-based measurements offer potentially enormous advantages for weak lensing because of high angular resolution and stability of the observing platform, allowing accurate characterization of the instrumental point-spread function (PSF).

The auto-correlation of galaxy shears measures (in projected form) the power spectrum of intervening dark matter fluctuations. Cross-correlation of a shear map with a map of foreground galaxies or clusters measures the average mass profile around these foreground systems, or, equivalently, the galaxy-mass and cluster-mass cross-correlation functions. These measurements can be combined with the clustering of the galaxies and clusters themselves to infer dark matter clustering, again constraining structure growth and expansion history. We expect these measurements to be competitive with, and largely complementary to, “cosmic shear” (auto-correlation) measurements from the same RST data set.

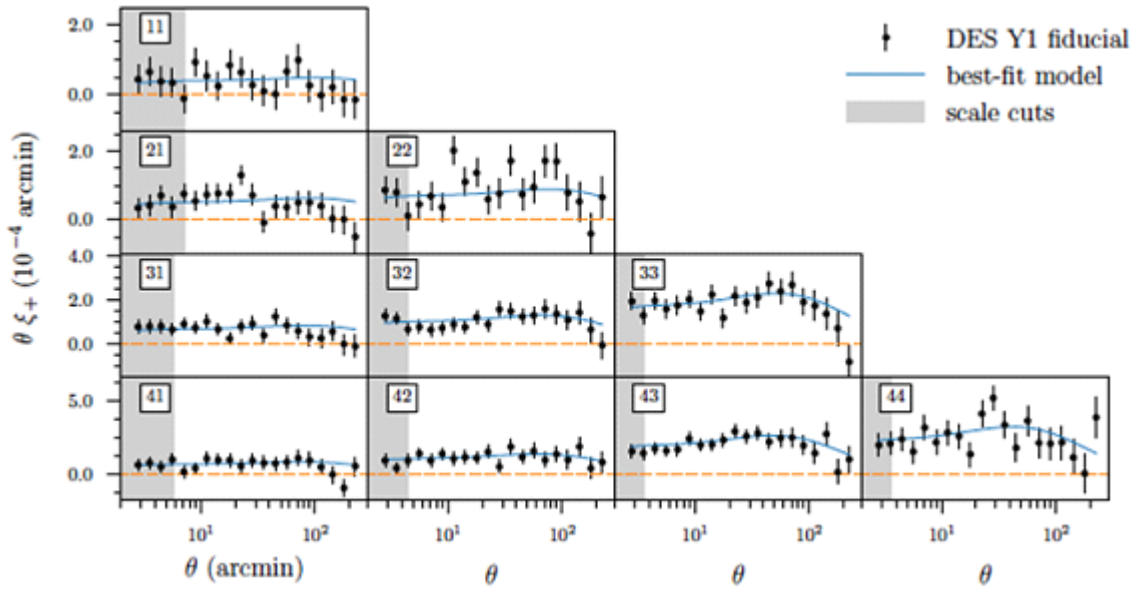

Figure 4 Measurements of the Cosmic Shear Correlation Function

Measurements of the cosmic shear correlation function as a function of angle from the Year 1 analysis of the Dark Energy Survey (Abbott et al. 2017). Galaxies are divided into four photometric redshift (photo-z) bins; panels along the diagonal show shear auto-correlations in the same photo-z bin while off-diagonal panels show cross-correlations of the shears of galaxies in different bins. Values of ξ_+ are multiplied by θ to better display large scale behavior. Blue curves in each panel show the predictions of a single underlying ΛCDM model, calculated using the estimated distribution of true redshifts in each photo-z bin. Note that galaxies at different redshifts still exhibit correlated shears because they are lensed by common foreground matter fluctuations.

2.1.5 Dark energy and Cosmology Summary

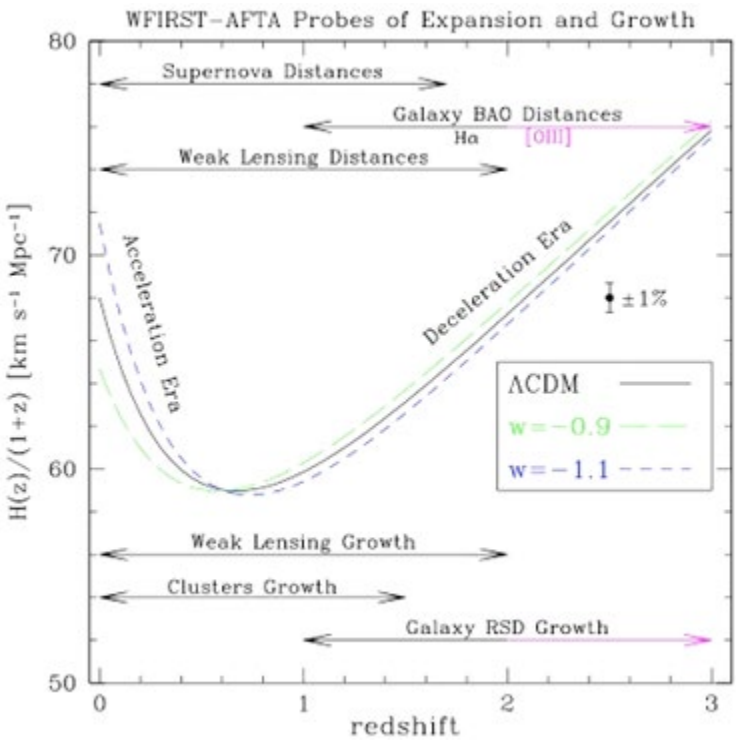

Figure 5 RST Probes of Cosmic Acceleration

Curves show theoretical predictions of the Hubble parameter H(z), divided by (1+z) so that a decreasing (increasing) trend towards low redshift indicates deceleration (acceleration). For models constrained by current data, the acceleration era begins at $z \approx 0.6$. Line segments show the redshift ranges mapped by the different RST dark energy probes, expansion history on the top and growth of structure on the bottom.

Figure 5 provides a conceptual overview of the RST dark energy program. The cosmic expansion history is probed by three distinct methods: supernovae, BAO, and weak lensing. Growth of structure is also probed by three methods: cosmic shear and clusters (both enabled by the weak lensing survey) and galaxy redshift-space distortions. While the different RST surveys cover different redshift ranges, all of the distance probes and all of the growth of structure probes have redshift ranges that overlap. The use of multiple overlapping methods allows joint analyses to break degeneracies that exist within a single method (e.g., the effects of distance and growth on weak lensing), to test the physical origin of deviations from ΛCDM (e.g., by comparing weak lensing and RSD measures of structure growth), and to cross-check results from approaches with very different sorts of systematic uncertainties. The multiplicity of high-precision cosmological measurements from RST will enable it to reach detailed, physically informative, and carefully tested conclusions about the origin of cosmic acceleration.

2.2 Exoplanets

The first discovery of planetary companions to Sun-like stars was, along with the discovery of dark energy, one of the greatest astronomical breakthroughs of the last quarter-century. These

discoveries have excited the astronomical community and the broader public as well. Since then, the pace of exoplanet discovery has increased each year. Early discoveries came mainly from radial velocity searches, which are most sensitive to massive planets in relatively short period orbits. Transit searches are also most sensitive to short period planets, but the ultra-high photometric precision of the Kepler mission enables detection of planets that are earth radius or even smaller. Gravitational microlensing is typically most sensitive at orbital separations of a few AU, and it can detect planets over a wide range of mass. Current direct imaging searches are sensitive to giant planets at large (10s of AU) orbital separations. There are now over 3000 confirmed exoplanets, discovered by all of these techniques, with Kepler driving much of the field's recent progress.

Nature has surprised astronomers with the enormous and unexpected diversity of exoplanetary systems, containing planets with physical properties and orbital architectures that are radically different from our own Solar System. Since the very first discoveries, we have struggled to understand this diversity of exoplanets, and in particular how our solar system fits into this menagerie.

RST will advance our understanding of exoplanets along two complementary fronts: the statistical approach of determining the demographics of exoplanetary systems over broad regions of parameter space, and, to the extent that the coronagraph technology demonstration is successful, the detailed approach of characterizing the properties of a handful of nearby exoplanets.

First, through its comprehensive statistical census of the outer regions of planetary systems using microlensing, including a complete assay of planets with the mass of Earth and greater and with separations spanning from the outer habitable zone to free floating planets, RST will complete the statistical census of planetary systems begun by Kepler. Indeed, RST will be sensitive to analogs of all of the planets in our Solar System with the mass of Mars or greater, and thus will allow us to place our Solar System in the context of known exoplanetary systems.

Second, the RST coronagraph will be capable, for the first time in human history, of directly imaging planets similar to those in our Solar System. It is expected to be capable of making detailed studies of the properties of giant planets and debris disks around nearby stars and will be the testbed for future coronagraphs capable of detecting signs of life in the atmospheres of Earth-like exoplanets. The coronagraph is a technology demonstration instrument, and as such it has no requirements on scientific performance. However, if its performance meets expectations it will be possible to use it to pursue scientific investigations.

2.2.1 Exoplanet Microlensing

Canonical theories of planet formation and evolution originally developed to explain our Solar System did not anticipate the incredible panoply of planetary systems that have been observed. These theories have since been expanded and altered to better describe the variety of planetary systems that we see. For example, the discovery of gas giant planets orbiting at periods of only a few days (also known as hot Jupiters), as well as evidence for the migration of the giant planets in our own Solar System, have highlighted the fact that these theories must account for the possibility of large-scale rearrangement of planet positions during and after the epoch of planet formation (Lin et al. 1996, Rasio & Ford 1996). These insights have also opened the way to

deeper understanding of previously unsuspected rearrangements in our own solar system. One current popular example is the so-called Nice Model, which theorizes the migration of the four giant planets evolved from an initial compact configuration into their present position (e.g., Levinson et al. 2011). Many of these theories also predict a substantial population of “free-floating” planets that have been ejected from their planetary systems through interactions with other planets (Juric & Tremaine 2008, Chatterjee et al. 2008).

The rapid advancement in exoplanet research has been driven by extensive observational searches around main-sequence stars and by the construction of more sophisticated planet formation models. Perhaps the most surprising discovery so far is the great diversity in the planets' dynamical properties, but these results are largely confined to planets that are unusually massive or reside in very close orbits. Nevertheless, the core accretion theory suggests most planets are much less massive than gas giants and that the critical region for understanding planet formation is just beyond the "snow-line", which is the region (1.5-4 AU) of greatest microlensing sensitivity (Ida & Lin 2005; Kennedy et al. 2006). Early results from ground-based microlensing searches (Beaulieu et al. 2006; Gould et al. 2006; Bennett et al. 2008) appear to confirm these expectations, but a more recent statistical analysis (Suzuki et al. 2016) is not consistent with the core accretion theory prediction of a planetary mass gap between the masses of Neptune and Saturn.

RST and Kepler complement each other, and together they cover essentially the entire planet discovery space. Kepler is sensitive to close-in planets but is unable to sense the more distant ones; RST is less sensitive to close-in planets, but surveys beyond the habitable zone better than Kepler. RST's sensitivity extends out even to unbound planets, offering the possibility to constrain their numbers and masses. Other methods, including ground-based microlensing, cannot approach the sensitivity and comprehensive statistics on the mass and semi-major-axis distribution of extrasolar planets that a space-based microlensing mission provides. Thus, RST provides the only way to complete the exoplanet census begun by Kepler and gain a comprehensive understanding of the architecture of planetary systems, needed to understand planet formation and habitability.

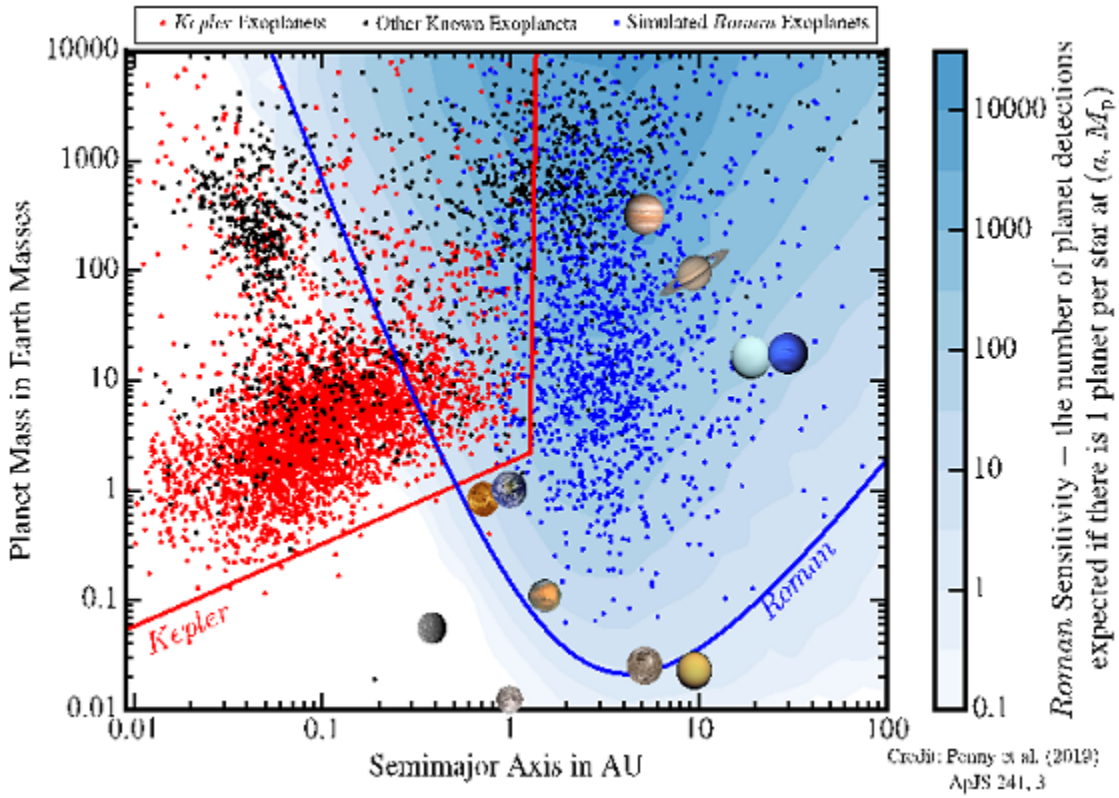

Figure 6 Complementarity of the Kepler Transit and RST Microlensing Observations

This figure illustrates the complementarity of the Kepler transit and RST microlensing observations. The red points are Kepler planet detections, while the blue points represent expected RST detections. Black points are planets detected by the radial velocity technique. RST is sensitive to planets in the habitable zone and beyond, which is in accessible to Kepler. (Figure courtesy of Matthew Penny).

The physical basis of microlensing is the gravitational bending of light rays by a star or planet. When a "lens star" passes close to the line of sight to a more distant source star, the gravitational field of the lens star deflects the light rays from the source star. The gravitational bending effect of the lens star "splits", distorts, and magnifies the images of the source star, so the observer sees a microlensing event as a transient brightening of the source as the lens star's proper motion moves it across the line of sight. The lensing magnification is determined by the alignment of the lens and source stars measured in units of Einstein ring radius, so even low-mass lenses can give rise to high magnification microlensing events (see Figure 7). Planets are detected via light curve deviations that differ from the normal stellar lens light curves (Mao & Paczynski 1991). A microlensing event's duration is given by the Einstein ring crossing time, typically 1-3 months for stellar lenses and a few days or less for a planet.

Microlensing observing programs rely upon the high density of source and lens stars towards the Galactic Bulge to produce the stellar alignments needed to generate microlensing events. This high star density also means that the Bulge main sequence source stars are not generally resolved

from one another in ground-based images. This means that the precise photometry needed to detect planets of less than a tenth of the Earth's mass is not possible from the ground unless the magnification due to the stellar lens is moderately high. Thus, ground-based microlensing is only sensitive to terrestrial planets located close to the Einstein ring (at ~2-3 AU). Full sensitivity to terrestrial planets in all orbits from the outer habitable zone to ∞ can come only from a space-based survey. The precise astrometry available from space also allows individual planet mass determinations for a much larger fraction of microlensing events.

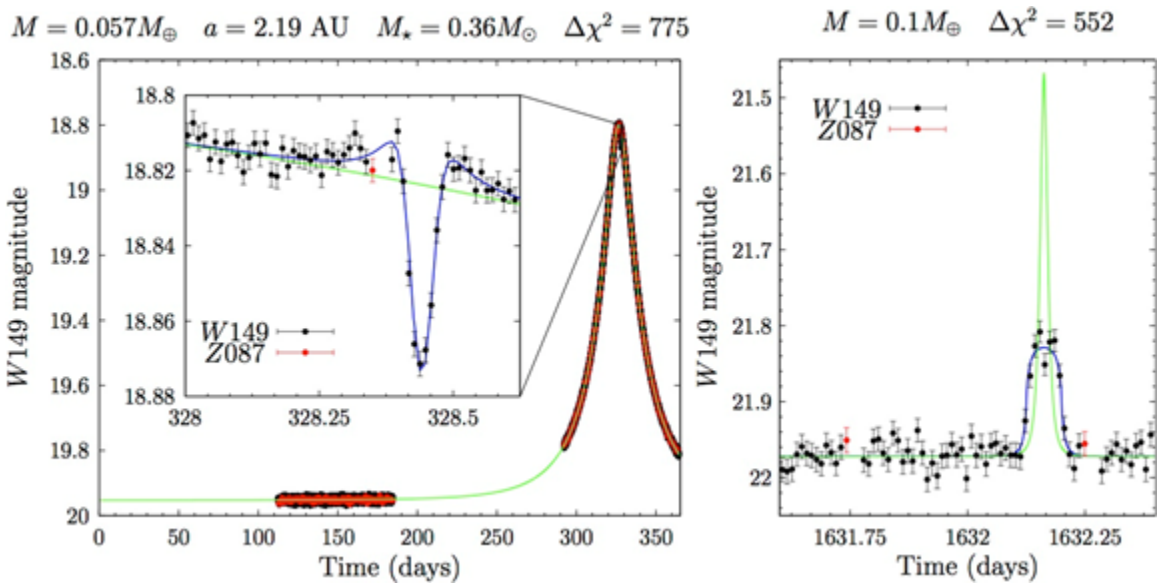

Figure 7 Examples of Simulated Event Light Curves with Detected Planetary Signals

Examples of simulated event light curves with detected planetary signals from simulations of a RST exoplanet survey. The left panel shows the detection of a Mercury-mass planet orbiting a 0.36 solar mass star with a semi-major axis of 2.19 AU. The right panel shows a simulated detection of a free-floating Mars-mass planet.

2.2.2 Direct-Imaging of Exoplanets and Disks

2.2.2.1 Exoplanets

Our understanding of the internal structure, atmospheres, and evolution of planets was originally developed through models that were tuned to explain the detailed properties of the planets in our own solar system. Our surveys of exoplanetary systems have led to the realization that there exists a diversity of worlds with very different properties and environments than those in our solar system, including gas giants under strong stellar irradiation (hot Jupiters), gas giants with massive heavy cores, water worlds, and "super-Earths" with masses intermediate to the rocky and the ice giants in our solar system. Subsequently, these models have had to be expanded and generalized to explain the properties of these new worlds, often including new and uncertain physics. Our understanding of these new worlds therefore remains primitive.

The best hope of understanding the physical properties of this diversity of worlds is through comparative planetology: detailed measurements of, and comparisons among, the properties of

individual planets and their atmospheres. These measurements provide the primary empirical constraints on our models.

Understanding the structure, atmospheres, and evolution of a diverse set of exoplanets is also an important step in the larger goal of assessing the habitability of Earthlike planets discovered in the habitable zones of nearby stars. It is unlikely that any such planets will have exactly the same size, mass, or atmosphere as our own Earth. A large sample of characterized systems with a range of properties will be necessary to understand which properties permit habitability and to properly interpret these discoveries.

Detailed characterization is currently only possible for relatively rare transiting systems. Unfortunately, transiting planets are themselves a relatively small subset of systems. Those that are bright enough for significant follow-up tend to be discovered from the ground. Ground-based transit discoveries tend to be a biased subset of systems, mostly including giant planets at short orbital periods that are subject to strong stellar irradiation. Kepler has detected many smaller and longer period transiting planets, but nearly all of these systems are far too faint for detailed characterization of the planets. Furthermore, atmospheric studies of transiting planets are only sensitive to very specific planet geometries and/or atmospheric pressures, therefore providing an incomplete view of the physical processes at work in the atmospheres of these systems. Finally, most transiting planets characterized to date are strongly irradiated by their host stars, impacting the thermal profiles and chemistries of their atmospheres.

Direct imaging surveys of planets orbiting nearby stellar systems offer a complementary and critical approach to studying the detailed properties of exoplanets. First, planets detected by direct imaging tend to be at longer orbital periods than those found by transits. Second, spectra of directly imaged planets provide powerful diagnostic information about the structure and composition of the atmospheres. These planets are not significantly heated by their host stars, so their spectra reveal their intrinsic temperature / pressure / composition profiles without complications of external heating. These reflected light spectra also sample the bulk compositions of planetary atmospheres and not just the thin upper atmospheres probed by transit studies. Finally, these planets can be found around the closest stars, which tend to be the best characterized. While ground-based direct imaging surveys have made enormous strides in recent years, with new, much more capable surveys coming on line soon, such surveys are ultimately limited by the contrast achieved in the kinds of planets they can study, being sensitive only to warm/massive young planets. RST will detect analogs to our cold Jupiter for stars in the solar neighborhood.

Establishing a diverse sample of characterized systems, and thus advancing our knowledge of exoplanet composition, requires a high-contrast, coronagraphic space-based survey of the nearest stars. RST is the first step in doing that. The large aperture, excellent wavefront quality, and high degree of stability make the telescope an excellent platform for direct imaging of exoplanetary systems and debris disks and an ideal testbed for critical technology needed in future missions.

Exoplanets are typically about a billion times fainter than their parent stars. A coronagraph is a set of optical elements that suppresses the star's light to create a region where a dim planet can be extracted. Due to optical imperfections in any system, all coronagraphs must be designed together with wavefront control via one or more deformable mirrors (DMs). The combined coronagraph and wavefront control system is characterized by the contrast, inner working angle,

spectral bandwidth, and stability achieved. Contrast is the degree to which the instrument can suppress scattered and diffracted starlight in order to reveal a faint companion. Inner Working Angle (IWA) is the smallest angle on the sky at which it can reach its designed contrast. This angle is typically only a few times larger than the theoretical diffraction limit of the telescope. The resulting residual stellar halo must also be stable over the time scale of an observation, so that the halo can be subtracted to reveal an exoplanet or disk. In principle, with a well-characterized and stable point spread function, various subtraction methods that have been developed and used on both ground and space images can be employed to average the background photon noise and extract faint planets that are below the raw contrast level. The recent history of planet imaging shows that recovering planets factors of 10 or more fainter contrast than the background is regularly accomplished, both on large ground telescopes and from the Hubble Space Telescope. We thus characterize the coronagraph instrument by its detection limit, that is, the limiting magnitude of a recoverable planet relative to the star from the combination of the coronagraph and wavefront control and data processing.

2.2.2.2 Dust and Debris Disks

A star and its planetary system both form from the same circumstellar disk. As a cloud of gas and dust collapses, the embryonic system evolves a preferential axis of rotation. Material undergoes gravitational collapse along that axis but cannot collapse freely in the perpendicular direction; conservation of angular momentum prevents matter from falling inward. However eventually friction and energy loss slows the orbital motion and allows gravitation to take over, with matter collapsing inward to form a star, and locally in orbit, to form planets.

Sun-like stars accumulate their mass within a million years, and planets typically form within 10 million years. Small rocky planetesimals come together to become full-size planets. The smaller ones can become terrestrial planets, while the larger ones continue to gravitationally attract gas and become gas or ice giant planets.

Young solar systems are violent places, with many planetesimals, proto-planets, and planets crammed into a relatively tight space. Orbits are initially eccentric and these bodies interact dynamically with each other and their central stars, causing frequent collisions. These collisions produce debris, as evidenced by the material in the asteroid belt and Kuiper belt of our own solar system. We also see this debris in observations of nearby young stars; many stars in the solar neighborhood were observed by IRAS and Spitzer to have far-infrared excess fluxes, indicative of reprocessing stellar radiation by small dust grains produced by collisions. A couple dozen of these extremely bright debris disks have been resolved in reflected visible or near-IR light with HST.

RST will be sensitive to debris disks with ~10 times the solar system's level of dust in the habitable zones and asteroid belts of nearby (~10 pc) sun-like stars. The high sensitivity and spatial resolution of RST images will map the large-scale structure of these disks, revealing asymmetries, asteroid belts, and gaps due to unseen planets. RST will be able to make the most sensitive measurements yet of the amount of dust in or near the habitable zones of nearby stars. This is important for assessing the difficulty of imaging Earth-like planets with future missions as well as for understanding nearby planetary systems. Finally, RST's photometric polarimetry measurements of these disks will constrain dust grain sizes and compositions.

2.3 General Observer

The General Observer (GO) science program of RST will have high impact over a broad range of modern astrophysics. The experience of Hubble suggests that the GO program will be every bit as important to the astronomical community and to the interested public as the dark energy and exoplanetary programs. The very wide field, large aperture, deep near-IR reach, excellent spatial resolution, and spectroscopic capabilities of the wide-field instrument will ensure that a multitude of GOs can pursue programs requiring degree-sized fields in the statistical realm for the first time. Examples include studies of stellar populations in the Milky Way and its neighboring galaxies and mapping large-scale structure through cosmic time. Many of these will be logical outgrowths of single object and small sample studies with HST, JWST, and other observatories, but they are likely to have outsized impacts, just as SDSS, Kepler, and other wide field surveys already have. The wide field of view instrument, both imaging and spectroscopy modes, will be available to the community for General Observer programs. Each of these will open new areas of discovery space that can be used for science investigations that are of most interest in the RST era. It is anticipated that the coronagraph will be available through a Participating Scientist Program.

Five representative General Observer programs are under study for the purpose of understanding mission performance requirements that may flow down from such programs. A sixth study investigating the requirements on the data archive is also under way, including characteristics of the archived datasets themselves, query tools, and data analysis tools. The five observing programs under study are:

1. History of the Galaxy: Using stellar populations to study the structure and evolution of the Milky Way, its globular clusters, and its dwarf satellites, and to reveal new characteristics of stellar evolution.

2. Nearby galaxies: Using resolved stellar populations in nearby galaxies to study their assembly histories and the evolution of their stellar content.

3. Galaxy evolution at high redshift: Using RST deep imaging data to study galaxy formation and evolution, early active galactic nuclei and quasars, the epoch of reionization, and the growth of structure from early times up to redshifts of about 1.

4. Cosmic Dawn: Using deep wide-field grism spectroscopy to study the epoch of the formation of the first galaxies and quasars, and the consequent reionization of the universe.

5. Solar System: the wide field of view and NIR bandpass of RST enable an interesting variety of Solar System studies: KBOs/TNOs/Centaurs/Binaries, irregular satellites of the giant planets, the Giant Planets, Asteroids/NEOs/PHAs, Comets, Occultations by Solar System objects, and Titan.

In addition to GO programs that pursue targeted observations, RST will support Guest Investigator (GI) studies that use data from the dark energy and exoplanet surveys to address a wide range of astrophysical questions, from the solar system to the most distant galaxies and quasars.

3 SCIENCE REQUIREMENTS FLOWDOWN

The RST Program Plan contains the Science Objectives and Level 1 requirements which drive the overall mission design. However, being a programmatic document, the RST Program Plan does not contain a detailed description of the flowdown from the Objectives to the RST requirements or the rationale for those requirements. The Baseline and Threshold Science Requirements held in the RST Program Plan, the Science Requirements contained here and the Design Reference Mission documented in the Operations Concept Document together validate that the RST mission will meet the Science Objectives outlined in the Program Plan.

Section 3-1 below states the mission science objectives, taken verbatim from the PLRA and repeated here for reference. Subsequent sections present the flowdown for each of the six RST science programs: the High Latitude Spectroscopic Survey (HLSS), the High Latitude Imaging Survey (HLIS), the Supernova Survey (SN), the Exoplanet Microlensing Survey (EML), the General Observer Program (GO), and the Guest Investigator Program (AR – archival research). For each science program, we begin with the governing science and survey capability requirements, which flow down from the PLRA objectives. These requirements in turn flow down to requirements on three categories of data records:

1. Science Data Records: the highest-level data products, such as source catalogs, time-series measurements, image mosaics, etc, used as input to the scientific analysis. These flow down to requirements on calibrated data records, and onto the Science Data Processing segment of the mission.

2. Calibrated Data Records: calibrated images, spectra, etc from which the science data records are derived. These requirements flow down to Raw Data Records, and to Science Data Processing, the Ground System, the Operations Concept and Calibration Plan, and in some cases directly to the flight hardware.

3. Raw Data Records: the raw data, such as the types of image and spectral data to obtain, which defines the filters, spectral elements, exposure times, operations concepts, etc. These requirements flow down directly to the flight hardware and Ground System mission segments.

3.1 Science Objectives

The Science Objectives, as specified in the RST Program Plan are as follows:

RST will conduct near-infrared (NIR) sky surveys in both imaging and spectroscopic modes, providing an imaging sensitivity for unresolved sources better than 26.5 AB magnitude.

RST will determine the expansion history of the Universe in order to test possible explanations of its apparent accelerating expansion, including Dark Energy and modification to Einstein's gravity, using the supernova, weak lensing, and galaxy redshift survey techniques, at redshifts up to $z = 2$ with high-precision cross-checks between the techniques.

RST will determine the growth history of the largest structures in the Universe in order to test the possible explanations of its apparent accelerating expansion including Dark Energy and modification to Einstein's gravity using weak lensing, redshift space distortions, and

galaxy cluster techniques, at redshifts up to z =2 with high-precision cross-checks between the techniques.

RST will carry out a statistical census of exoplanetary systems in the Galaxy, from the outer habitable zone to free floating planets, including analogs to all of the planets in our Solar System with masses greater than Mars, by monitoring stars toward the Galactic Bulge using the microlensing technique.

RST will devote a substantial fraction of the mission lifetime to a peer-reviewed General Observer program that will allow for a broad range of scientific studies of astrophysical targets in our solar system, in the Galaxy, and beyond, with access to the full sky within the mission lifetime.

RST will include a public archive and peer-reviewed Guest Investigator program for archival research that will enable a broad range of scientific studies of astrophysical targets in our solar system, in the Galaxy, and beyond.

The six observing programs map to these objectives as follows. The High-Latitude Spectroscopic and Imaging Surveys map to Objectives 1, 2, 3, and 6, providing near-infrared surveys over large areas, statistical data sets for precision measurements of the cosmic expansion history and the growth of matter clustering, and an archive that supports an enormous range of science investigations. The Supernova Survey maps most directly to Objective 2, measuring the cosmic expansion history, but its depth and time-domain sampling over many square degrees also complement the wide area surveys (Objective 1) and enable a wide variety of other investigations (Objective 6). The Exoplanet Microlensing Survey maps directly to Objective 4, the statistical census of planetary systems, and again provides a unique resource for Guest Investigator studies of stars, planets, and the structure of the Galaxy (Objective 6). The General Observer program maps directly to Objective 5. As with Hubble Space Telescope, many observations conducted in the GO program will likely find applications beyond their original design goals, enabled by the data archive and Guest Investigator program (Objective 6).

3.2 Flowdown from Objectives to Science Requirements

Each observing program is addressed independently. There are subsections for each program that give the flowdown from science requirements through science data records, calibrated data records, and raw data records, as defined above. The introduction to each section describes the reasoning leading from the Objectives to the science requirements. For the HLIS, HLSS, SN, and EML programs we adopt the following general approach. We define a reference survey based on current expectations of what RST can achieve in a notional allocation of observing time. We define quantitative figures of merit (FoM) based on a forecast of performance of that reference survey. Baseline science requirements are defined such that, if the program is allocated the observing time assumed for the reference survey, then it will achieve the reference figure of merit to within some specified margin. For the high-latitude survey, this margin was taken to be the amount by which the reference survey exceeds the performance of the corresponding survey submitted to the Astro-2010 Decadal Survey. This calculation is described in detail in Figure of Merit Computations for the HLS Reference Survey (RST-SCI-DESC-0080). Threshold requirements are defined with a larger margin. The actual allocation of observing time to programs will not be made until closer to launch, and the performance of an individual program

will ultimately depend on its time allocation. For moderate variations around the time assumed for the reference surveys, figures of merit defined by the variance of inferred values of physical parameters will typically scale linearly with time allocation, at least if that variance is dominated by statistical uncertainties. Large changes in observing time could cross thresholds that change performance more drastically. This approach to defining the science requirements enables clear definition of performance requirements for all mission segments, and definition of a sample design reference mission that meets the Science Objectives, while not precluding future optimization of the observing strategies. A representative allocation of mission time, based on the requirements of the individual programs given here, is presented in the Mission Operations Concept Document (RST-SYS-PLAN-0013).

3.3 High Latitude Spectroscopic Survey (HLSS)

As discussed in Sections 2.1.2 and 2.1.3, the HLSS enables constraints on the cosmic expansion history through BAO measurements of the angular diameter distance $D_A(z)$ and the Hubble parameter H(z), and it enables constraints on the growth of structure through RSD measurements of the matter clustering amplitude and its time derivative. In the regime described by linear perturbation theory, the parameter combination constrained by RSD is $\sigma_m(z)f(z)$, where $[\sigma_m(z)]^2$ is a scaling factor for the amplitude of the linear matter power spectrum and $f(z) = d\sigma_m/d\ln a$, with $a = (1+z)^{-1}$.

The wide-field infrared sensitivity of RST enables it to carry out a slitless spectroscopic survey for Hα (λ = 0.6563 μm) emission-line galaxies in the redshift range z ≈ 1-2. This redshift range, especially z > 1.3, is difficult to probe efficiently with optical redshift surveys from the ground. At z > 2, the Lyα forest and Lyα emission line galaxies improve the prospects for ground-based surveys. Dark energy science requirements for the HLSS are therefore defined in terms of its ability to provide a cosmologically powerful redshift survey in the z=1-2 redshift range. The HLSS will also measure redshifts of [OIII] (λ = 0.5007 μm) emitters, enabling a survey that extends to higher redshifts at lower galaxy space density and providing additional leverage for probing the galaxy population in the prime redshift range.

The rms statistical error for BAO and RSD quantities scales as $(V_{eff})^{-1/2}$, where the effective volume is

$$V_{eff} = \int dV \left\{1 + {}^{1}/_{nP}\right\}^{-2} .$$

Here n is the galaxy number density and P is the amplitude of the galaxy power spectrum at comoving wavenumber $k \approx 0.2$ h Mpc^{-1}. BAO measurements are expected to be robust to theoretical and observational systematic uncertainties provided that the completeness and contamination levels of the redshift survey are well understood. Cosmological inferences from RSD measurements are subject to systematic uncertainties in theoretical models of non-linear galaxy bias, which become increasingly important to smaller scales. RSD parameter constraints are usually obtained by modeling the measurements up to a maximum wavenumber $k_{max} \approx 0.1 - 0.2$ h Mpc^{-1} such that theoretical systematics are subdominant. Improvements in theoretical modeling will likely allow larger values of k_{max} to be useful by the time of RST, but the design of the desired data set does not depend much on the anticipated value of k_{max}.

3.3.1 Reference Survey and Figures of Merit

For the HLSS reference survey we adopt a primary survey area of 2000 deg^2, a redshift range $1.05 < z < 1.9$ ($\lambda = 1.35 – 1.90$ μm), and a point-source emission line flux sensitivity of 1.0×10^{-16} erg cm^{-2} s^{-1} at 1.8 μm. Our forecasts of FoM performance are based on a full operational model of this survey that includes the wavelength-dependent sensitivity of the grism observations and estimates of the fraction of the survey area with different numbers of spectroscopic exposures, and losses of some pixels of some exposures due to cosmic rays. The resulting predictions of $nP_{0.2}$ based on current estimates of the Hα luminosity function and clustering bias of Hα emitters are shown in Figure 8. For z<1.75, where the influence of dark energy is expected to be most significant, the survey is designed to provide nP>1, so that the BAO measurement uncertainty is dominated by cosmic variance within the survey volume and not by shot noise on the galaxy distribution.

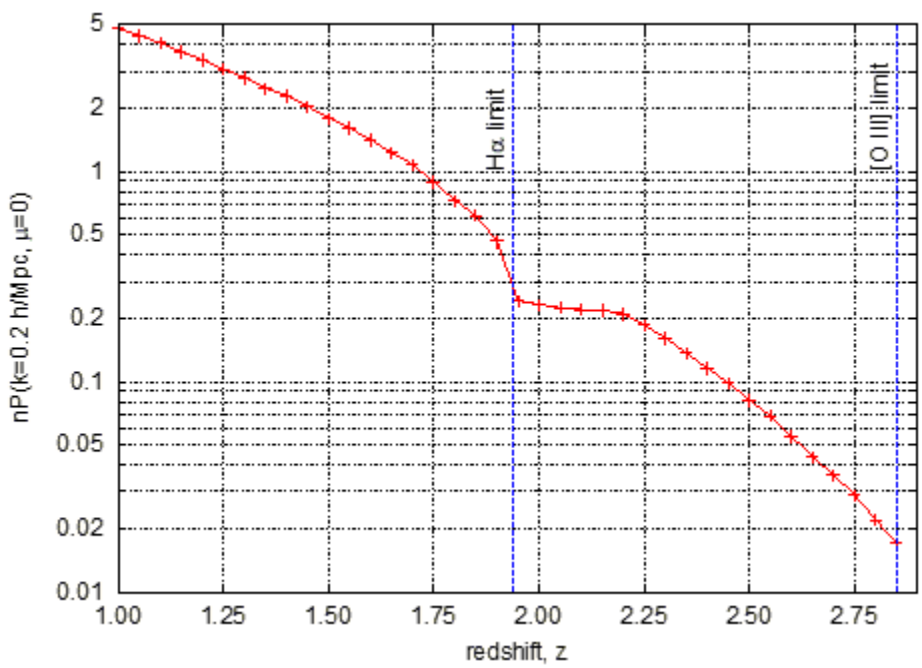

Figure 8 Ratio of Clustering to Shot Noise.

Ratio of clustering to shot noise is plotted as a function of redshift for the reference survey. This ratio is computed at k=0.2 h/Mpc, and for modes with wave vector perpendicular to the line of sight (mu=0). Vertical lines show the redshift limits for H alpha and [O III] corresponding to observer-frame wavelength of 1.93 microns.

For this forecast we have assumed a completeness of 0.6 when converting the number density of galaxies predicted by the luminosity function to the number density assumed to be in the survey. We have assumed a bias for Hα ELGs of b(z) = 1+0.5z. The bias relation has been rescaled to agree with Geach et al. (2012) measurement of b=2.4 at z=2.23 for f > 5×10^{-17} erg s^{-1} cm-^{2}.

The reference survey also includes observation of 20 deg^2 at 10× the exposure time for standard HLSS fields, to enable calibration of the completeness of the main survey and tests for a variety

of possible systematics. These deep fields require approximately 10% of the total observing time of the HLSS.

Based on current models of observatory performance, the reference survey (including the deep fields) can be completed in 0.64 years of observing time (including overheads for slewing and target acquisition).

For BAO we define the reference figure of merit in terms of the aggregate fractional uncertainties on D_A and H over the redshift range $1 < z < 3$. Specifically, we define F_D and F_H to be constant factors that multiply $D_A(z)$ and $H(z)$, respectively, relative to the predictions of our fiducial ΛCDM cosmological model, over this entire redshift range. The reference figure of merit is

$$FoM_{BAO,ref} = [\sigma(F_D)\sigma(F_H)]^{-1}$$

where $\sigma(F_D)$ and $\sigma(F_H)$ are the forecast rms errors in these quantities for the reference survey described above. For this forecast we assume perfect knowledge of the BAO sound horizon scale r_d, since we are interested in characterizing the measurement capability of the HLSS. We further assume that density field reconstruction will allow factor-of-two mitigation of non-linear degradation of the BAO signal, and we assume that all scales can be used in the BAO measurement. With these assumptions, our current forecasting tools Figure of Merit Computations for the HLS Reference Survey (RST-SCI-DESC-0080) yield $FoM_{BAO,ref} = 11300$ for the reference survey described here. As described in the document Figure of Merit Computations for the HLS Reference Survey (RST-SCI-DESC-0080), this value for the FoM exceeds the corresponding value for the galaxy redshift survey considered by the 2010 Decadal Survey in their evaluation of the RST mission (based on the JDEM-Omega mission concept) by a factor of 1.53 for measurements of BAO.

For RSD we define the reference figure of merit in terms of the aggregate fractional uncertainty on the growth rate parameter $\sigma_m(z)f(z)$ over the redshift range $1 < z < 3$. Specifically, we define F_G to be a constant factor that multiplies $\sigma_m(z)f(z)$ relative to the predictions of our fiducial ΛCDM cosmological model, over this entire redshift range. The reference figure of merit is

$$FoM_{RSD,ref} = [\sigma(F_G)]^{-2}$$

where $\sigma(F_G)$ is the forecast rms error in this quantity for the reference survey. Note that we use an inverse variance so that the FoM scales linearly with data volume, just like the FoM defined for BAO. For this forecast we assume that linear perturbation theory can be used up to $k_{max} = 0.2$ h Mpc^{-1} to constrain F_G and that higher wavenumbers are not used. With this assumption, our forecasting tools yield $FoM_{RSD,ref} = 6070$ for the reference survey described here. It is reasonable to expect that eventual analyses of the RST data set will allow stronger constraints thanks to improvements in theoretical modeling methods and use of higher order clustering statistics.

3.3.2 Baseline Dark Energy Science Requirements for the HLSS

To derive the baseline level of performance for the HLSS, we adopt a scale factor of 1.5, which as noted above gives a FoM matching the performance equivalent to the Astro-2010 submission for the HLSS.

HLSS 2.0.1: RST shall be capable of executing a high-latitude spectroscopic survey that can, if allocated 0.64 years of total observing time, achieve BAO constraints that yield

$$\mathrm{FoM}_{\mathrm{BAO}} \geq \mathrm{FoM}_{\mathrm{BAO,ref}} / 1.5 = 7533,$$

including statistical errors and observational systematic uncertainties, with $\mathrm{FoM}_{\mathrm{BAO}}$ and $\mathrm{FoM}_{\mathrm{BAO,ref}}$ computed as described in Section 3.3.1.

HLSS 2.0.2: RST shall be capable of executing a high-latitude spectroscopic survey that can, if allocated 0.64 years of total observing time, achieve RSD constraints that yield

$$\mathrm{FoM}_{\mathrm{RSD}} \geq \mathrm{FoM}_{\mathrm{RSD,ref}} / 1.5 = 4047,$$

including statistical errors and observational systematic uncertainties, with $\mathrm{FoM}_{\mathrm{RSD}}$ and $\mathrm{FoM}_{\mathrm{RSD,ref}}$ computed as described in Section 3.3.1.

Comment: Below we define survey capability and data record requirements that will, if met, lead to capabilities that satisfy HLSS 2.0.1 and 2.0.2. These two high-level requirements should be viewed as governing principles that can be used to evaluate alternative survey strategies, technical trades, and descopes.

Comment: For both of these requirements, potential observational systematic uncertainties include uncertain corrections for incompleteness, contamination, catastrophic redshift errors, and edge effects.

Allocation of Margin

To guide the definition of further baseline requirements, we allocate the factor of 1.5 FoM margin relative to the reference survey in two broad categories as follows:

A factor 0.85 in survey area (1700 deg^2 vs. 2000 deg^2)

A factor 0.78 in observational systematics ($0.85 \times 0.78 = 0.66$).

Margin on the sampling density $nP_{0.2}$ is implicitly incorporated within the survey area category.

Given the sensitivity of the effective volume to $nP_{0.2}$, a shortfall in flux sensitivity, completeness, galaxy density, or galaxy bias relative to the assumptions in our forecast would likely be accommodated by increasing the exposure time for the HLSS at the expense of survey area. The margin in survey area also allows for observational inefficiencies (e.g., slew and settle times) and for time devoted to calibration observations specific to the HLSS other than the deep fields already incorporated in the reference survey.

In general, there is room to trade margin among these categories while satisfying the governing baseline requirements. For example, if the redshift range is larger than $1.1 \leq z \leq 1.9$, then the margin for survey area can be made larger.

Other requirements are those needed to allow reliable redshift determinations and the construction of galaxy redshift catalogs with the information needed to enable accurate clustering measurements, including accurate maps of survey depth.

3.3.3 High-Latitude Spectroscopic Survey – Survey Capability Requirements

The principal requirement for the BAO/RSD program is the measurement of 3D positions (RA/Dec/redshift) for a large sample of galaxies with a characterizable selection function. The 3D measured positions of galaxies need only be accurate enough not to cause significant degradation of the large-scale structure measurement at mildly nonlinear scales. A redshift range of $1 < z < 2$ provides sufficient cosmic volume to enable the large statistics required for the BAO survey while providing significant overlap with the supernova survey.

The key survey capabilities needed for RST to satisfy the science requirements above are as follows:

> **HLSS 2.0.3:** RST shall be capable of executing a slitless spectroscopic survey covering the wavelength range $1.35\ \mu m \leq \lambda \leq 1.90\ \mu m$ with RMS redshift errors $\sigma_z \leq 0.001(1+z)$, reaching emission line flux sensitivity of 1.0×10^{-16} erg cm^{-2} s^{-1} for a point source at 1.8 μm with a net survey speed that is at least 0.34 deg^2/hr.

Comment: The wavelength range corresponds to redshifts $1.1 \leq z \leq 1.9$ for Hα emission at 0.6563 μm. This wavelength range also allows measurement of [OIII] emission line redshifts (0.5007 μm) at $1.7 \leq z \leq 2.9$. A wider wavelength range would be desirable as it increases the redshift range and survey volume and therefore adds margin for meeting other baseline requirements. However, a wider wavelength range increases noise and therefore degrades sensitivity. The spectral resolution achieves the required rms redshift accuracy, discussed further below.

Comment: The flux sensitivity is that assumed in our $nP_{0.2}$ calculations and FoM forecasts for the reference survey. Flux sensitivity is defined by the ability to detect a line at $S/N \geq 6.5$ at the median sky background level and assuming no losses of exposures due to chip gaps, cosmic rays, etc. We anticipate that 5σ detections will typically be usable for galaxies in the clustering sample, but also that significant fractions of the survey area will have higher background or loss of an exposure that reduces the S/N, motivating our choice of a 6.5σ threshold under ideal conditions.

Comment: The survey speed includes overheads and is sufficient to observe 1700 deg^2 in 0.64 years with just under 10% of the time allocated to deep field calibrations.

> **HLSS 2.0.4:** Roman shall be capable of conducting an HLSS with an average completeness ≥ 0.6.

Comment: We define completeness to be the ratio of the number of galaxies in the HLSS that are usable for BAO and RSD analyses to the number of galaxies expected to exceed the survey flux sensitivity limit based on the redshift-dependent Hα luminosity function. The nP0.2 and FoMref values for the reference survey are computed with a factor of 0.6 incorporated, so completeness at or above this level will not degrade the FoMs relative to the reference values. Estimates of incompleteness and experience with existing surveys suggests that 0.7 is achievable, so a requirement at 0.6 builds in some margin. This high-level requirement flows to requirements on the distribution of dithers and roll angles in the observing strategy and on the ability of data reduction software to identify emission lines while eliminating contaminants.

HLSS 2.0.5: Galaxies counted towards meeting requirements HLSS 2.0.3-2.0.4, shall have RMS redshift errors $\sigma z \leq 0.001(1+z)$, after excluding galaxies larger than 0.54" in radius and excluding outliers, with a fraction of outliers less than 10% of the sample smaller than 0.54" in radius , and with outliers defined as $|z_{obs} - z_{true}|/(1+z_{true})>0.005$.

Comment: Calculations by Wang et al. (2010), illustrated in Figure 9, show that values of $\sigma z/(1+z) > 0.001$ clearly degrade the results, while precision better than 0.001 provides diminishing returns. In grism observations, larger galaxies have somewhat larger redshift errors at a given S/N. However, only a small fraction of galaxies in the HLSS are expected to exceed 0.54" in radius, as shown in Figure 10.

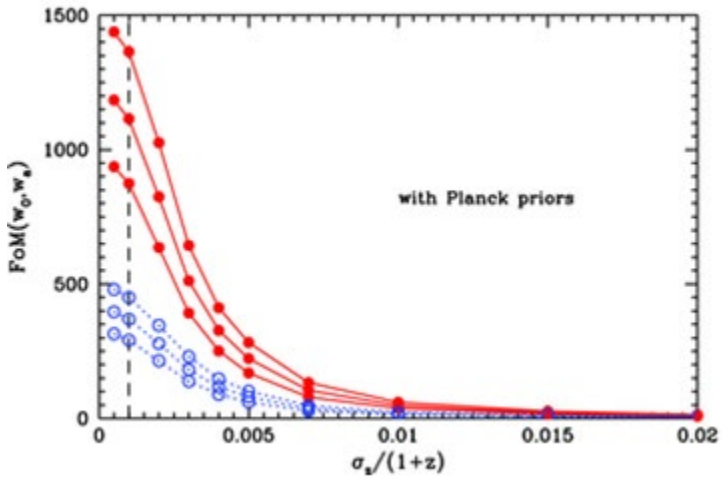

Figure 9 Dependence of DE Figure of Merit

Uncertainties >0.001 significantly degrade the results. The red curve assumes the growth rate of structure $f_g(z)$ is measured; the blue curve results from marginalizing over $f_g(z)$. From Figure 2 of Wang et al. 2010.

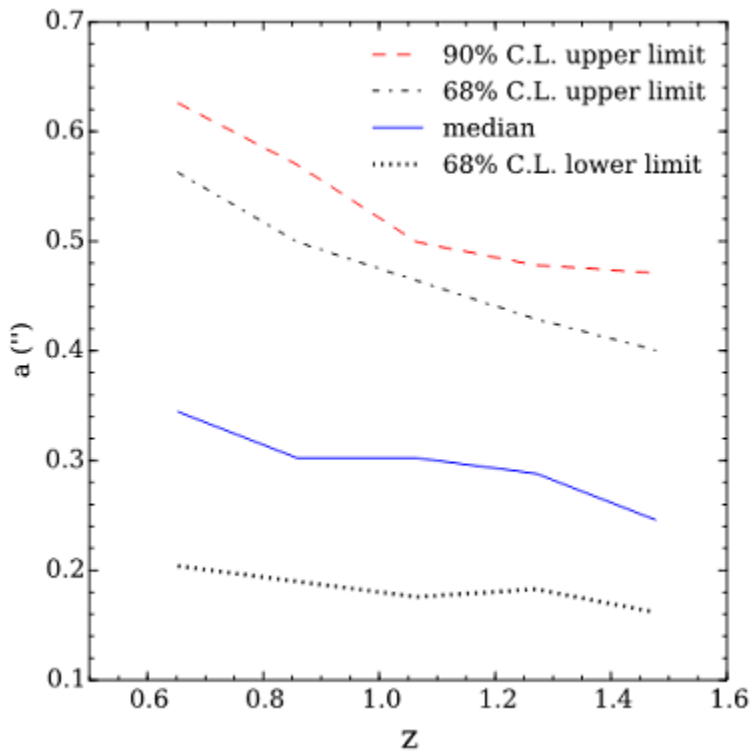

Figure 10 90% upper limit of semi-major axis continuum size of Hα ELGs

The 90% upper limit of semi-major axis continuum size of Hα ELGs with Hα line flux > 10^{-16} ergs/s/cm^2, and 0.55<z<1.85, based on 1773 galaxies from WISP (WISP team, private communication).

3.3.4 High-Latitude Spectroscopic Survey – Science Data Records

Higher-level science products include a catalog of each source in the field, that contains positions, classifications, photometric and spectroscopic redshifts (when assigned), links to the calibrated spectra, etc. The catalog also includes emission line wavelengths, equivalent widths, and integrated fluxes.

High-level science products should also include information on the effective depth of the survey with position on the sky, and any other information needed to understand the galaxy selection functions in three dimensions. Examples include, for each galaxy: the net exposure time (losses include chip gaps, spectral overlap with adjacent sources, cosmic rays, etc), number of distinct roll angles, changes in PSF size with position in field or observing conditions, etc.

> **HLSS 2.1.1:** RST shall provide sufficient information to characterize completeness and survey depth as a function of sky position and redshift, with sufficient detail and accuracy that associated systematic uncertainties in galaxy clustering cause ≤ 20% degradation in the BAO and RSD figures of merit.

Comment: Uncertainties in corrections for completeness and survey depth are the principal source of observational systematic uncertainty in the BAO and RSD measurements. This requirement allows these effects to use most but not all of the FoM margin allocated to

observational systematics (0.80 vs. 0.75). This requirement can be verified by analysis, though the required analysis is fairly complex. It may require the ability to inject artificial sources into the true data stream to measure how efficiently they are recovered.

> **HLSS 2.1.2:** RST shall provide sufficient information to enable determination of the incidence of outliers, to a fraction of 2.5×10-3 of the full galaxy sample over the entire survey redshift range.

Comment: Outliers dilute the clustered galaxy fraction with spatially uncorrelated contaminants from other redshifts. If the outlier fraction is ε then the galaxy power spectrum is depressed by a factor (1-ε)2. For BAO the dilution is a minor issue (it reduces S/N), but for RSD it is a problem because it reduces the galaxy bias by (1-e) without changing the linear redshift-space distortion parameter b (observable for growth rate fg), introducing an error of (1-ε) in the inferred rate of structure growth fgs8(z). Uncertainty of 2×10-3 in ε leads to 0.2% systematic error in the growth rate after it is corrected for the bias due to completeness.

Comment: The deep field calibration observations are crucial to meeting this requirement, and analysis of those observations should be sufficient to achieve it.

> **HLSS 2.1.3:** RST shall associate spectra (or a range of spectral image pixels) with the corresponding objects in the imaging catalog.

> **HLSS 2.1.4:** RST HLSS catalog spectra derived from individual exposures shall include information on flux uncertainty, effective line-spread function (LSF) as a function of position and wavelength, data quality flags, and an estimate of contamination from the overlap of different spectra.

Comment: Information on the line-spread function may be in the form of model parameters.

> **HLSS 2.1.5:** RST shall produce a single net spectrum for each source by combining HLSS spectra from multiple roll angles.

> **HLSS 2.1.6:** RST shall be capable of obtaining spectra at nearly opposing roll angles to account for possible offsets of the emitting region from the center of the broad-band image.

> **HLSS 2.1.7:** RST shall provide the following additional information for each net extracted spectrum (HLSS 2.1.5): uncertainties in the measured fluxes and wavelengths, effective line-spread function as a function of wavelength, data quality flags, and additional data generated in producing the spectra that characterize or support the spectra generation process.

Comment: Information on the line-spread function may be in the form of model parameters.

> **HLSS 2.1.8:** RST shall provide HLSS science data records with redshifts as well as best fit spectral templates associated with that redshift.

> **HLSS 2.1.9:** RST shall provide HLSS science data records with wavelengths and integrated fluxes of emission lines, as applicable.

Comment: These are basic requirements on the data records needed to allow science analysis and quality assurance.

> **HLSS 2.1.10:** RST shall provide HLSS science data records with relative position measurement uncertainties less than 3.4" over the entire survey area.

Comment: We need to measure galaxy positions to better than ~$0.1h^{-1}$ Mpc (which corresponds to 3.4″, assuming that 105 h^{-1} Mpc subtends 1 degree), in order to measure galaxy clustering accurately. This should be met easily if HLIS 2.2.5 is met, which makes systematic errors in the astrometry negligible. Given the pixel scale of 0.11″, this requirement is automatically met within each field, and is tied to the precision of astrometry across different fields.

> **HLSS 2.1.11:** RST shall be capable of providing images and corresponding source catalogs of the HLSS fields that reach JAB=24.0, HAB=23.5, and F184AB=23.1 for an reff=0.3″ source at 10sigma to achieve a reference image position, in 3 filters.

Comment: Provided the HLSS covers area already observed in the HLIS, this requirement will be met automatically. This requirement applies to any HLSS fields that are counted toward the minimum survey area requirement but are not covered by the HLIS. Imaging in at least three filters is required to build a minimal spectral template for grism spectral decontamination. See HLIS 2.1.11.

3.3.5 High-Latitude Spectroscopic Survey –Calibrated Data Records

> **HLSS 2.2.1:** RST shall archive HLSS calibrated spectra for each grism exposure.

> **HLSS 2.2.2:** RST shall provide HLSS calibrated spectra with an uncertainty of the wavelength measurement σ_λ of $\sigma_\lambda/\lambda \leq 0.001$.

Comment: The wavelength calibration uncertainty is needed to allow redshift measurement uncertainty at the same precision (HLSS 2.0.5).

> **HLSS 2.2.3:** RST shall provide HLSS calibrated spectra with an uncertainty in the wavelength calibration that does not introduce biases to the wavelength measurement by amounts greater than $\sigma\lambda/\lambda \leq 10^{-4}$ on any angular scales exceeding 0.064 degrees within a field, and $\sigma\lambda/\lambda \leq 1\times10^{-4}$ from field to field.

Comment: Variations in the wavelength calibration within a field, and from field to field on large scales, wash out the clustering signal by de-correlating the projected component of the clustering signal on those angular scales. Within a field, the acceptable level of wavelength error is $\sigma_\lambda/\lambda \leq 10^{-4}$, which is 10% of the errors on individual redshift measurements (0.001), to avoid increasing the overall redshift error by a significant factor. The angular scale is set by the optimal smoothing scale for BAO reconstruction, ~ 5 Mpc/h. At z=3, this subtends 0.064 degrees for a flat universe with Ω_m=0.3 and a cosmological constant. For field to field, the acceptable level of wavelength error is 2×10^{-5}, which comes from comparing two adjacent fields. Since we expect ~10^4 galaxies per deg^2, we have ~2810 galaxies per FOV of 0.281 deg^2. If the galaxies have a redshift error of 10^{-3} each, then one can measure systematic offsets between fields (statistically) at the 10^{-3}/sqrt(2810) level, which is 1.9×10^{-5}. At that level the power from the systematics is sub-dominant to the power from the redshift error.

HLSS 2.2.4: RST shall provide calibrated spectra with relative spectrophotometric flux calibration uniform to 2 percent (with the goal of 1%) over the area and wavelength range of the survey.

Comment: We emphasize that these are requirements on the relative uniformity of the spectrophotometric calibration, and not on its absolute value.

Comment: Spatial errors or wavelength-dependent errors in the spectrophotometric calibration will introduce artificial spatial fluctuations in the number density of galaxies, which could contaminate the cosmological signal. We start by setting a requirement on the spatial uniformity of the mean number density as a function of physical scale. We require that the non-cosmological fluctuations in the mean number density (or the selection function of the survey) be < 1% (sqrt variance) when averaged over spatial scales between 10 Mpc/h to 200 Mpc/h. At small scales, this is ~two orders of magnitude smaller than the cosmological signal, while at the ~BAO scale of 100 Mpc/h, this is ~one order of magnitude smaller than the cosmological signal. These fluctuations equal the cosmological signal at ~400 Mpc/h. These physical scales correspond to ~0.5 degrees to 6 degrees at a redshift of 1.5. We convert this to a requirement on the spectrophotometric calibration accuracy, assuming the Model I luminosity function of Pozetti et al. At the flux limit of RST, this yields a requirement of 1% relative spectrophotometric calibration, averaged over angular scales of 0.5 degrees to 6 degrees.

3.3.6 High-Latitude Spectroscopic Survey – Raw Data Records

The implementation approach for measuring the requisite number of galaxy redshifts is to perform slitless spectroscopy over the entire wide-field instrument field of view. Imaging data of the same fields is required for properly extracting the spectra, and having photometric redshifts is desirable for minimizing the possibility of mis-identification of emission lines. Thus, observation efficiency is maximized if the region surveyed for this program lies within the boundaries of the HLIS.

The high latitude spectroscopic survey must support multiple roll angles to reduce spectral confusion and unambiguously associate an emission line with its host galaxy. Furthermore the angles must be such as to provide counter-dispersion – the roll angle should change by ~180° to suppress systematic errors in wavelength determination associated with the astrometric offset between the continuum galaxy image and the Hα emitting region. It is in principle possible to do this either by using 2 separate dispersers with opposite dispersion, or by using a single disperser and waiting ~6 months for the counter-dispersed image. Accomplishing both purposes of obtaining spectra at approximately 180° roll offset, and obtaining spectra with small roll offsets to vary the overlap of spectra of adjacent galaxies requires exposures at a minimum of three different roll angles. Because some data will be lost to cosmic rays, spectra falling into gaps in the focal plane array, etc, exposures at four roll angles should be planned for each field so as to ensure adequate data at the minimum of three roll angles.

HLSS 2.3.1: RST shall provide raw spectral images in the archive for each downlinked detector readout with each raw data record including a unique dataset identifier for each exposure, the exposure time, the time of exposure, all individual downlinked detector readouts used to make the exposure, the observatory pointing orientation and any additional engineering data the Science Center uses for subsequent processing.

HLSS 2.3.2: RST shall provide HLSS raw spectral images with a spectral dispersion between 10 Å/pix and 12 Å/pix over the full bandpass and across the full field.

Comment: Gratings tend to give constant dispersion in linear space, rather than R-space. The above dispersion would give point-source spectral resolution $R=\lambda/\Delta\lambda$ in the range $550 \leq R \leq 800$, for a 2-pixel resolution element.

HLSS 2.3.3: RST shall provide raw spectral images for the HLSS with wavelength range of at least 1.32 to 1.93 µm.

Comment: The wavelength range here comes directly from HLSS 2.0.3, with 1.5% extension on either end because it is problematic to use emission lines that fall within 1.5% of the bandpass edges. A wider wavelength range would increase the redshift range of the survey while increasing the background noise.

Comment: A wavelength range satisfying $\lambda_{max}/\lambda_{min} \geq 1.82$ is highly desirable for the [OIII] redshift survey as it allows the use of multiple lines to reject line misidentifications. Specifically, this ratio ensures that we cannot have [OII] (373nm) falling off the blue end of our coverage while Hα (656.28nm) falls off the red end.

HLSS 2.3.4: RST shall provide HLSS raw spectral images with 50% of the energy enclosed in a circle of radius <0.21" at 1.5 µm for a monochromatic point source, excluding diffraction spikes and non-first order light and including the effects of pointing jitter, for at least 95% of the exposures and over 95% of the FOV.

Comment: This limit of 0.21″ is required by source separation in the input catalog for spectral extraction.

HLSS 2.3.5: RST shall be capable of providing HLSS raw spectral images of each field with a minimum of 3 dispersion directions, with two being 180 +/- 30 degrees opposed.

HLSS 2.3.6: RST shall be capable of obtaining 20 spectroscopic observations in the HLSS deep fields with dispersion directions of the observations roughly evenly distributed between 0 and 360 degrees.

Comment: The first mode corresponds to the standard HLSS observations, the second to the observations for the deep calibration fields discussed in the description of the reference survey.

3.4 High Latitude Imaging Survey

3.4.1 High-Latitude Imaging Survey – Science Requirements

The High-Latitude Imaging Survey (HLIS) enables constraints on the cosmic expansion history and growth of structure through weak lensing (WL) measurements, including cosmic shear, galaxy-galaxy lensing, and cluster-galaxy lensing. Our requirements discussions focus principally on cosmic shear, with galaxy-galaxy lensing and cluster-galaxy lensing providing margin for achieving the demanding goals on cosmological measurement precision.

The weak lensing technique uses the shear of distant galaxies by gravitational lensing, which is determined by an integral of the tidal field along the line of sight to the source galaxy. The

strength of the lensing signal as a function of the redshift of source galaxies is sensitive both to the growth of cosmic structure at intervening redshifts $0<z<z_{source}$ and to the distance-redshift relation (since the same amount of mass produces more shear on more distant sources). In addition to measurements of cosmic shear (the correlated ellipticities of source galaxies lensed by the same foreground structure), the correlation of lensing shear with foreground galaxies of known redshift z_{fg} probes the relation of these galaxies to the matter field; this "galaxy-galaxy lensing" signal can be combined with measurements of galaxy-clustering to infer the amplitude of matter fluctuations. A weak lensing survey must provide wide angle sky coverage with a high density of usable sources across a wide redshift range (local to z~2), provide photometric redshifts so that the galaxies can be sliced into bins to study evolution of the signal and remove "intrinsic" (not lensing induced) shape correlations, and achieve exquisite control over coherent systematic errors in the shear signal. The latter includes both "additive" shear errors, i.e., apparent shear induced by imperfect correction for instrument effects (aberrations, anisotropic jitter, geometric distortions, etc.) that are not present in the sky, and "multiplicative" shear errors, where the calibration of the observed shear is incorrect. Some sources of error (*e.g.*, failure to recover full sampling) can lead to both additive and multiplicative errors.

The imaging component of a weak lensing survey is inherently sensitive to sources at any redshift, so long as they are bright enough in the bands used and large enough compared to the PSF to enable shape measurement. Unlike for the HLSS, the HLIS redshift range cannot be independently tuned and traded against depth or area given the constraints of the RST mission. For example: we have found that for the Reference survey (see below), 50% of the source galaxies are predicted to be at $z_{src}<1$, 90% at $z_{src}<2$, and 98.5% at $z_{src}<3$. The HLIS requirements are designed to control systematics over this entire redshift range.

An important consideration is the number of filters used for shape determination. Cross-spectra between repeated measurements of the same sky footprint with sufficiently different (e.g. rolled) tiling patterns acquired at different epochs provide a powerful means to suppress additive shear systematic errors, since the true weak lensing signal remains the same but the systematic errors can be de-correlated. Generating one shear map per filter is the simplest implementation, as the number of passes is restricted by efficiency considerations and multiple filters will be needed for photometric redshifts. At least two shear maps are necessary to perform a cross-power analysis. However, this provides only one cross-power spectrum, so it is impossible to check cross-powers against each other, and moreover there is no way to determine from this one cross-cc power spectrum whether the calibration (multiplicative error) of the two input maps is consistent. A third shear map mitigates both of these issues. (Other methods, such as galaxy-galaxy lensing, could be used for consistency tests.) The Reference Survey therefore assumes three shape measurement filters, although it is possible that further developments with other surveys will favor a different implementation.

Multiple filters are also important for addressing wavelength-dependent PSF issues in galaxy shape measurements (Voigt et al. 2011; Cypriano et al. 2010); with a single shape measurement filter, the difference in PSF between galaxies and calibration stars can easily become a limiting systematic that is both difficult to detect and problematic to correct, especially in galaxies that have a radial color gradient. Robust photometric redshifts require a combination of optical and NIR photometry, to suppress confusion between the spectral breaks near 4000 Å and 1216 Å. RST measurements must therefore complement ground-based photometry in sufficient filters and

at a depth sufficient for determining photometric redshifts for the entire galaxy sample used for the shear measurements.

Given that the source redshift distribution cannot be independently varied, a reasonable proxy for the statistical power of a WL survey is its aggregate statistical precision – the ability to measure the linear power spectrum amplitude σ_8 with all other parameters held fixed. The "dark energy figure of Merit" (FoM) would be an alternative metric that is more closely tied to the ultimate science goal. However, weak lensing alone suffers from parameter degeneracies between dark energy parameters and other cosmological parameters (primordial perturbations, baryon abundance, neutrinos…) and so "practical" dark energy constraints always come from combining WL with other probes (e.g. the CMB). By contrast, the aggregate precision metric depends only on RST weak lensing, and the additional supporting data sets (optical imaging for photo-z's, and spectroscopy or any other calibration data). The JDEM FoMSWG forecasted that Stage III weak lensing projects (those currently underway) would measure σ_8 to 1% (1σ, stat+sys); RST should enable a large advance over this.

The RST weak lensing survey is designed to reach an aggregate statistical precision of 0.132% (1σ), where by "statistical" we refer to mode counting, galaxy shape noise, and photometric noise alone. The Reference survey is one implementation of this, with an area of 2000 deg^2 and an effective source density of 30 galaxies/arcmin^2, which meets this target. Observational systematic errors are required to be sub-dominant, in the sense that they would reach the level of systematic errors only after a survey with 5× the area of the Reference Survey. This ensures that RST would remain statistics-limited even in an extended mission that dedicated significant time to a continuation of the HLS. Astrophysical systematic errors are not under our direct control, but we have written requirements on RST in cases where aspects of the mission design could potentially mitigate these errors. Further understanding of these systematic errors could in principle motivate choosing a different point on the depth vs. area curve than the Reference Survey.

The basic observable for cosmic shear WL is the lensing power spectrum – the variance C_{LL} of spherical harmonics of the shear map as a function of angular wavenumber L -- measured in tomographic bins of source photometric redshift (photo-z). The combination $L(L+1)C_{LL}$ is the contribution to the variance of cosmic shear per logarithmic interval $\Delta \ln L$. The shape of C_{LL} depends on the shape of the matter power spectrum P(k), and the amplitude depends on the distance-redshift relation $D_A(z)$ and on the history of matter clustering $\sigma_m(z)$, where $(\sigma_m)^2$ is a scaling for the amplitude of the matter power spectrum. Analysis in photo-z bins provides sensitivity to the redshift dependence of these functions, but the kernel of the cosmic shear integrals is broad in redshift, so it is difficult to decompose the constraints into narrow bins of $D_A(z)$ and $\sigma_m(z)$. The shape of P(k) depends on cosmological parameters that are constrained well but not perfectly by cosmic microwave background measurements. The predicted shape of P(k) can change in modified gravity models that have an effective scale-dependence or environment-dependence in the strength of gravity.

Figure 11 shows the predicted cosmic shear angular power spectrum for 17 tomographic bins of source galaxy photometric redshift together with the projected statistical errors for the RST WL survey. For multipole L less than a few hundred, the statistical errors are dominated by sample variance in the lensing mass distribution within the survey volume, while for high L or the

extreme redshift bins the errors are dominated by shape noise, *i.e.*, the random orientations of the source galaxies that are available to measure the shear. For a given photo-z bin the statistical errors at different L are uncorrelated. Across photo-z bins, the errors at lower L are partly correlated because the same foreground structure contributes to the lensing of all galaxies at higher redshift; the errors decorrelate at high L when they become dominated by shape noise,

which is independent for each set of sources. While Figure 11 displays the auto-spectra for the 17 photo-z bins, there are also 17×16/2 = 136 cross-spectra that provide additional information.

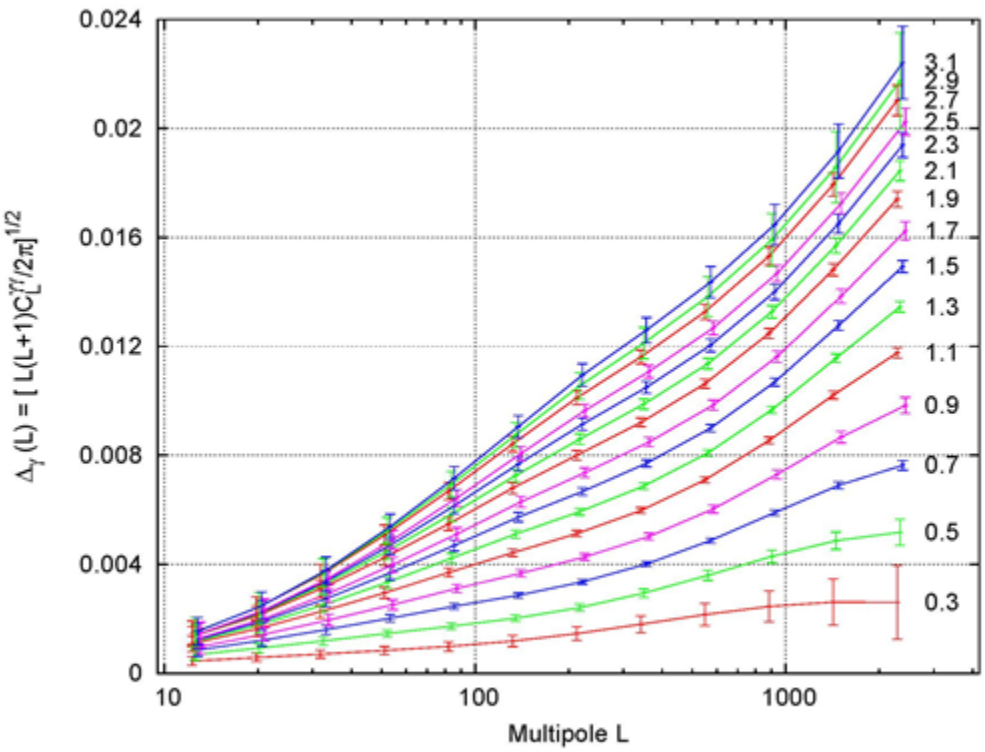

Figure 11 Predicted Cosmic Shear Angular Power Spectrum and Associated Statistical Errors for the WL Survey

The predicted cosmic shear angular power spectrum and associated statistical errors for the WL survey, for 17 tomographic bins of source photometric redshift as labeled. L is the angular multipole, and $L(L+1)C_L\gamma\gamma$ is the contribution to the variance of cosmic shear per logarithmic interval $\Delta \ln L$.

The cosmological sensitivity of the WL experiment arises from the dependence of the predicted lensing power spectrum on parameters describing dark energy and structure growth. An overall increase in the amplitude of matter clustering would raise all of the model curves in Figure 11 by the same factor, while a change in the *rate* of structure growth would shift the curves relative to

each other. Changes in the distance-redshift relation would also shift the curves relative to each other, as the lensing signal depends on the distance to lenses and sources. The mix of correlated and uncorrelated errors makes it difficult to read the aggregate precision of the WL measurement off a plot like Figure 11. We find that the overall measurement precision of the amplitude of the WL power spectrum (i.e., a constant multiplicative offset across all bins) is 0.29%. For an approximate scaling argument that gives a similar result, see §5.4 of Weinberg et al. (2012).

Even when the ellipticity of a galaxy is well measured, the estimate of its shear has a low signal-to-noise ratio, because typical shears are ~ 0.005 while the dispersion of galaxy ellipticities is ~ 0.3. Large numbers of WL sources are needed to overcome the impact of this "shape noise." The primary determinant of the statistical power of a WL data set is the total number of galaxy shapes measured, which is the product of the survey area and the effective source density N_{eff}. The effective source density incorporates signal-to-noise weighting of individual galaxy ellipticities, and it omits galaxies that are too small (relative to the imaging PSF) to yield reliable ellipticity estimates in the presence of measurement biases.

The leading sources of systematic error in deriving cosmological constraints from WL measurements are:

1. Systematic biases in the shear measurements themselves. These are usually separated into additive biases, which add to all shears coherently across a large area, and multiplicative biases, which rescale the estimated shears relative to the true shears.

2. Systematic biases in photo-z estimates. Photo-z estimates do not need to be highly accurate on a galaxy-by-galaxy basis, but the true redshift distribution of galaxies in bins of photo-z must be known to high accuracy, including the mean redshift, the dispersion, the skewness of the core distribution, and the outliers arising from catastrophic errors.

3. Contamination of the true WL signal by intrinsic alignments of galaxy ellipticities with the ellipticities of their neighbors or with the tidal gravitational field of the surrounding dark matter distribution.

4. Systematic errors in the prediction of the WL signal as a function of cosmological parameters. The primary challenge is accurately modeling the baryon distribution and the impact of the baryons on the dark matter; baryonic effects have little impact on large scales, but they become important in the highly non-linear regime, e.g., on angular scales smaller than the virial diameters of large halos.

Controlling shape measurement systematics requires excellent knowledge of the imaging PSF, including any dependence on field position, galaxy flux, galaxy color, and so forth. Controlling photo-z systematics requires excellent photometric calibration, large and deep spectroscopic calibration data sets, and measurements and modeling of the angular cross-correlation of source galaxy populations with large scale structure traced by brighter galaxies in spectroscopic redshift surveys. Controlling intrinsic alignment systematics requires tomographic analyses that can discriminate between intrinsic alignment and true lensing signatures, interpreted using parametric models that are flexible and accurate enough to represent intrinsic alignment effects. Controlling modeling systematics requires marginalizing over parameterized descriptions that are flexible and accurate enough to represent the effects of baryonic/non-linear physics; tighter

priors on these effects from empirically constrained numerical simulations reduce the statistical errors that arise from this marginalization.

HLIS requirements are designed to produce a statistically powerful data set with the data quality needed to control shape measurement, photo-z, and intrinsic alignment systematics, and the ability to conduct internal cross-checks that could reveal unrecognized systematics. The different responses of cosmic shear, cluster-galaxy lensing, and galaxy-galaxy lensing to all four of these categories of systematic error is itself a powerful tool for systematics control.

3.4.2 Reference Survey and Figures of Merit

For the HLIS reference survey used to define baseline requirements, we adopt the same 2000 deg^2 area as the HLSS, and acquire imaging to a depth sufficient to obtain an effective source density to $N_{eff} = 30$ $arcmin^{-2}$ in the Y, J, H, and F184 filters. This provides margin for observing inefficiencies and the possibility that some fraction of sources cannot be used because of unreliable shape measurements or photo-z estimates. We define the reference figure of merit in terms of the aggregate fractional uncertainty on the amplitude of clustering $\sigma_m(z)$ for a fixed distance-redshift relation. Specifically, we define F_{WL} to be a constant factor that multiplies $\sigma_m(z)$ at all redshifts, relative to the predictions of our fiducial ΛCDM cosmological model. The reference figure of merit is

$$FoM_{WL,ref} = [\sigma(F_{WL})]^{-2}$$

where $\sigma(F_{WL})$ is the forecast rms error in this quantity for the reference survey. With this inverse-variance definition, the FoM scales linearly with survey area in the absence of systematic errors. For this forecast we include statistical errors and marginalization over a description of baryonic effects, but we do not incorporate other systematics. Our forecasting tools yield an uncertainty of 0.132% in F_{WL} for the reference survey, or $FoM_{WL,ref} = 573000$. The corresponding value for the Astro 2010 version of the HLIS was 321000, hence the present survey exceeds the expectations of the New Worlds New Horizons report by a factor of 1.78; see RST-SCI-DESC-0080 Figure of Merit Computations for the HLS Reference Survey for details of this calculation. Figure 11 shows a forecast of the shear angular power spectrum and its associated statistical errors for 17 tomographic photo-z bins.

In practice there is substantial degeneracy between the expansion history and structure growth constraints from WL. However, for characterizing the statistical power of the survey and the impact of systematics, it is simplest, and sufficient, to focus on a single-parameter constraint with other quantities held fixed. The degeneracy between growth and expansion history will be broken largely by combining the WL measurements with SN and BAO constraints, which depend only on expansion history.

3.4.3 Baseline Dark Energy Science Requirements for the HLIS

To derive the baseline level of performance for the HLIS, we adopt a scale factor of 1.75, which as noted above gives a FoM matching the performance equivalent to the Astro-2010 submission for the HLIS.

> **HLIS 2.0.1:** RST shall be capable of executing a high-latitude imaging survey that can, in 1.07 years of total observing time, achieve WL constraints that yield

$$\mathrm{FoM}_{\mathrm{WL}} \geq \mathrm{FoM}_{\mathrm{WL,ref}} / 1.75 = 327400,$$

including statistical and systematic errors, with $\mathrm{FoM}_{\mathrm{WL}}$ and $\mathrm{FoM}_{\mathrm{WL,ref}}$ computed as described above.

While $\mathrm{FoM}_{\mathrm{WL,ref}}$ is computed based on cosmic shear alone, the $\mathrm{FoM}_{\mathrm{WL}}$ for the HLIS will include the constraints from galaxy-galaxy lensing and cluster-galaxy lensing, which provide margin from additional statistical power and their leverage for constraining systematics. Additional margin comes from the use of three shape measurement bands, which provides greater statistical power than the $N_{\mathrm{eff}} = 30$ arcmin^{-2} reference case, as well as providing a method to diagnose and mitigate systematic effects through the comparison of auto- and cross-correlations.

Since the reference $\mathrm{FoM}_{\mathrm{WL}}$ is computed without contributions from shape measurement, photo-z, or intrinsic alignment systematics, meeting this Level 1 requirement implies keeping the contribution of these systematics sub-dominant relative to the statistical errors of the reference survey.

Allocation of Margin

We define baseline Level 2 requirements for the HLIS such that, if these requirements are satisfied, we expect the baseline requirement, $\mathrm{FoM}_{\mathrm{WL}} \geq 0.57 \times \mathrm{FoM}_{\mathrm{WL,ref}}$, to be satisfied. We allocate the margin relative to the reference survey in broad categories as follows:

- A factor 0.85 in survey area (1700 deg^2 vs. 2000 deg^2)
- A factor 0.9 in effective source density (27 arcmin^{-2} vs. 30 arcmin^{-2})
- A factor 0.95 in shape measurement systematics
- A factor 0.83 in photo-z systematics
- A factor 0.95 in intrinsic alignment systematics ($0.85 \times 0.9 \times 0.95 \times 0.83 \times 0.95 = 0.57$).

The margin in survey area allows for observational inefficiencies (e.g., slew and settle times exceeding the margin already built in to the estimates) and for time devoted to calibration observations specific to the HLIS.

In general, there is room to trade margin among these categories while satisfying the baseline requirement. For example, if the effective source density exceeds 27 arcmin^{-2}, then there is room to accommodate larger photo-z systematics or a smaller survey area. If four filters are not required over the full survey area to control systematics, then the number of shape measurements can be increased (considerably) by observing a larger area in one or two bands.

Other requirements are those needed to allow the construction of galaxy catalogs with the information needed to enable accurate WL and galaxy clustering measurements, including accurate maps of survey depth.

We do not define individual thresholds (as opposed to baselines) for the Level 2 requirements. The HLIS threshold is a factor of 4 lower in $\mathrm{FoM}_{\mathrm{WL}}$, and the best way of meeting this threshold would likely depend on which of the baseline requirements cannot be met.

3.4.4 High-Latitude Imaging Survey – Survey Capability Requirements

The weak lensing science analysis will require shape measurements of source galaxies; the statistical power of the survey depends on the effective number density n_{eff} and area A. Achieving the science goals also requires control over biases in shear determination (both additive and multiplicative). These galaxies must have photometric redshifts, which come from a combination of RST NIR data and ground-based optical data. Finally, calibration of the photometric redshifts will include deep field data from RST as well as spectroscopic data from other observatories.

The survey capabilities needed on RST to satisfy the science requirements above are as follows:

Survey Statistical Power

> **HLIS 2.0.2:** RST shall be capable of executing a High Latitude Imaging Survey to measure galaxy shapes with a total effective galaxy density of at least $n_{eff} = 27$ per arcmin^2 in at least two bands, and three bands for at least half of these galaxies, and photometry in 4 NIR bands to support photometric redshift determination, with a net survey speed that is at least 0.20 deg^2/hr.

Comment: The effective number density is defined by the equation:

$$n_{\mathrm{eff}} = \frac{1}{A_{\mathrm{survey}}} \sum \frac{\sigma_{\mathrm{int}}^2}{\sigma_{\mathrm{int}}^2 + \sigma_{\mathrm{meas}}^2},$$

where σ_{int} is the intrinsic RMS dispersion in galaxy ellipticities per component, σ_{meas} is the RMS measurement noise per component, the sum is over all galaxies, and A_{survey} is the survey area.

Comment: The 3 bands required for shape measurement count as 3 of the 4 photometric bands.

Comment: The area includes edge effects in the sky tiling. Losses due to bright stars or image defects at scales < 1 arcmin are counted as loss of galaxy number density rather than survey area.

Comment: The survey speed includes overheads and is sufficient to observe 1700 deg^2 in 1.07 years, with ~10% of the time allocated to deep field observations. Time is defined here to include the time for observations in all 4 filters.

Shear Measurement Systematic Error Control

The survey statistical precision defines the required level of control for measurement systematics. Given the possibility of an extended mission that would allow a larger area HLS, we have set our requirements for additive and multiplicative shear errors so that RST shape measurement remains statistics-limited (in the sense that $\sigma_{sys}<\sigma_{stat}$) even in the event that an extended mission covers 10,000 deg^2 (5x reference area at reference depth). This has been assessed using the criterion that $Z < 1$, where $Z = \sqrt{\Delta \boldsymbol{C} \cdot \boldsymbol{\Sigma}^{-1} \Delta \boldsymbol{C}}$ depends on the data vector $\boldsymbol{C}$ (vector of all power spectra and cross-spectra in each bin), its systematic error $\Delta \boldsymbol{C}$, and its statistical covariance matrix $\boldsymbol{\Sigma}$. *Any* function of the data vector is then biased by no more than Z statistical standard deviations. This criterion depends on not just the amplitude of the additive or

multiplicative bias, but also its dependence on angular scale and on redshift. The FoMSWG Fisher code (Albrecht et al. 2009) was used to construct Σ .

The angular scale dependence is addressed by breaking the contributions to Z down into four angular ranges, each half a decade in scale: $\log_{10} l$ = 1.5—2.0, 2.0—2.5, 2.5—3.0, and 3.0—3.5. (The cosmic shear signal at $\log_{10} l > 3.5$ is strongly affected by baryonic uncertainties so it is not included in this budget.) The contributions to Z are broken down so that 6.25% of the total budget (in an RSS sense: Z^2=0.0625) is allocated to each of these four ranges, and 25% to the multiplicative bias. (The remaining 50% of the systematic error budget is reserved for errors other than shape measurement.) This partitioning of the systematic error budget is not unique and trades among the different terms may be made. In each case, the Z-statistic is first estimated for a redshift-independent error (additive or multiplicative). Then, for each possible redshift dependence of the additive or multiplicative systematic error, one computes the factor:

$$S = \frac{Z(\text{true redshift dependence})}{Z(\text{all redshift bins set to the most contaminated bin})}$$

The S-factor is by construction 1 for any systematic error that is redshift-independent. It thus captures the amount by which the redshift dependence enhances (S>1) or reduces (S<1) the significance of the systematic. The systematic error budgets, quoted in HLIS 2.0.3 and 2.0.4 below, are thus on additive and multiplicative biases scaled by the S-factor. For the most common types of systematic errors, such as PSF ellipticity induced by astigmatism, we have found that S<1, but this should be checked for each case.

HLIS 2.0.3: RST shall enable shear measurements with additive shear errors A limited in RMS per component over the range of angular multipoles $1.5 < \log_{10} \ell < 3.5$ as specified below:

$$\sqrt{\sum A^2 S} < 7.0 \times 10^{-5} \quad \text{for} \quad 1.5 < \log_{10} \ell < \mathbf{2.0}$$

$$\sqrt{\sum A^2 S} < 9.9 \times 10^{-5} \quad \text{for} \quad 2.0 < \log_{10} \ell < \mathbf{2.5}$$

$$\sqrt{\sum A^2 S} < 1.4 \times 10^{-4} \quad \text{for} \quad 2.5 < \log_{10} \ell < \mathbf{3.0}$$

$$\sqrt{\sum A^2 S} < 1.9 \times 10^{-4} \quad \text{for} \quad 3.0 < \log_{10} \ell < \mathbf{3.5}$$

where the sum is over independent terms in the additive systematic budget.

The total additive systematic budget, obtained via RSS of the scale bins, is 2.7×10^{-4}.

HLIS 2.0.4: RST shall enable shear measurements with multiplicative shear errors M shall be known to

$$\sqrt{\sum M^2 S} < 3.2 \times 10^{-4}$$

where the sum is over independent terms in the multiplicative systematic budget.

Comment: Requirements HLIS 2.0.3 and HLIS 2.0.4 includes sources of additive shear with both hardware (detector, optics) and software (biases due to data reduction pipeline) origin, after all post-processing.

Comment: HLIS 2.0.3 and HLIS 2.0.4 serve as top-level error budgets that are subdivided into individual contributions, usually combined in an RSS sense. The budgets from each effect (e.g. astrometric errors) can be traded against each other so long as the top-level budget is met. These error budgets are described in the Wide-Field Instrument Calibration Plan (RST-SCI-PLAN-0006).

Deep Field

HLIS 2.0.5: RST shall be capable of observing a deep field of at least 6 deg^2 within the HLIS with a depth five times greater (in inverse variance) than the main survey in each of the HLIS filters, and with at least twice the number of dither and roll positions as the broader HLIS.

Comment: The deep field is to be used for characterizing noise-related biases in shape measurement, selection, and photometric redshifts. Due to the large number of dithers, it can also be used to understand the impact of undersampling and sparse dither patterns on photometry, astrometry, and shape measurements in the HLIS.

Comment: The deep field should be situated to overlap with other deep multi-wavelength data; overlap with deep fields for the optical telescope used for photometric redshifts is particularly valuable.

3.4.5 High-Latitude Imaging Survey – Science Data Records

High-level science products needed for weak lending analysis include: mosaiced images; catalogs of each source; and tools for working with the data.

Mosaics

HLIS 2.1.1: RST shall be capable of producing mosaic images of the HLIS fields using data in each filter, and using coordinates tied to the astrometric frame defined by the ICRF.

HLIS 2.1.2: RST shall be capable of producing HLIS mosaics that include information on the flux uncertainty or effective depth as a function of position, data quality flags, and additional data generated in producing the mosaics that characterize or support the mosaic generation process.

Weak lensing analyses can use as input either mosaics, the calibrated images, or some combination of both (for example, object detection on a mosaic but with parameters determined by a χ^2 fit to the calibrated images). It is likely that the final WL analysis for RST will use more

than one object selection/shape measurement method, possibly using different levels of data processing as input.

Even shape measurement methods that work on stacked images will require access to metadata to understand noise correlations or other sources of systematic error. The "additional data" described in HLIS 2.1.2 will thus include links to individual exposures, information needed to reconstruct weights, etc.

Object Catalogs

HLIS 2.1.3: RST shall be capable of producing a catalog containing information for each detected source in the HLIS field, including positions, classifications, photometry (e.g. aperture photometry, model fits, adaptive moment photometry), and limited time domain information for variable sources.

HLIS 2.1.4: RST shall be capable of producing a catalog containing information for each detected source in the HLIS field, image moments (through at least 2nd order) in each filter at each epoch, and object-appropriate derived data. Examples of object-appropriate derived data include photometric redshifts and morphological parameters for galaxies, parallaxes and proper motions for stars.

HLIS 2.1.5: The RST shall be capable of including in the HLIS catalog information on the statistical uncertainties for each quantity in the catalog as well as data quality flags where numeric uncertainties are not applicable.

HLIS 2.1.6: Deleted

HLIS 2.1.7: RST shall be capable of providing HLIS science data products with the angular mask and noise map of the lensing sample.

HLIS 2.1.8: RST shall provide a means for users to determine a redshift probability distribution for an arbitrary sample of objects that reflects a true N(z) with an error on that estimate.

HLIS 2.1.9: RST shall enable users to determine redshift probability distributions p(z) for galaxies in each tomographic bin of the HLIS lensing sample per the table below on the fraction of probability within $|z_{phot}-z_{spec}|/(1+z)$ of the true redshift.

Comment: This way of phrasing the requirement takes an arbitrary p(z) into account and is more closely related to the ultimate N(z) requirement than the typically used σ_z and outlier fraction measurement. It also reflects the fact that the galaxy population is diverse, and so different populations will have different photo-z properties given the photometry.

Fraction of Sample	68% of p(z) within
~50%	0.04
~30%	0.08
~20%	0.15

Fraction of Sample	90% of p(z) within
~70%	0.12
~20%	0.24
~10%	0.45

HLIS 2.1.10: RST shall enable users to determine the N(z) of each tomographic bin of Δz_{phot}=0.05 such that the systematic uncertainty in the mean redshift of the bin, Δz, is given by $\Delta z/(1+z)<0.002$.

Comment: This is the top-level requirement on photo-z calibration. The 0.002 is based on the requirement that the photo-z errors degrade the aggregate precision by a factor of $1.2^{1/2}$ (i.e. 20% in RSS) for the Reference survey, and assuming that the errors in the photo-z calibration are correlated over a range of Δz =0.2 in redshift.

HLIS 2.1.11: RST shall be capable of providing HLIS science data record with S/N ≥ 18 (matched filter detection significance, combining all exposures) per shape/color filter for a galaxy with an exponential disk profile and r_{eff} = 180 mas and mag AB = 24.4/24.3/23.7 (J/H/F184).

Comment: These depths differ from those quoted in the PLRA BSR #2 because these are for S/N=18 and those in the PLRA are for S/N=5.

HLIS 2.1.12: RST shall be capable of providing a sample of spectroscopic redshifts over the entire HLIS footprint, covering $0<z\leq2.5$ and with a known selection function.

Comment: At high z, this will come from the RST HLSS. At low z, the approved 4MOST survey will do this in the Southern Hemisphere and DESI will in the North. The low redshifts might also be possible internally to RST data using rest-frame NIR lines.

Simulation Tools

In addition to data products themselves, certain tools will be needed to understand underlying systematic effects in the data. These include:

HLIS 2.1.13: RST shall provide simulation packages that can "observe" simulated fields (e.g. from a catalog of galaxies, with an x-y-λ data cube of each) and feed the results into the data reduction pipeline, all the way through to simulated catalogs.

HLIS 2.1.14: RST shall provide a simulation package that can inject simulated galaxies (e.g. from x-y-λ data cubes) or stars into the real images and re-run (portions of) the data processing. This is needed to assess completeness/selection effects, the impact of blending on objects of known properties, and the impact of nearby stars on the measurement of galaxy photometric properties. In principle, much of this could be done from observing simulated skies, but these hybrid simulations are useful because they have the correct instrument noise properties and level of crowding by construction.

3.4.6 High-Latitude Imaging Survey – Calibrated Data Records

Rigorous calibration of the telescope, WFI, and data processing algorithms will be crucial for meeting requirements on photometric, astrometric, and shape measurement errors. Requirements on these measurements are a total of contributions from all error sources in the signal chain. In particular, the H4RG detectors have multiple response characteristics (e.g. QE, IPC, persistence, etc.) and noise (dark current, read noise, etc.), and measurement errors due to these must sum to less than the total allotted error budget. Spatial variations in the detector properties must be characterized on the relevant scales: variations across a single star or galaxy can induce measurement errors in that source, whereas variations across the detector can induce correlations that bias the weak lensing signal. Calibrations may be achieved directly from science data or dedicated calibration fields unless doing so is prohibitively difficult or time-consuming (survey time). In that case, meeting calibration requirements may require laboratory experiments (if the effect is stable) or using on-board hardware to produce a stimulus. The approach to calibration is described in detail in the RST Wide-Field Instrument Calibration plan (RST-SCI-PLAN-0006).

The high-level calibration needs for RST are summarized here, organized by the type of calibration.

General

> **HLIS 2.2.1:** RST shall be capable of archiving HLIS calibrated images with the PSF for each exposure specified as a function of position on the focal plane and incorporate any World Coordinate System information needed for subsequent stages of processing.

Comment: The PSF can be provided in the form of model parameters and software that computes the PSF from the model.

> **HLIS 2.2.2:** RST shall be capable of providing HLIS calibrated data records with the relative photometric calibration in each HLIS filter spatially uniform on angular scales $l<3200$ to better than 10 millimag RMS.

This requirement flows from the photo-z requirement: variations in the photometric calibration lead to systematic variations of the $P(z_{phot}|z_{spec})$ function across the survey, which both distorts the lensing and galaxy clustering power spectra, and may make the photo-z calibration fields not representative.

Point Spread Function

The PSF ellipticity must be known well enough to ensure that we meet the additive shear error requirement, and the PSF second moment ($I_{xx} + I_{yy}$) must be known well enough to meet the multiplicative shear error requirement. The data set requirements on PSF knowledge were calculated to use 50% (in a root-sum-square sense) of the shape measurement error budget (which also includes other terms, such as residuals from the data processing algorithms and detector effects Calibration Plan (RST-SCI-PLAN-0006). The PSF knowledge requirements apply to all sources of PSF fluctuations in the same range of multipoles (large scales: $l < 3200$) that will be used for the WL power spectrum. They also include detector effects that, if not suitably corrected or accounted for, bias PSF measurements (e.g. nonlinear pixel response, cross-talk, correlated read noise, etc.).

A convenient representation of the systematic uncertainty in a galaxy ellipticity measurement is given by Eq. 15 of Paulin-Henriksson et al (2008):

$$\sigma_{sys}^2 = P^{\gamma-2}\left\langle\left(\frac{R_{PSF}}{R_{gal}}\right)^4\right\rangle \times \left[2\sigma_{\epsilon_{PSF}}^2 + \left(\left\langle|\epsilon_{gal}|^2\right\rangle + \left\langle|\epsilon_{PSF}|^2\right\rangle\right)\left(\frac{\sigma[R_{PSF}^2]}{R_{PSF}^2}\right)^2\right]$$

where $P^{\gamma}\approx 1.84$ is related to the mean galaxy ellipticity ε_{gal}, R_{PSF} and R_{gal} are the half-light radii of the PSF and galaxies, and ε_{gal} and ε_{PSF} are the elipticities of the galaxies and PSF. Several key considerations are apparent from this equation: R_{PSF} should be kept as close to the diffraction limit as possible, as the smaller R_{PSF} is, the smaller R_{gal} can be, which increases the density of usable galaxies; and both ε_{PSF} and $\sigma_{\varepsilon PSF}$ should be as small as possible.

> **HLIS 2.2.3:** RST shall be capable of providing HLIS science data records with the PSF ellipticity, defined by the moment ratios e1=(Ixx-Iyy)/(Ixx+Iyy) and e2=2Ixy/(Ixx+Iyy), determined to an error of $\leq 5.7\times10^{-4}$ RMS per component on angular multipole scales $32 < l < 3200$.

Comment: The top-level requirement is dependent on the angular distribution (as per HLIS 2.0.3). The angular distribution from HLIS 2.0.3 corresponds to placing 1.7×10^{-4} of the shear systematic at $32 < l < 100$; 2.3×10^{-4} at $100 < l < 320$; 3.1×10^{-4} at $320 < l < 1000$; and 3.8×10^{-4} at $1000 < l < 3200$. If these budgets are exceeded in one bin, the top-level systematic error budget will have to be re-allocated.

> **HLIS 2.2.4:** RST shall be capable of providing HLIS science data records with the PSF size, defined by the second moment Ixx+Iyy, determined to a relative error of $\leq 7.2\times10^{-4}$ RMS on angular multipole scales $l < 3200$.

The "PSF" as defined in HLIS 2.2.3 and HLIS 2.2.4 includes the pixel response as well as the optical PSF and image motion.

Astrometric Calibration

> **HLIS 2.2.5:** RST shall be capable of providing HLIS calibrated data records with the astrometric solution in the WFI images having a relative error (offset between two images of the same galaxy or star, possibly taken at different times during the survey) of < 1.3mas.

> **HLIS 2.2.6:** RST shall be capable of providing HLIS calibrated data records with the astrometric solution in the WFI images having an absolute error, relative to the astrometric frame defined by the ICRF of:
>
> <26 mas RMS per component for $\log_{10} l = 1.5$—2.0
>
> <11 mas RMS per component for $\log_{10} l = 2.0$—2.5
>
> <5.1 mas RMS per component for $\log_{10} l = 2.5$—3.0
>
> <2.2 mas RMS per component for $\log_{10} l = 3.0$—3.5.

Comment: Requirement HLIS 2.2.5 flows from the avoidance of systematic error due to stacking (or joint fitting) of two images that are offset, which can make an intrinsically circular object appear elliptical. The 1.3 mas figure in HLIS 2.2.5 is estimated from the requirement of knowledge of jitter, with the expectation that smearing of images from combination of images with a systematic astrometric offset will have a similar effect.

Comment: Requirement HLIS 2.2.6 is present because distortions in the astrometric solution will imprint a spurious shear on all objects in the sky, in proportion to the gradient of the astrometric error. The l=1 moment of astrometric errors (which correspond to errors in the cosmic aberration and global rotation of the coordinate system) are excluded as they do not produce shear. The l<32 range (largest angular scales) produce spurious shear, but outside the band where HLIS 2.0.3 sets requirements. The limits have been chosen to limit astrometric gradients to <1% of the additive shear error budget in an RSS sense. (This number could be traded if necessary.)

Requirement HLIS 2.2.6 corresponds to allocating 1% of the HLIS 2.0.3 budget in an RSS sense to the astrometric distortion. This number can be traded against other terms in the error budget.

Individual Pixel Behaviors and High Spatial Frequency Peculiarities

NIR detector arrays exhibit peculiarities in individual pixels, in the sense that basic parameters (gain, IPC, pixel QE and area, centroid, 2nd and higher moments of the pixel response function) could vary on all spatial scales on a detector array, all the way down to individual pixels. Many physical causes could be associated with these variations, including – but not limited to – differences among the readout channels (128 columns wide); lattice planes (the "cross-hatch" pattern seen on some HxRG detector arrays); or defects in specific pixels (e.g. contamination by dust particles on the pixel surface).

For RST, we distinguish between the low spatial frequencies that are in band for the weak lensing shape measurement (i.e. correspond to scales used for cosmological measurement), and the high spatial frequencies. The transition is at $l = 3200$, which is the maximum spatial frequency used in the cosmological forecasts; this corresponds to a Fourier mode with wavelength 3700 pixels on the focal plane: 360 deg ÷ (3200 × 3.06×10^{-5} deg/pix) = 3700 pix. Errors on larger scales (smaller spatial frequencies) are covered by HLIS 2.2.3, 2.2.4, 2.2.5, and 2.2.6. Errors in knowledge of the pixel behaviors at smaller scales are covered here, by HLIS 2.2.7. These errors are out of band for weak lensing. However, they affect the measurements of individual objects; the stars used for PSF determination are of greater concern than the lensing source galaxies because the signal is concentrated into fewer pixels. Therefore, we set a requirement that the high spatial frequency errors be small compared to the statistical uncertainties on an individual PSF star.

> **HLIS 2.2.7:** RST shall be capable of providing a map of the pixel-to-pixel variations in the pixel response functions. For a postage stamp image of a star containing a total count of 87,000 electrons in an HLIS exposure, the individual pixel response function map shall introduce an error of no more than 0.5σ in the 0th, 1st, or 2nd moments. Here "σ" represents the RMS statistical error, including Poisson and read noise.

Comment: The mean total counts from the S/N>100 stars in an H band HLS exposure is 87,000 electrons. The 0.5σ specification quantifies our criterion that the errors induced by knowledge of

the pixel peculiarities are small compared to the statistical errors; it corresponds to a 25% increase in errors in an RSS budgeting sense. See Calibration Plan (RST-SCI-PLAN-0006) for details.

Comment: The "0th moment" of a pixel response function is just the flat field, and is the integral over the pixel, ∫ QE dA. One must go to the 2nd moment to start distinguishing pixel-to-pixel variations in QE from area.

Comment: As described in the Calibration Plan, the most likely approach to HLIS 2.2.7 on orbit is via many highly dithered observations of a dense stellar field (such as the microlensing field).

Photometric Calibration

> **HLIS 2.2.8:** RST shall be capable of providing HLIS calibrated data records with the variation of the total system response known as a function of position within the field of view, such that the total flux of a source with a known Spectral Energy Distribution (SED) can be corrected to a common filter system at the ~0.5% level when imaged at any point on the focal plane.

Comment: This is basically a requirement that the relative photometric calibration across the field of view be known to 0.5%. It is specifically worded in terms of a source with known SED because the filter bandpass will vary over the field, and so it is only by specifying an SED that one can meaningfully describe how the total system response varies as a function of position.

> **HLIS 2.2.9:** RST shall be capable of providing calibrated data records with absolute photometry of point sources calibrated in one or more of the standard filters to <2%, with a goal of 1%.

> **HLIS 2.2.10:** RST shall be capable of providing calibrated data records with photometric zeropoints varying by less than 0.5% over the duration of the high latitude imaging survey program.

> **HLIS 2.2.11:** RST shall be capable of providing calibrated data records with relative photometric zero-points of the filters known to <0.5%, relative to a standard star.

Comment: The calibrated fluxes of the galaxies will be used for determining photometric redshifts. This requires accurate relative fluxes in different bands (HLIS 2.2.11), and consistent fluxes over the duration of the survey (HLIS 2.2.9).

Comment: Comment: The absolute flux calibration (HLIS 2.2.9) is needed primarily for purposes of combining RST data with data from other observatories and doing a joint photometric redshift fit; thus HLIS 2.2.9 could be replaced with a requirement for transfer standards that would allow both datasets to be placed on a common flux scale.

3.4.7 High-Latitude Imaging Survey – Raw Data Records

The observing plan for the high latitude imaging survey is to acquire imaging data in four bands: Y, J, H, F184. The depth in each band will be sufficient for photometric redshift determination, and the depth and sampling will be sufficient for shear measurements in the three reddest filters:

J, H, F184. These bands will provide data that seamlessly overlap with ground-based photometry from LSST to obtain photo-z's for all of the WL source galaxies.

Raw Image Properties

HLIS 2.3.1: RST shall be capable of providing HLIS raw images in the archive for each detector exposure with each raw data record including a unique dataset identifier for each exposure, the exposure time, the time of exposure, all individual downlinked detector readouts used to make the exposure, the observatory pointing orientation and any additional engineering data the Science Center uses for subsequent processing.

HLIS 2.3.2: RST shall have the capability of providing HLIS raw images of galaxies in 4 filters (Y, J, H, and F184).

Image Quality and Sampling

HLIS 2.3.3: RST shall be capable of providing HLIS raw images with a system PSF EE50 radius ≤ 0.12 (Y band), 0.12 (J), 0.14 (H), or 0.14 (F184) arcsec, excluding diffraction spikes and non-first order light and including the effects of pointing jitter, for at least 95% of the exposures and over 95% of the FOV.

HLIS 2.3.4: RST shall be capable of providing HLIS raw images in at least 2 passes at different roll angles, and dithered so that >90% of the survey area receives 5 exposures (J and H bands) or 4 exposures (Y and F184 bands) of the survey area, in the survey mode defined by HLIS 2.0.2.

Comment: The observing strategy must provide coverage of the sky that is uniform at the depths needed, must provide for adequate sampling of the PSF, and must be consistent with obtaining accurate photometry for all objects. The approach to accomplishing this is as follows. The survey region will be covered completely in two passes for each filter. In each pass, there will be 3—4 exposures of a given field (depending on filter: the bluest filters require better sampling), with a small diagonal step between exposures of a size slightly larger than a chip gap. The second pass will be similar, except that the roll angle will be shifted. This tiling pattern provides 4-8 exposures for any given spot on the sky, with >90% of the sky having 5 or more exposures.

Comment: We do not require shape measurements in the Y band, so the sampling requirements are less stringent even though Y is bluer than J. There is still a requirement for calibration by repeated visits, and to be able to identify true sources in the presence of cosmic rays and other image defects.

Comment: The change in roll angle between the two passes ensures that the repeat visits to different spots on the sky are observed by a random distribution of pairs of positions on the focal plane, facilitating accurate photometric calibration.

Comment: The number of dither positions required is assessed with image simulations. This was studied in pre-phase A using IMCOM (Rowe et al. 2011), and in Phase B this will be studied further using GalSim.

Deep Fields

HLIS 2.3.5: RST shall be capable of acquiring at least 15,000 spectroscopic redshifts in the HLIS deep field (see HLIS 2.0.5), representing the full extent of color space for detected galaxies. (Spectra could be from RST observations or from ground-based observatories).

HLIS 2.3.6: RST shall be capable of periodic acquisition of HLIS deep field imaging observations throughout the HLIS observing program.

Comment: One of the purposes of the deep fields is to track changes in photometric calibration. The purpose of this requirement is so that the deep fields required by HLIS 2.0.5 are not taken all at one epoch.

Handling of Multiple Reads Per Exposure

The RST NIR detectors will be continuously read out, resulting in many samples of each pixel per exposure. However the downlink budget may not support downlinking every sample.

HLIS 2.3.7: RST raw data records shall consist of at least 6 ground-configurable combinations of samples per microlensing exposure.

Comment: The non-destructive readout capability of the RST NIR detectors enables recovery of information from pixels that saturate during an exposure, or that are affected by charge deposition from cosmic-rays. Availability of such data also enables diagnostic measurements of various non-linear response effects (such as the "brighter-fatter" effect), image motion during an exposure, etc. Onboard combinations of individual detector readouts include simple sums, differences, and/or averages of frames.

HLIS 2.3.8: Deleted

HLIS 2.3.9: Deleted

HLIS 2.3.10: Deleted

HLIS 2.3.11: Deleted

HLIS 2.3.12: Deleted

HLIS 2.3.13: Deleted

3.5 Supernova

3.5.1 Supernova Survey Science Requirements

The supernova technique relies on Type Ia supernovae as distance indicators to measure the expansion history of the universe and thus yield information about the accelerating expansion and the nature of dark energy.

Luminosity distance depends directly on cosmological parameters such as the (potentially evolving) equation-of-state of dark energy. Measuring the luminosity distance at various redshifts can thus constrain these parameters. In practice, we measure relative distances between nearby ($z \sim 0$) and high-redshift supernovae. Doing so removes the need for absolute distances,

which rely on knowing the Hubble constant. To measure the luminosity distance to a SN Ia (modulo knowledge of the current expansion rate), one observes the rest-frame luminosity L_{SN}, and determine the luminosity distance D_L directly from the relation $F = L_{SN}/4\pi D_L^2$. By measuring supernovae at a variety of redshifts, the evolution of $D_L(z)$ can be determined. The difficulty in practice is in knowing the proper L_{SN} for a given supernova, the corrections to apply for extinction in the host galaxy and the Milky Way and for intervening gravitational lensing, determining the supernova's redshift, and in understanding instrumental systematic effects.

Type Ia's have an intrinsic luminosity spread of an order of magnitude at blue rest-frame wavelengths, but the peak luminosity is empirically found to be well correlated with the light curve shape (LCS) and the color of the supernova. Once these correlations are accounted for, the intrinsic dispersion in LCS-corrected peak luminosity is 9-18%, corresponding to distance errors per supernova of 4.5-9%. The low end of this error range is achieved by observations that measure rest-frame IR wavelengths, and by spectrophotometric observations that make it possible to match narrowly defined SN subpopulations. Rest-frame IR observations offer two further advantages: (1) the effects of dust extinction are drastically lower than at optical wavelengths; and (2) the intrinsic dispersion of (uncorrected) peak luminosities is much smaller in the NIR, reducing sensitivity of the derived distance to uncertainties in the LCS measurement.

Residuals from the width-luminosity relation are correlated with the properties of the SN host galaxy (*e.g.*, Sullivan et al. 2010, Kelly et al. 2010, Lampeitl et al. 2010); empirical corrections for this correlation have been applied in recent analyses (*e.g.*, Betoule et al. 2014). Ongoing surveys of local and distant SNe have much more extensive photometric and spectroscopic coverage than the early surveys that discovered dark energy, so they are teaching us a great deal about the SN population as well as improving cosmological constraints. In particular, it appears that, with RST's photometry of the SNe and their host galaxies, these host-galaxy correlations can be utilized to further tighten the distance measurement uncertainties, and make them robust against population drifts within the range of SNe Ia behaviors (and their host galaxy dependencies) seen currently in the ground-based surveys.

Our ultimate goal is to constrain the nature of dark energy. While there are several possible ways of quantifying our knowledge about dark energy, the Dark Energy Task Force (DETF - Albrecht et al. 2006, arXiv:astro-ph/0609591; Albrecht et al. 2009, arXiv:0901.0721) suggested that the community use the dark energy figure of merit (FoM), equivalent to the reciprocal of the area of the error contour containing the 95% confidence in the w0-wa plane. Wang (2008 arXiv:0803.4295) proposed the a variant that is mathematically represented as

$$\mathrm{FoM} = \det\,[C(w0, wa)]^{-1/2}$$

where C is the covariance matrix for w0 and wa. This definition is equivalent in the limit of Gaussian uncertainties, is more readily computed, and has since been widely adopted. Larger FoMs indicate greater accuracy. For the planning purposes, the FoM is a reasonable choice.

The standard for performance of a large space mission such as RST (a so-called Stage IV experiment) proposed by Albrecht et al (2006) and widely adopted by the community was to improve on the FoM of the experiments then in progress ("Stage II") by a factor of 10. The current best values from Stage II experiments are 31.3 (Betoule et al 2014) and 32.6 (Alam et al., 2016), leading to a target value (in round numbers) for the FoM of the RST SNIa program of

325. This FoM is computed using existing data on the CMB (from the Planck collaboration 2016) and on BAO (Anderson et al 2014) but no other RST datasets.

In the absence of systematic uncertainties, one can examine the statistical uncertainties for SN distances to quickly determine the FoM. Here, we define the statistical distance uncertainty to a particular redshift (using SNe in a redshift bin of Δz) to be

$$\sigma_{stat} = [(\sigma_{meas})^2 + (\sigma_{int})^2 + (\sigma_{lens})^2]^{1/2} / \sqrt{N_{SN}} ,$$

where σ_{meas} is the measurement uncertainty for a particular SN (which in practice should depend on redshift), σ_{int} is the intrinsic scatter for SNe Ia (which could depend on redshift), σ_{lens} is the uncertainty caused by gravitational lensing magnification, which depends on redshift and we model as $\sigma_{lens} = 0.07 \times z$ mags, and N_{SN} is the number of SNe Ia in a particular redshift bin of width Δz

For current SN samples, σ_{int} varies from ~0.08 – 0.16 mag. The intrinsic scatter is effectively how well we can measure the distance to a particular SN in the absence of all other uncertainties. Unaccounted SN physics, line-of-sight effects, and uncertain dust corrections are all expected to contribute to σ_{int}. The exact value of σ_{int} is wavelength dependent with SNe Ia being more standard in the restframe NIR (at redshifts $z < 0.3$, where obtainable with RST) than in the optical and NUV (e.g., Foley et al., 2008, 2016; Ellis et al., 2008, Mandel et al. 2011), and more standard with spectrophotometric matching in the restframe optical (Fakhouri et al 2015).

The measurement uncertainty, σ_{meas}, will depend primarily on the S/N of the total set of observations, but other aspects like the wavelength coverage and cadence will also contribute. The lensing uncertainty depends on foreground structures, which could, in principle, be measured and (at least partially) corrected. However, left uncorrected, σ_{lens} is simply an additional increase in the observed scatter that will inflate the overall statistical uncertainty.

As noted above, our goal is to achieve a FoM of 325. If we assume that systematic uncertainties will account for half of the error budget (see below), then we require any strategy to have a statistical-only FoM > 650. For a flat redshift distribution to $z = 2$, this requires

$$\sigma_{stat} / \sqrt{N_{SN}} \leq 0.01 \text{ mag.}$$

on average for 0.1bins in z, smaller at low z and larger at higher z, approaching 0.015 at $z = 2$, as shown in Figure 12, where the distance errors are one half the magnitude errors.

Making the optimistic assumption that we will have data adequate to match the best standardization previously achieved of $\sigma_{int} = 0.08$ mag across all redshifts, we can thus determine the required measurement error:

$$\sigma_{meas} = [(\sigma_{stat})^2 N_{SN} - (\sigma_{int})^2 - (\sigma_{lens})^2]^{1/2}$$

$$\leq [X^2 - 0.08^2 - (0.07 \times z)^2]^{1/2}$$

At the maximum redshift of $z = 2$, this corresponds to $\sigma_{meas} = 0.08$ mag.

The final FoM measurement will also include systematic uncertainties. Although one would like to decrease statistical and systematic uncertainties independently, there is often a trade between

the two. Therefore, we will examine the case where $FoM_{stat} = 650$ and including systematic uncertainties decrease the FoM by at most a factor of 2.

The key sources of potential systematics for the RST supernova survey are:

- Photometric calibration across the redshift range of the RST SNe and between the RST sample and calibration samples in the local universe. This includes absolute calibration of the photometric system, non-linearity in the detector response, and the zero-point in each filter.
- Contamination of non-standardizable SNe, which currently include SNe Ia similar to the fast-declining SN 1991bg, SNe Iax, and all core-collapse SNe.
- The SN spectral model and its possible evolution with redshift.
- Environmental effects that effect distance measurements and are currently corrected by measuring host-galaxy properties. These corrections may evolve with redshift as host and SN properties change, on average, with cosmic time.
- Mis-calibrated dust reddening corrections, including uncertainties in MW reddening and possible evolution of galactic dust properties with redshift. Extinction effects must be disentangled from intrinsic correlations between SN luminosity and color.
- Mis-estimation of the effects of intervening gravitational lenses, generally in the form of intervening massive galaxies and galaxy clusters.
- Possible evolution of the SN population or contamination of the Type Ia sample by other populations that are systematically less or more luminous. SN properties are known to be correlated with the properties of their host galaxies.
- Biases in the estimated redshifts of supernovae in the cosmological analysis sample or in the luminosities of supernovae selected for redshift measurement and cosmological analysis.
- Selection biases imprinted on the sample when making choices for spectroscopic follow-up observations of the SNe and of their host-galaxies (to determine, e.g., redshift).

These effects can generally be grouped into three categories:

1. Systematic effects are directly related to precise and accurate measurement of astrophysical flux. For these effects, proper characterization of RST hardware, adequate in-flight calibration procedures and necessary future measurements of exterior calibrators, and precise models for those exterior calibrators are all necessary.
2. Systematic effects that require adequate information about individual SNe. This includes mitigating possible contamination, spectral-model, and particular evolutionary biases.
3. Systematic effects that require sufficient information about the SN population. This includes mitigating possible spectral-model, environmental, dust-reddening, population evolution, and selection biases.

An important aspect of the RST SN program is the ability to constrain many of these systematics by obtaining near-infrared spectrophotometry to provide spectral diagnostics that can distinguish intrinsic color variations from the effects of dust extinction (Chotard et. al. 2011) and match high and low-z SNe with similar properties to suppress evolutionary effects in the mix of supernovae.

To guide the establishment of an error budget and forecast the performance of the supernova survey, we use the error model described above and extend it to consider systematic uncertainties. We assume the intrinsic dispersion in Type Ia luminosities can be reduced to σ_{int} = 0.09 mag (slightly less optimistic than the sample calculation above), after correction for light curve shape and spectral properties. The other contribution to statistical errors is gravitational lensing magnification, which we model as $\sigma_{lens} = 0.07 \times z$ mags. The overall statistical error in a $\Delta z = 0.1$ redshift bin is then

$$\sigma_{stat} = [(\sigma_{meas})^2 + (\sigma_{int})^2 + (\sigma_{lens})^2]^{1/2} / \sqrt{N_{SN}} ,$$

where N_{SN} is the number of SNe in the bin.

To describe the systematic error, a full hierarchical Bayesian error model has been developed (Rubin et al, in prep) that preserves all of the correlations between sources of systematic uncertainties and across redshift bins, and takes advantage of the IFC spectrophotometry to minimize systematics associated with photometric calibration and K-corrections (as determined in Saunders et al, 2015) and to reduce evolutionary systematics (Fakhouri et al, 2015). For the range of SN reference surveys considered here, the final Figure-of-Merit results match well to those obtained with a highly simplified model in which the systematic error per bin is taken to be

$$\sigma_{sys} = 0.01\ (1+z) / 1.8 \text{ mag},$$

with no correlation of errors between redshift bins; for the purposes of this discussion we use this highly simplified model, though the full analysis uses the full hierarchical Bayesian model.

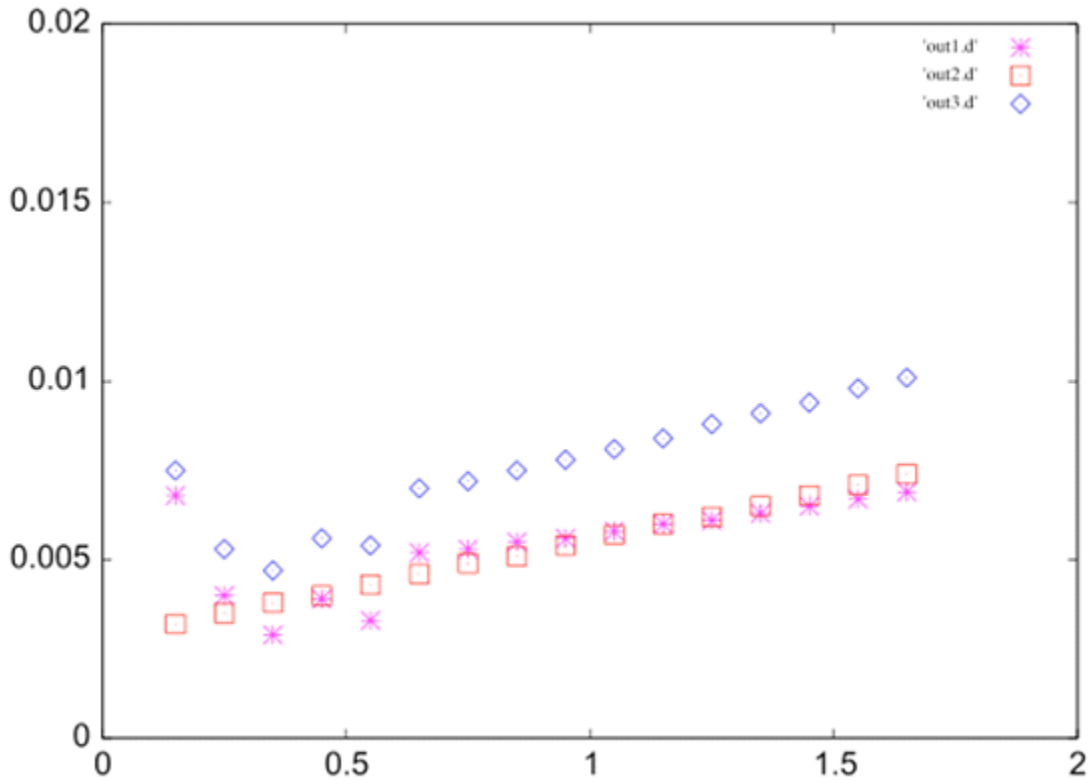

Figure 12 The statistical (squares), systematic (asterisks), and total (diamonds) relative uncertainties on the distance σDL/DL are plotted for each Δz = 0.1 bin.

The total error for a bin is just the quadrature sum of the statistical and systematic errors. The diamonds in the above Figure show the total distance error (which is half the flux error) based on the present RST observatory design and the simplified error model above. By design, the statistical and systematic errors are comparable, except in the lowest redshift bin where the volume is small. With the simplified error model, one gains by improving statistics in low redshift bins (where the exposure times are shorter) until one hits the systematics limit, and then one gains by going to higher redshifts, which continue to provide new information. In the simplified model, the total error is about 0.5% per bin near z = 0.5, then climbs to 1% at the highest redshifts because of the combination of increased contribution of lensing to the statistical error and the assumed redshift behavior of the systematic error.

The flux measurement can be related to the luminosity distance $D_L(z)$ by (all quantities expressed as monochromatic magnitudes):

$$m(\lambda_{obs}) = M(\lambda_{em}) + A_{MW}(\lambda_{obs}) + A_{host}(\lambda_{em}) + \mu + 2.5 \log(1+z),$$

where:

$$\lambda_{obs} = (1 + z)\, \lambda_{em}$$

$A_{MW}(\lambda_{obs})$ is the foreground Milky Way extinction at wavelength λ_{obs}

$A_{host}(\lambda_{em})$ is the host galaxy extinction at wavelength λ_{em}

$M(\lambda_{em})$ is the absolute magnitude corresponding to intrinsic flux of the supernova at wavelength λ_{em}

$\mu(z) = 5.\ \mathrm{Log}\ (D_L(z) / 10\mathrm{pc})$

$M(\lambda)$ and $m(\lambda)$ are traditional energy-based monochromatic magnitudes derived from f_λ; if derived from f_ν, (*e.g.* AB magnitudes), the sign of the term $2.5\log(1+z)$ is reversed. The template rest-frame spectrum $M(\lambda)$ (or $M(\nu)$) must be normalized to an absolute B-magnitude M_B, typically -19.

Recall that the desired precision on D_L is "sub-percent"; thus in what follows, the top-level requirement will be given as $\sigma_{DL}/D_L < 0.01$. To convert to an uncertainty on μ:

$$D_L = 10\mathrm{pc} \times 10^{0.2\mu},$$

So the corresponding uncertainty propagation is

$$\sigma_{DL} = d(D_L) / d\mu \times \sigma_\mu = 0.2\ \ln(10) \times 10\mathrm{pc} \times 10^{0.2\mu} \times \sigma_\mu,$$

$$\text{or}\ \ \sigma_{DL}/D_L = 0.2\ \ln(10)\ \sigma_\mu = 0.4605\ \sigma_\mu.$$

Thus a 1% requirement on σ_{DL}/D_L corresponds to ~2% for σ_μ.

Performance requirements can be derived by considering the various terms in the equation relating the distance modulus $\mu(z)$ to the observed fluxes of a given supernova. Rearranging the equation to compute μ gives:

$$\mu = m(\lambda_{obs}) - M(\lambda_{em}) - A_{MW}(\lambda_{obs}) - A_{host}(\lambda_{em}) - 2.5\ \log(1+z).$$

The term $M(\lambda_{em})$ is the absolute magnitude (defined as the magnitude that would be observed at a distance of 10pc) of the supernova at the specified wavelength. As noted above, the intrinsic variation of this quantity is roughly an order of magnitude, but correlation of M with light curve shape and with certain spectral features allows one to reduce the intrinsic scatter to as low as 9%. There are many ways to use SN data to derive a precise peak absolute magnitude, but a simple and popular prescription is

$$M = M_0 - \alpha(x_1 - 1) + \beta c.$$

where M_0 is a fiducial peak absolute magnitude, x_1 is a light-curve shape parameter, c is a color parameter, and α and β are hyperparameters describing the relation between peak luminosity and light-curve shape/color. This particular parameterization does not differentiate between the extrinsic color-luminosity relation of dust reddening/extinction and internal relations related to SN physics (although the full hierarchical Bayesian model does differentiate between these relations). As a single parameter (and a single hyperparameter) are used to describe two independent relations, there is the possibility of biases between SNe dominated by one effect and those dominated by the other. Other parameterizations attempt to directly address this by explicitly having a (strictly non-negative) reddening term and a color-luminosity relation dictated by known reddening laws.

Regardless of the interpretation of the color correction, the determination of both of these correction terms requires both a fit to the light curve shape to determine the stretch parameter, and a measurement of the SN color. These in turn set the requirements on the observing cadence and photometric accuracy of the flux measurements. Achieving a low value of 9% for σ_{int} requires proper sampling and photometric accuracy in measurements of the light curve before and after peak brightness.

Because the variation of intrinsic luminosity of the supernovae introduces a statistical uncertainty, this uncertainty may be reduced by increasing the size of the supernova sample. The net contribution to the error budget is $\sigma_M = \sigma_{int} / \sqrt{N_{SN}}$. For example: if $\sigma_{int} = 9\%$ and $N_{SN} > 100$, then the net contribution to the uncertainty budget is under 1%.

3.5.2 Reference Survey and Figures of Merit

We consider here a three-tier reference survey for the supernova measurements, using 6 months of observing time distributed over 2 years at 5-day intervals. The nominal survey area is 4.96 square degrees. This entire region is imaged in 4 filters with an exposure time of 600 seconds for each pointing, taking a little less than half of the 30 hours available for each visit. The prism exposures are distributed into 3 tiers: a 4.96 sq degree wide field, a 1.12 sq deg medium tier, and an 0.84 sq deg deep tier. The prism exposure times in the three tiers are 600sec, 3600 sec, and 9000 sec, respectively. While not yet optimized, this survey strategy provides >100 SNIa per $\Delta z = 0.1$ redshift bin for $0.7<z<1.8$.

The supernova surveys described by e.g. Hounsell et al 2018 achieve DETF FOM values ranging from 200 up to ~400 including systematic uncertainties, depending on optimization of the survey strategy, assumptions on success of systematic uncertainty control, and depending on whether ground-based data are used at low-redshift. This indicates that the requirement of 325 is plausible. The statistical FoM achievable in these surveys ranged from 500 to 700, depending on the observing strategy.

3.5.3 Baseline Dark Energy Science Requirements for the SN Survey

We define baseline Level 2 requirements for the Supernova Survey such that, if these requirements are satisfied, we expect the baseline requirement, $FoM_{SN} \geq 0.5 \times FoM_{SN,ref}$, to be satisfied (taking $FoM_{SN,\,ref}$ to be ~650, as above). We allocate the margin relative to the reference survey in broad categories as follows:

- A factor 0.8 in FoM if total exposure time drops by 20%
- A factor 0.9 in FoM if flux calibration due to count-rate nonlinearity uncertainty increases from 0.3% to 0.4% systematics
- A factor 0.8 in FoM if flux calibration due to fundamental color calibration uncertainty increases from 0.5% to 1%
- A factor 0.9 in FoM if the intrinsic gray-dispersion increases from 0.08 to 0.1 mag (for a combined drop in FoM of $0.8 \times 0.9 \times 0.8 \times 0.9 = 0.52$).

SN 2.0.1: RST shall be capable of executing a supernova Type Ia survey that can, if allocated 0.5 years of total observing time, achieve constraints that yield

$$FoM_{SN} \geq FoM_{SN,Ref} / 2 = 325,$$

The margin in survey area allows for observational inefficiencies (e.g., slew and settle times) and for time devoted to calibration observations specific to the SN Survey.

In general, there is room to trade margin among these categories while satisfying the baseline requirement.

3.5.4 Supernova Survey Capability Requirements

Achieving the desired constraints on the expansion history of the universe leads to the requirement:

> **SN 2.0.2:** RST shall enable a supernova survey that can measure the distance modulus $\mu(z)$ over the redshift range $0.2 \leq z \leq 1.7$, with observational noise contributions to the uncertainty $\sigma\mu \leq 0.02$ per $\Delta z=0.1$ bin.

Type Ia supernovae are the most useful standard candles. Limiting the statistical noise contribution to the uncertainty in the distance modulus leads to the requirement:

> **SN 2.0.3:** RST shall enable a SN survey to observe more than 100 SNe-Ia per $\Delta z=0.1$ bin.

Uncertainties in the redshifts of individual supernovae, especially biases in the redshifts, can significantly degrade the precision of the dataset. Allocating half of the total uncertainty (0.5%) in the luminosity distance $D_L(z)$ to the uncertainty in redshift leads to the requirement:

> **SN 2.0.4:** RST shall enable a SN survey with the systematic bias in redshift, $\sigma_z /(1 + z)$, less than the values in the following table:

Z	0.3	0.6	0.9	1.2	1.5
σ_z / (1+z)	0.001	0.0016	0.0019	0.0022	0.0024

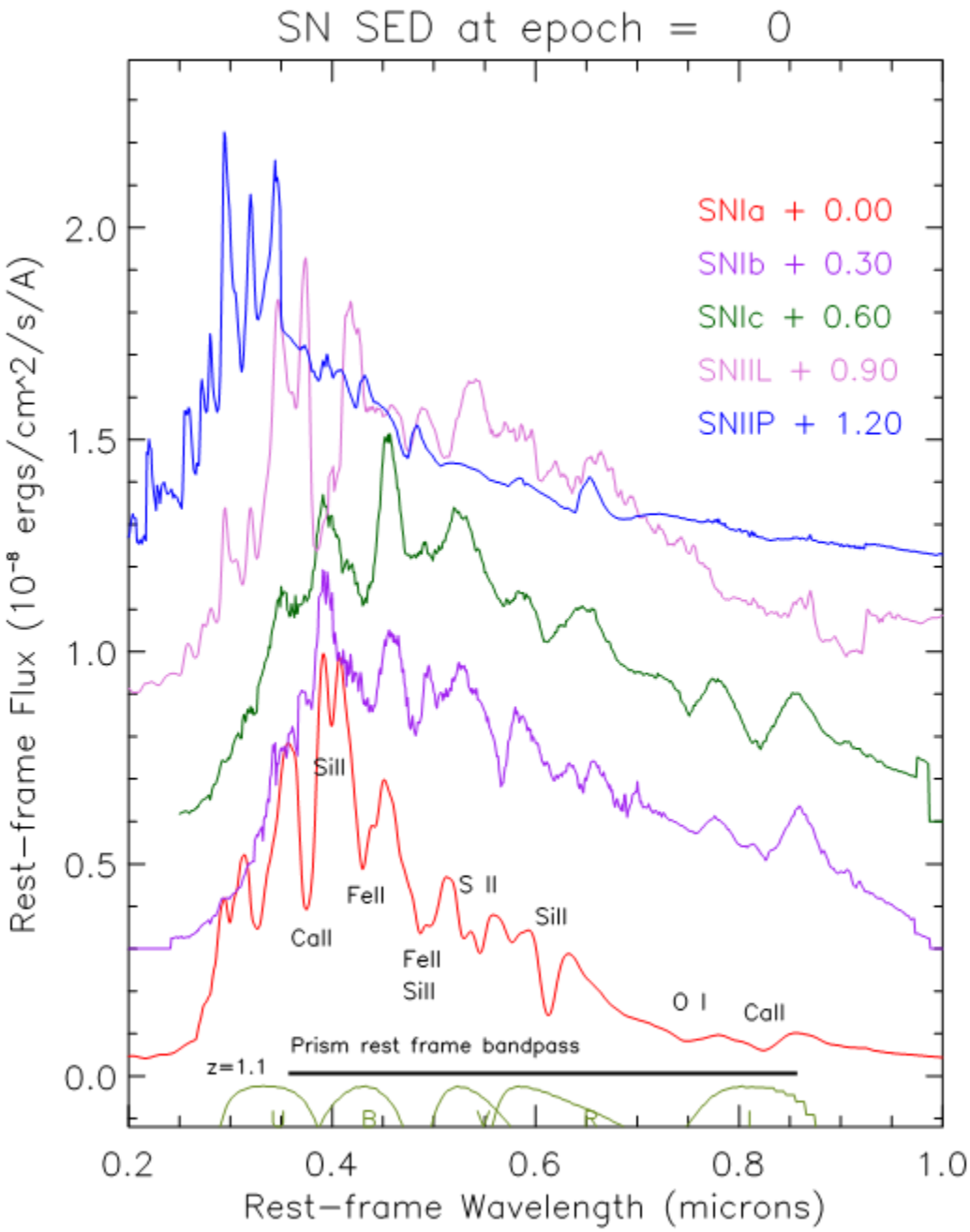

Figure 13 Spectral Energy Distributions of Various SN Types are Shown, at Peak Flux

This plot of supernova spectral energy distributions illustrates how spectral features can be used to identify the SN types, and that the features are strong enough to use for redshift measurement. The green curves at the bottom show the traditional filter bandpasses used to characterize SNe, and the black horizontal bar shows the rest-frame prism bandpass at z=1.1.

3.5.5 Supernova Survey: Science Data Records

SN 2.1.1: RST shall be capable of producing mosaic images of the SN fields in each filter at each epoch of observation, using coordinates tied to the astrometric frame defined by the International Celestial Reference Frame (ICRF).

SN 2.1.2: RST shall be capable of including information in the SN mosaics on the flux uncertainty for each pixel, data quality flags, and additional data generated in producing the mosaics that characterize or support the mosaic generation process.

SN 2.1.3: RST shall be capable of producing, quarterly throughout the survey and at the end of the survey, a mosaic image of the SN fields that combines data from individual epochs to form a deep “static sky” image. Producing this "static sky" image on approximately quarterly time frame supports GI deep field science.

SN 2.1.4: RST shall be capable of producing a catalog containing information for each detected source in the SN fields, including positions, classifications, photometry (e.g. aperture photometry, model fits, adaptive moment photometry), and limited time domain information for variable sources.

SN 2.1.5: RST shall be capable of producing a catalog of each source in the SN fields containing object-appropriate derived data. Examples of object-appropriate derived data include photometric and spectroscopic redshifts and morphological parameters for galaxies, parallaxes and proper motions for stars, and light curves for variable sources.

SN 2.1.6: RST shall be capable of including in the SN catalog information on the statistical uncertainties for each quantity in the catalog as well as data quality flags where numeric uncertainties are not applicable.

3.5.6 Supernova Survey: Calibrated Data Records

SN 2.2.1: RST shall be capable of archiving SN calibrated images with the PSF for each exposure specified as a function of position on the focal plane, the effective bandpass as a function of position and incorporate any World Coordinate System information needed for subsequent stages of processing.

Comment: The PSF can be provided in the form of model parameters and software that computes the PSF from the model.

Because the luminosity distance of a given supernova is derived from wavelengths that include, e.g., the rest-frame B magnitude at the peak of the light curve, and because the rest-frame B-band (for example) will appear at different wavelengths in the instrument depending on the redshift of the supernova, inaccuracies in the relative photometric calibration as a function of wavelength will lead directly to systematic errors in the derived cosmological results. Over its instrumental wavelength range RST itself must be able to calibrate fluxes against known standard stars, which other projects have calibrated (or will calibrate) across wavelengths to fundamental physics standards and/or test stellar models. Variations in the calibration over time would lead to systematic errors in the lightcurve shapes and in host galaxy subtraction. The absolute calibration of the photometry is not critical, except if needed for combining RST data with data from other observatories, such as for determining photometric redshifts of host galaxies. SN 2.2.5 below is

included for this reason. (Again, this requirement is that RST calibrate to known standard stars, and not add significant additional uncertainty.)

SN 2.2.2: RST shall be capable of providing knowledge of the relative instrumental bias on the photometric calibration (defined as (Ftrue(λ) – Fmeas(λ)) / Ftrue(λ), where F(λ) is the flux calibration) that must be <0.005 between any two filter bands in the instrument.

SN 2.2.3: RST shall be capable of providing photometric calibration accuracy such that the reported flux from a source of AB 26th mag is 25,119±75 times fainter than an AB 15th mag source, after calibration.

Comment: Ongoing work on secondary flux standards may enable an increase in the bright end magnitude to 18 (AB).

SN 2.2.4: RST shall be capable of providing calibrated spectra with a wavelength accuracy of $\sigma_\lambda/\lambda < 0.001$ for spectra used to determine redshifts.

SN 2.2.5: RST shall be capable of providing calibrated data records with absolute photometry of point sources calibrated (against standard stars) in one or more of the standard filters to <2%, with a goal of 1%.

SN 2.2.6: RST shall be capable of providing calibrated data records with photometric zeropoints varying by less than 0.5% over the duration of the supernova program.

SN 2.2.7: RST shall archive SN program calibrated spectra for each prism exposure.

SN 2.2.8: RST shall provide spectra with relative spectrophotometric flux calibration as a function of wavelength accurate to 3%, when calibrated against standard stars.

Comment: High-precision relative fluxes will be derived from the imaging data.

SN 2.2.9: Deleted

3.5.7 Supernova Survey: Raw Data Records

SN 2.3.1: RST shall be capable of providing raw images in the archive for each detector exposure with each raw data record including a unique dataset identifier for each exposure, the exposure time, the time of exposure, all individual downlinked detector readouts used to make the exposure, the observatory pointing orientation and any additional engineering data the Science Center uses for subsequent processing.

Because the luminosity distance of a given supernova is derived from the rest-frame B magnitude at the peak of the light curve, and because the rest-frame B-band will appear at different wavelengths in the instrument depending on the redshift of the supernova, inaccuracies in the relative photometric calibration as a function of wavelength will lead directly to systematic errors in the derived cosmological results.

Furthermore, the extinction correction to be applied to the data is derived by fitting spectral templates to the observed fluxes. Systematic biases in the photometric calibration over the full waveband will lead to systematic errors in the extinction and thus in the distance modulus. A representative extinction curve is shown in Figure 14. At short wavelengths this curve can vary

significantly from one line of sight to another, and it can vary from one galaxy to another. Over most of the bandpass shown, a two parameter fit is usually sufficient to characterize the shape of the curve, e.g. R_V and A_V in the nomenclature of Cardelli, Clayton, and Mathis (1989 ApJ 345 245 – but see also Fitzpatrick 2007 ApJ 663 320 and Fitzpatrick and Massa 2009 ApJ 699 1209). Because the extinction curve is shallow in the NIR, but steep in the blue where the uncertainty has the greatest impact, it is helpful to be able to compare the SN spectrum against a template over a broad wavelength range when estimating the extinction in the host galaxy of the supernova.

Choosing SN survey fields to have a line of sight through the Milky Way in regions of low extinction will limit the potential impact of uncertainties in the estimation of foreground extinction. These considerations lead to the requirement:

> **SN 2.3.2:** RST shall be able to observe supernovae in fields with low Galactic extinction, such that $E(B-V) \leq 0.02$ over 90% of the area, and low zodiacal light background. Here, Galactic extinction is that defined by Schlafly & Finkbeiner 2011 (ApJ 737, 103).

Because supernova light curves have a duration of many months, the yield of properly-observed light curves is vastly reduced if the supernova survey fields cannot be observed continuously throughout a year.

> **SN 2.3.3:** The RST field of regard shall be large enough to provide a continuous viewing zone (CVZ) that encompasses regions of the sky suitable for observing supernovae.

Achieving a small variation in intrinsic luminosity requires an empirical correction based on the shape of the light curve for each supernova. The light curve must be sampled on both the leading and trailing edges, with sampling intervals ideally no longer than 4 days in the SN rest-frame in order to resolve the shape of the light curve [For examples, see Guy et al 2007, A&A 466 11 (SALT2), Conley et al 2008, ApJ 681 482 (SiFTO), Jha, Riess & Kirschner 2007, ApJ 659 122 (MLCS2k2)]. Because the minimum redshift of the RST sample is 0.2, this corresponds to an observing cadence of 5 days for discovery and initial monitoring. The light-curve shape is a function of wavelength, hence the light curve must be monitored in multiple imaging bands and/or spectrophotometrically. Measuring the supernova flux requires subtraction of the host-galaxy flux, hence the host galaxy must be measured after the supernova has faded. In the rest-frame B-band, the rise-time is approximately 19 days (Conley et al 2006 AJ 132 1707) and the fall-time to 10% of peak luminosity is 45-60 days. The light curve fall-times are roughly twice as long in the rest-frame I–band and at longer wavelengths. Thus, the final follow-up measurement of the host galaxy flux must be done at least 6 rest-frame months after discovery, or $6(1+z)$ months in the observers frame after discovery. These considerations lead to the requirements:

> **SN 2.3.4:** RST shall enable a SN survey that monitors the SN fields with an uninterrupted sampling cadence ≤ 5 days.

> **SN 2.3.5:** RST shall have the capability of providing raw images of SN fields in up to six filters that span roughly 0.5 – 2.0 μm.

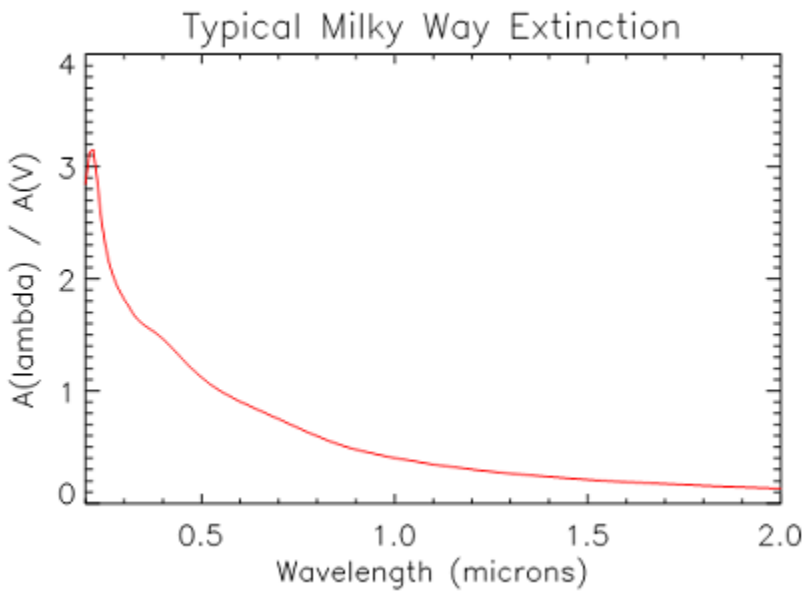

Figure 14 Typical Milky Way Extinction Curve

Figure 14 shows a typical Milky Way extinction curve. The steep rise at shorter wavelengths means that small uncertainties in the overall level of extinction result in much larger uncertainties at blue wavelengths than in the NIR.

Definitive classification and redshift determination of a supernova is best done with spectra. SN typing, and to some extent sub-typing, can be performed with multi-band imaging light-curves if a comprehensive set of spectral templates is available. Spectra of SNIa are unique in lacking any features of HI, and in having strong absorption by both SiII and SII. The combination of the CaII absorption features (the H&K lines 3934, 3969A and the NIR triplet: 8498, 8542, 8662A) and the SiII and SII features is important for sub-typing. As can be seen in Figure 15, a spectral bandpass of 0.75-1.8microns spans all these lines for a redshift of 1.1 ensuring that a spectral template library can be obtained at a redshift near the midpoint of the range of interest for RST.

SN 2.3.6: RST shall be capable of obtaining spectra over the bandpass 0.75-1.8 microns, with spectral dispersion lambda/delta_lambda>70 per two-pixel resolution element at all wavelengths, and <170 per two-pixel resolution element at wavelengths longer than 0.8 microns.

SN 2.3.7: RST shall provide raw spectral images with 50% of the energy enclosed in a circle of radius < 0.17" at 1.2 microns for a monochromatic point source, excluding diffraction spikes and including the effects of pointing jitter, for at least 95% of exposures and over 90% of the field of view.

SN 2.3.8: RST shall be able to obtain a prism spectrum of a flat-spectrum source with a signal to noise of 10 per 2-pixel resolution element in 600 seconds for a source magnitude of AB=22.3 at 1.2 microns.

SN 2.3.9: Deleted

SN 2.3.10: Deleted

SN 2.3.11: Deleted

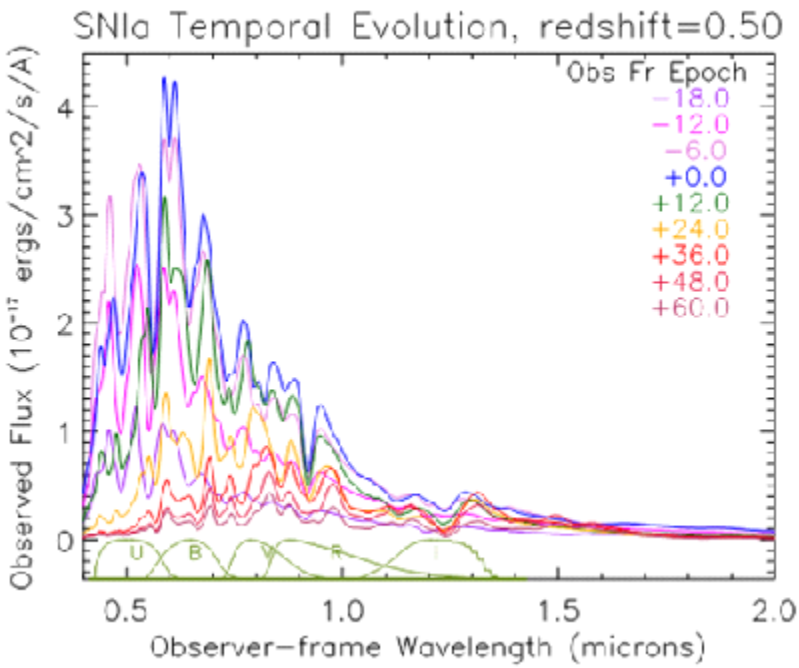

Figure 15 SNIa Spectra at Various Points in its Evolution

SNIa spectra at various points in its evolution are plotted, for a SN at redshift 0.5. The spectra peak at short wavelengths at early times, shifting to longer wavelengths as later times. Redshifted filter curves are shown at bottom.

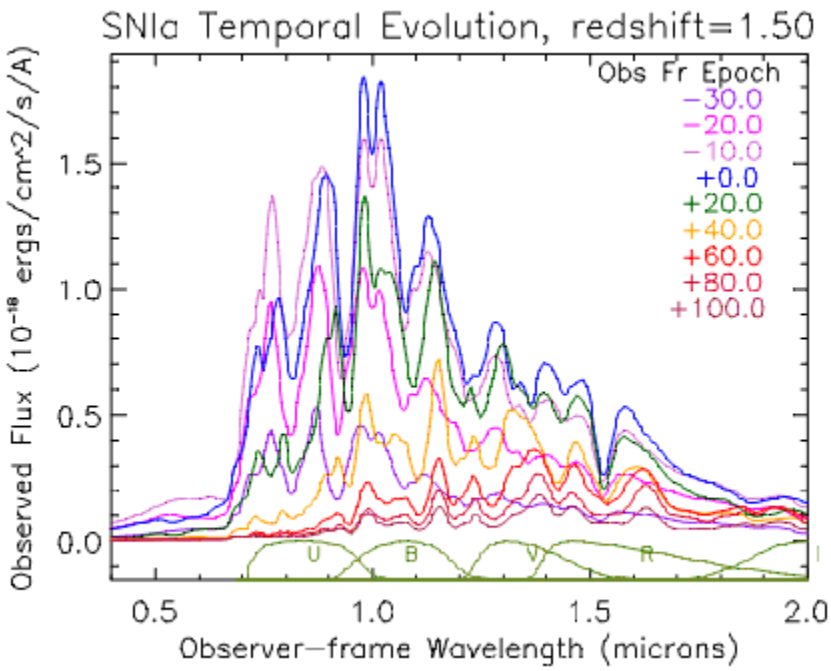

Figure 16 Same as for the figure above, but for redshift=1.5.

Proper characterization of the SNe requires uninterrupted monitoring of their evolution. This is accommodated by placing the survey area near the ecliptic poles, in a part of the observatory field of regard that is accessible continuously throughout the mission.

SN 2.3.12: Deleted

SN 2.3.13: Deleted

3.6 Exoplanet Microlensing

The primary RST Microlensing Science Objective, which will enable RST to provide (along with Kepler) the ultimate empirical dataset with which to test theories planet formation and evolution, is to:

Carry out a statistical census of planetary systems in the Galaxy, from the outer habitable zone to free floating planets, including analogs to all of the planets in our Solar System with the mass of Mars or greater.

3.6.1 Exoplanet Microlensing - Science Requirements

Testing theories of planet formation requires accurate and precise measurements of the demographics of planets over a wide range of planet and host star parameters. *Kepler* has begun this process by measuring the radius and period distribution of planets with periods of less than roughly one year and planet sizes of roughly greater than one Earth radius. Furthermore, *Kepler* has detected thousands of planets in this regime, and as a result of the uncertainty arising from Poisson fluctuations in the empirically determined distributions of planet radii and period in this regime is relatively small.

The RST microlensing survey will complete this census by detecting a (roughly) similar number of planets with masses greater than that of the Earth and periods of greater than roughly one year. Again, to provide similarly stringent constraints on exoplanet demographics as *Kepler*, RST should detect a comparable number of planets as Kepler, assuming a similar occurrence rate as *Kepler*.

Furthermore, since typical microlensing observables do not automatically ensure estimates of host star properties, the RST microlensing survey must ensure that the majority of the microlensing planet detections are accompanied with the requisite data to allow for accurate (<~ 20%) estimates of the host star masses, and thus the exoplanet masses and projected separations.

When setting our reference microlensing survey parameters, we choose values that will enable us to measure the distribution function of planets in mass ratio and projected semimajor axis in units of the Einstein ring radius with sufficient precision to measure the shape and normalization of this distribution function, and detect features that may be in it (i.e., a break at a given mass). Since theories that predict the expected distribution of planets in the region of parameter space where the microlensing survey will be sensitive are exceptionally uncertain, differ dramatically between different theorists, and even differ between different versions of simulations by the same authors, it is difficult to know exactly what features to expect and therefore predict a priori how many planets must be detected to meaningfully constrain planet formation in the region where microlensing is sensitive.

We therefore generally take our cues from previous surveys, in particular the *Kepler* survey. The first *Kepler* sample included ~1200 planets, and while a detailed analysis of this sample revealed many interesting results (Howard et al. 2012) dividing the sample up into ~10 bins in planet radius resulted in a ~10% uncertainty per bin. While there were enough detections to constrain the overall slope of the radius distribution precisely, the precision per bin was still insufficient to clearly reveal a large break in the distribution of radii at ~4 R_{Earth} that has subsequently been clearly confirmed with the expanded sample of nearly 4000 confirmed *Kepler* planets. Note that this break is a "smoking gun" of one formation scenario of planet formation; it is exactly just such signatures that we are searching for with this survey. Note also that this sample spanned a much smaller range of semimajor axes than the RST survey will.

Similarly, given the poorer-than-expected precision with which Kepler was able to measure η_{Earth}, it is of great interest to improve the precision of that measurement. This sets our desired yield in the parameter space near the habitable zone (as defined by both the stellar insolation flux and planet mass) of FGK stars.

A measurement of the frequency of Mars-mass objects will likely strongly constrain planet formation theories, which generally predict that objects of that mass are likely the building blocks of planet formation. Therefore, measuring the frequency of such objects (and, hopefully, planets less than this mass) is essential for constraining these planet formation theories. We therefore set a desired yield of Mars-mass objects.

A notable feature of the RST microlensing survey is that it should be possible to measure the host star mass and distance of at least a subset of the planetary microlensing events, with the RST data alone. This allows us to convert from the dimensionless quantities that are routinely measured in microlensing events (the planet/star mass ratio and projected separation in units of

the Einstein ring radius) to the physical quantities of planet mass and projected separation in physical units (i.e., Astronomical Units). This will allow more direct comparisons with radial velocity, transit, direct imaging, and astrometric surveys. Furthermore, it will allow the determination of the variation of planet frequency with host star mass and Galactocentric distance. We therefore have set a limit on the desired fraction of planetary host star masses that can be measured to a given precision.

Finally, we wish to measure the frequency of free-floating planets. Planet formation theories general predict many planets are ejected in the process of planet formation, but the mass distribution of these ejected (and thus free-floating) planets depends strongly on what fraction of planetary systems are formed via 'violent' dynamical interactions, and what fraction are formed in a more quiescent manner. Conversely, a measurement of the mass function and total mass of free-floating planets will provide a strong constraint on planet formation models. It is expected that low-mass planets will be ejected in larger numbers than higher-mass planets, simply due to energetic considerations. We therefore set our desired yield for free-floating planets by setting a requirement for the frequency of free-floating Earth-mass planets.

Next we define a reference survey that will allow us to achieve our goals above: accurately measure the mass function of planets beyond the snowline, measure the frequency of Mars-mass objects, measure the masses of a significant fraction of the host stars, and measure the mass function of free-floating planets.

Reference Microlensing Survey

Our methodology for estimating the yield of planet detections is described in detail in Penny et al. (2019 ApJS 241:3) and summarized briefly in the appendix. The appendix also describes the uncertainties that are inherent in estimating this yield.

For our reference survey, we adopt a fiducial planet mass M_p and semimajor axis a function that is derived from that of Cassan et al. (2012, Nature, 481, 167). Specifically, the distribution function we adopt is:

$$\frac{\mathrm{d}^2 N}{\mathrm{d}\log a\ \mathrm{d}\log M_p} = 0.24^{+16}_{-10}\left(\frac{M_p}{95 M_{Earth}}\right)^{-0.73\pm0.17} \text{ for } M_p > 5M_{Earth}$$

and

$$\frac{\mathrm{d}^2 N}{\mathrm{d}\log a\ \mathrm{d}\log M_p} = 2.06 \text{ for } M_p > 5M_{Earth}.$$

While more up-to-date distribution functions that include more data exist (e.g., Suzuki 2016, ApJ, 833, 145), we have chosen to adopt this fiducial mass function for several reasons. First, doing so provides consistency between the planet yields we estimate here and those from previous versions of the RST mission. Second, it is clear that further improvements on the distribution function of cold planets can be expected. Finally, the precise choice of the distribution function is not essential, as it simply provides a reference yield that we can use to set our Level-2 requirements. We assume one free-floating Earth-mass planet per star.

To define the reference survey, we assume a detector area of 0.282 square degrees and total of seven fields, for a total survey area of 1.974 square degrees. We choose the number and location of the fields in order to roughly optimize the microlensing event rate, as described in Penny et al. (2019). We cycle through our fields such that we achieve a 15 minute cadence per field, which leads to a typical exposure time of 53s once overheads (slew and settle times and read times) are included. This yields a source noise photon flux such that, given the properties of the telescope, primary microlensing filter, and detector, one can achieve a SNR=100 on a H_{AB}=21.4 magnitude star. We assume that exposures are taken in two other filters once every 12 hours. We assume a total of 6 microlensing seasons, each 62 days long centered around quadrature with respect to the location of the Bulge fields. We assume that the first two seasons are taken at opposite quadrature and the last two seasons are taken at opposite quadrature, in order to provide the ability to measure parallaxes of stars in the field.

With these assumptions, we estimate of the yield of bound exoplanets (again assuming our fiducial mass function) to be 1474 (See Table 1). The yield of free-floating Earth-mass planets assuming one per star is 23.

The yield for the baseline survey is computed assuming 80% of the survey area or survey duration of the reference survey, and the threshold survey yield is computed assuming an additional factor of two reduction.

Table 1 Yield of bound planets for the reference, baseline, and threshold surveys.

M/MEarth	0.1-0.3	1	10	100	1000	3000-10000	Total	FFE
Reference	20	181	545	412	224	91	1474	23
Baseline	16	144	436	330	179	73	1179	19
Threshold	8	72	218	165	90	36	589	9

3.6.2 Exoplanet Microlensing – Survey Capability Requirements

The Baseline Science Requirements for studying the demographics of bound planets beyond the snowline, and measuring the mass function of free-floating planets are as follows:

EML 2.0.1: RST shall be capable of measuring the mass function of exoplanets with masses in the range 1 $M_{Earth} < m < 30\ M_{Jupiter}$ and orbital semi-major axes ≥ 1 AU to better than 15% per decade in mass.

EML 2.0.2: RST shall be capable of measuring the frequency of bound exoplanets with masses in the range 0.1 $M_{Earth} < m < 0.3 M_{Earth}$ to better than 25%.

EML 2.0.3: RST shall be capable of determining the masses of, and distances to, host stars of 40% of the detected planets with a precision of 20% or better.

EML 2.0.4: RST shall be capable of measuring the frequency of free floating planetary-mass objects in the Galaxy from Mars to 10 Jupiter masses. If there is one M_{Earth} free-floating planet per star, measure this frequency to better than 25%.

EML 2.0.5: RST shall be capable of estimating η_{Earth} (defined as the frequency of planets orbiting FGK stars with mass ratio and estimated projected semimajor axis within 20% of the Earth-Sun system) to a precision of 0.2 dex via extrapolation from larger and longer-period planets.

Comment: Given our input assumptions, and assuming that the requirements at Level 3 and below are satisfied, the data provided by RST will allow us to meet all of our level 2 baseline requirements above with a roughly 20% margin, in the sense that the requirements above will be satisfied given our assumptions with a yield that is 80% of our reference survey yield. Note that a factor of 0.8 fewer detections leads to a Poisson uncertainty on the mass function, frequency of Mars mass planets, Earth mass free-floating planets, and our estimate of η_{Earth} that is $0.8^{-1/2}$=1.12 times higher on the mass function, and leads to a number of host stars with mass measurements with precisions of 20% that is 0.8 times lower.

Allocation of Margin

In the case of the microlensing survey, the yield depends almost exclusively on the number of star-years monitored, the microlensing event rate in the target fields, and on the (photon-noise) signal to noise ratio for a star of a fiducial stellar magnitude. We have limited ability to maximize the number of stars per square degree down to a given magnitude that we can monitor in a given field. Both the number of stars per square degree and the event rate in our fields is set by the stellar density. This density is highest toward the Galactic Bulge, and while we may optimize these quantities by small adjustments in the field, there are fundamental limits in our ability to maximize them. Similarly, we have limited ability to maximize the event rate in our fields[1]. Given that our cadence is essentially fixed (see below), the signal to noise ratio of a star of a given magnitude depends primarily on the aperture of the telescope and the filter in which most of the observations are collected, while the area monitored is determined by the size of the WFI detector and the number of fields we can observe with a given cadence. Of these, we can and do optimize the number of fields given a prescribed amount of overhead, which itself is set by the slew and settle time and readout time, such that we achieve the required signal to noise ratio on our fiducial star. Therefore, for a fixed set of observatory properties, our primary freedom in allocating margin is to alter the product of total number of square degree times the total number of days that we monitor our fields. For the number of host star mass measurements we require, we have a bit more flexibility, but as we argue below, we expect that our primary method of measuring host star masses by combining a measurement of the flux of the lens with a measurement of the source crossing time and/or a direct measurement of the lens-source proper motion. We expect the number of lens flux measurements to scale (to first order) linearly with the planet yield. The latter method of measuring the proper motion does depend on the cadence of the microlensing survey seasons; in particularly we desire as long of a time baseline between the first and last seasons as possible.

We therefore allocate our margin as follows:

- A factor of 0.8 in the total number of square degrees-days of the survey to go from the reference to baseline survey, and an additional factor of 0.5 for the threshold survey (Section 4.2.4).

Microlensing Survey Implementation Considerations

Microlensing events require extremely precise alignments between a foreground lens star and a background source star, which are both rare and unpredictable. Furthermore, the probability that a planet orbiting the lens star in any given microlensing event will give rise to a detectable perturbation is generally much smaller than unity, ranging from a few tens of percent for a Jupiter-mass planet and a typical low-magnification event, to less than a percent for planets with mass less than that of the Earth. These planetary perturbations have amplitudes ranging from a few percent for the lowest-mass planets to many tens of percent for the largest perturbations, but are brief, ranging from a few days for Jupiter-mass planets to a few hours for Earth-mass planets.

Also, the time of a planetary perturbation with respect to the peak of the primary event is unpredictable. Thus detecting a large number of low-mass exoplanets with microlensing requires monitoring of a very large number of stars (>~10^8) continuously with relatively short cadences (<~15 minutes) and photometric precision of a few percent or better. Practically, a sufficiently high density of source and lens stars, and thus a sufficiently high microlensing event rate, is only achieved in lines of sight towards the Galactic Bulge. However, these fields are also crowded, and this high star density means that high spatial resolution is needed to resolve out the individual stars in order to achieve the required photometric precisions and to identify the light from the lens stars.

As described above and detailed in Penny et al. (2018, in prep), these requirements below are based on the results of sophisticated simulations of a microlensing exoplanet survey. However, to understand the order of magnitude of these requirements, simple back-of-the-envelope estimates are provided. Consider, as a specific example, the goal of detecting at least ~180 bound Earth-mass planets, as expected in our reference survey. The typical detection probability for an Earth-mass planet at 2AU is ~1.5%, and thus ~180/0.015 ~ 1.2×10^4 microlensing events must be monitored to detect ~180 such planets, assuming every star hosts such a planet. The average microlensing event rate in the RST microlensing survey fields is ~5×10^{-5} events/year/star, and thus $1.2\times10^4/5\times10^{-5}$ ~ 240 million star-years must be monitored. The typical stellar density down to J=23 is ~few x 10^8 stars per square degree, and thus we have the first data requirement below that at least ~2 square degrees must be monitored. In order to detect and accurately characterize the perturbations due to Earth-mass planets, which typically last a few hours and have amplitudes of several percent, photometric precisions of a few percent, continuous monitoring, and cadences of less than 15 minutes are needed, as this is roughly half the typical crossing time of the typical source. Since this is essentially the shortest timescale of any significant features we expect in microlensing events, this sets our minimum cadence.

Typical microlensing events last roughly 40 days, so seasons longer than this (in order to acquire sufficient baseline) are needed. Finally, given the areal density of ~few x 10^8 stars per square degree, an angular resolution of <10^{-4} degrees (<0.4 arcseconds) is needed to resolve the faintest stars. These numbers are obviously approximate, but provide a roughly sense of the order-of-magnitude of the survey requirements.

Given the extinction by dust present along lines of sight to the Galactic Bulge, the highest signal-to-noise ratio for measurement of lightcurves will be obtained by means of a broad near-infrared filter.

Typically, the measurement of a microlensing light curve provides allows extraction only of the Einstein ring crossing time. The desired quantities of planet mass and separation from the host

star can be determined if the distances to the source and host star can be determined and if the mass of the host star can be determined. The source star is typically assumed to be in the Galactic Bulge, and therefore its distance is roughly known, although RST may be able to measure the source star distances directly via parallax.

The mass and distance to the host lens can be determined in a variety of ways. Simply put, there are three distinct additional pieces of information that can be extracted from microlensing events that will provide a mass-distance relation to the host star. Since these mass/distance relations are all different, combining any two of these will yield an estimate of the mass and distance to the host star separately. We review the basic methodology of how to measure these additional pieces of information here in order to clarify our lower-level requirements, but refer the reader to Bennett, Anderson & Gaudi (2007, ApJ, 660, 781) for details.

1. **Angular Einstein Ring Radius**: The first piece of information that one can obtain for most planetary microlensing events is the source crossing time $t_\star$. This is measured whenever the source passes over a region of the magnification due to the lens with a significant second derivative[2], as is typically the case for planetary microlensing perturbations. This can then be combined with the timescale (a routine observable in microlensing events) to determine the angular size of the source in units of the angular Einstein ring radius θ_E. The source color and magnitude is also a routine observable in microlensing events, provided one has data in multiple filters taken when the source is magnified, then yields the angular radius of the source and thus the angular Einstein ring radius. In essence, the angular source size provides a standard "angular ruler" with which to measure θ_E. With an estimate of the source distance, the angular Einstein ring radius gives a relation between the mass and distance to the lens.

   A generally related quantity to $t_\star$ that one can measure is the relative lens-source proper motion μ. This can be measured in a variety of ways: by resolving the lens and source before or after the microlensing event, by measuring the image elongation as the source and lens separate, or by measuring a color-dependent centroid shift if the source and lens are sufficiently well separated and have sufficiently different colors. The relative proper motion combined with the Einstein timescale t_E yields θ_E.

2. **Lens flux**: If one can measure the lens flux, and estimate the extinction to the lens, then one can again determine a mass-distance relation to the lens, once one adopts a mass-luminosity relationship. The requires resolving out all unrelated stars from the blended lens+source flux, measuring the source flux (which, as we mention above, is a routine observable), and then subtracting the source flux from the blend to measure the lens flux. In most cases, we will want to measure the lens-source relative proper motion using the full time series of RST microlensing survey data with the color dependent centroid or image elongation methods (Bennett et al. 2006, ApJL, 647, L171, 2007 ApJ, 660, 781). The lens-source proper motion measurements will avoid confusion with binary companions to the source or lens stars. For the higher-mass and/or more nearby lenses, we expect this to be the dominant method of estimating the lens mass.

[2] In these instances, the source is 'resolved' by the magnification structure of the lens; this is commonly known as "finite source effects."

3. **Microlensing parallax**: If one has a "standard ruler" in the observer plane, and one can measure "microlensing parallax", the effect of non-inertial or non-cospatial observers on the microlensing event and compare them to this ruler, then one infer the linear Einstein ring radius projected on the observer plane, ř, which is itself a vector with a direction equal to that of the relative lens-source proper motion. Again, given an estimate of the source distance, this provides a mass-distance relationship to the lens.

Microlensing parallax can be measured in several ways. First, for relatively long events, one can use the acceleration of the Earth to infer the microlensing parallax. The most easily measurable component of this vector produces the largest effect on microlensing events near quadrature, which is fortuitously the time around which the RST microlensing season will be centered. One can also measure the microlensing parallax from non-cospatial observers, given the (known) projected physical separation between them. In the case of RST, it will only be separated from ground-based observatories by ~0.01 AU, which is much smaller than the typical projected Einstein ring radius of microlensing events of ř ~ 8 AU. However, it is comparable to the projected Einstein ring radius of planets with the mass of Earth or smaller. Thus, if perturbations from these planets can be detected from both the ground and RST simultaneously, this will yield ř.

3.6.3 Exoplanet Microlensing – Science Data Records

The microlensing survey requires several data products, produced at several different time intervals during the survey.

The primary data products used in the analysis are the calibrated 'moment curves', which are generalizations of a light curve: photometry, astrometry, ellipticity, etc., as a function of the epoch of observation. These should be produced on a daily timescale, with as many of the detector systematics removed as possible.

Supersampled and stacked images of the microlensing fields generated at the end of each season will be used for source identification and to measure source motions.

In order to calibrate the microlensing event rate and planetary detection sensitivity, we require injection and recovery tests of the light curves.

The final, end-of-survey data products will include the final moment curves calibrated with all available data, a source catalog containing positions, proper motions, colors, and other basic data for each object in the field, detection efficiencies for microlensing events and planets, a catalog of binary and planetary detections, and calibrated detector artifacts and their change over time.

EML 2.1.1: RST shall be capable of providing supersampled stacked images of the microlensing fields after every microlensing season.

EML 2.1.2: RST shall be capable of producing a catalog of each source in the microlensing fields containing positions, fluxes, with object-appropriate derived data. Examples of object-appropriate derived data include object classification, parallaxes and proper motions for stars and limited time domain information for variable sources.

EML 2.1.3: RST shall be capable of producing a catalog of each microlensing event in the microlensing fields containing positions, fluxes, object classification information with

event-appropriate derived data. Examples of event-appropriate derived data include links to the corresponding source catalog entries and moment curves.

EML 2.1.4: RST shall be capable of including information in the microlensing catalog on statistical and systematic uncertainties for each quantity in the catalog and/or data quality flags, as applicable.

EML 2.1.5: RST shall be capable of providing calibrated photometry and position measurements for each microlensing event on a daily basis, and ellipticity measurements every 8th day.

EML 2.1.6: RST shall be capable of providing science data records with relative astrometric measurements having a systematic precision of ≤100 μas over each microlensing season, for sources imaged on the same detector in at least two passbands.

3.6.4 Exoplanet Microlensing - Calibrated Data Records

Typically, the measurement of a microlensing light curve allows extraction only of the Einstein ring crossing time. The desired quantities of planet mass and separation from the host star can be determined if the distances to the two stars can be determined and if the mass of the host star can be determined. The primary star-star lensing events typically last ~40 days. The distances to the stars and their masses can be determined from their spectral types and brightness; the stars will not be spatially resolved, but the change in colors and brightness during the event combined with relative proper motion over a period of years may enable placing the stars on a color-magnitude diagram and thus determine their distances and masses (Bennett et al. 2007). Furthermore, the changing line-of-sight geometry during the event modifies the shape of the primary lensing light curve, allowing an independent measurement of the distances to the stars (Gould 1992, Gould et al. 2014). Subtle distortions in the microlens light curves due to the orbital motion of the planet about the host will also enable constraints on the period, inclination, and eccentricity of the orbit in a subset of cases. Measurements in multiple filters are required to determine spectral types, and high-precision relative photometry is required for analysis of the light curve shapes.

EML 2.2.1: RST shall be capable of archiving microlensing calibrated images and incorporate any World Coordinate System information needed for subsequent stages of processing.

EML 2.2.2: RST shall be capable of providing calibrated data records for photometry and position of microlensing events on a daily basis, and every 8th day for ellipticity.

EML 2.2.3: RST shall be capable of providing calibrated data records with relative astrometric measurements having a statistical precision of ≤1 mas per measurement for a star of H_{AB}=21.4 in at least two passbands.

Comment: Astrometric precision of the source stars of the microlensing survey is important for several reasons. The ability to measure the astrometric precision of a star to a given precision determines the ability to measure the relative lens-source proper motion, the color-dependent centroid shift, and potentially the parallax of the source. A statistical requirement of a ~1 mas astrometric precision for an H_{AB}=21.4 is derived from the fact the FWHM of the PSF is ~0.10”

and we require a SNR~100 for a star with H_{AB}=21.4. Since the ability to centroid a PSF is roughly FWHM/SNR~0.10”/100~1 mas.

> **EML 2.2.4:** RST shall be capable of providing calibrated data records with the FWHM for 99% of stars brighter than H(AB)=21.4 with a precision ≤1% in both axes after every 8 consecutive day interval.

Comment: As discussed above, one of the ways to measure the relative lens-source proper motion is to measure the elongation of the PSF as the lens and source separate. The above requirement is derived from the requirement of being able to measure the FWHM in each axis to a given precision per measurement, which is the minimum requirement for being able to measure elongation over the course of the mission.

> **EML 2.2.5:** RST shall be capable of providing calibrated data records with the FWHM of each source measured in both axes of a H_{AB}=21.4 star to ≤0.2% for each observing season of the microlensing survey.

> **EML 2.2.6:** RST shall be capable of providing calibrated data records with relative photometric measurements in the primary microlensing filter having a systematic precision of ≤0.1% over a season.

Comment: Planetary perturbations from planets near the edge of our detection sensitivity, which are also those planets that are inaccessible from the ground, produce deviations that are often only a few tenths of percent. These include perturbations from habitable zone planets, as well as the lowest mass planets. In addition, the ability to measure long-timescale deviations from simple microlensing events (such as those due to parallax) will depend on the ability to distinguish, e.g., trends due to systematic errors in the photometry from intrinsic asymmetries in the microlensing events themselves.

> **EML 2.2.7:** RST shall be capable of providing calibrated data records with relative photometric measurements from separate seasons tied to ≤0.1% for any individual star.

Comment: Accurate measurements of the timescales of events that span a significant fraction of a season require the ability to precisely tie the photometry from different seasons together. Similarly, the ability to measure microlens parallax will depend critically on the ability to distinguish systematic offsets from different seasons from true asymmetries.

> **EML 2.2.8:** RST shall be capable of providing calibrated data records with absolute photometry of point sources calibrated in one or more of the standard filters to <3%.

> **EML 2.2.9:** RST shall be capable of providing calibrated data records with relative zero-points of the filter photometry known to <1.4%.

3.6.5 Exoplanet Microlensing - Raw Data Records

Microlensing events require extremely precise alignments between a foreground lens star and a background source star, that are both rare and unpredictable. Furthermore, the probability that a planet orbiting the lens star in any given microlensing event will give rise to a detectable perturbation is generally much smaller than unity, ranging from a few tens of percent for a Jupiter-mass planet and a typical low-magnification event, to less than a percent for planets with

mass less than that of the Earth. These planetary perturbations have amplitudes ranging from a few percent for the lowest-mass planets to many tens of percent for the largest perturbations, but are brief, ranging from a few days for Jupiter-mass planets to a few hours for Earth-mass planets.

Also, the time of the perturbations with respect to the peak of the primary event is unpredictable. Thus detecting a large number of low-mass exoplanets with microlensing requires monitoring of a very large number of stars (>~10^8) continuously with relatively short cadences (<~15 minutes) and photometric precision of a few percent or better. Practically, a sufficiently high density of source and lens stars, and thus a sufficiently high microlensing event rate, is only achieved in lines of sight towards the Galactic Bulge. However, these fields are also crowded, and this high star density means that high spatial resolution is needed to resolve out the individual stars in order to achieve the required photometric precisions and to identify the light from the lens stars.

These requirements below are based on the results of sophisticated simulations of a microlensing exoplanet survey. However, to understand the order of magnitude of these requirements, simple back-of-the-envelope estimates are provided. Consider, as a specific example, the goal of detecting at least 150 Earth-mass planets. The typical detection probability for an Earth-mass planet at 2AU is ~1.5%, and thus ~150/0.015 ~ 10^4 microlensing events must be monitored to detect ~150 such planets, assuming every star hosts such a planet. The average microlensing event rate in the RST microlensing survey fields is ~5×10^{-5} events/year/star, and thus $10^4/5\times10^{-5}$ ~10^{-5} ~200 million star-years must be monitored. The typical stellar density down to J=23 is ~10^8 stars per square degree, and thus the equivalent of ~2 square degrees must be monitored for a year. In order to detect and accurately characterize the perturbations due to Earth-mass planets, which typically last a few hours and have amplitudes of several percent, photometric precisions of a few percent, continuous monitoring, and cadences of less than 15 minutes are needed. Finally, given the areal density of ~10^8 stars per square degree, an angular resolution of 10^{-4} degrees (0.4 arcseconds) is needed to resolve the faintest stars.

Given the extinction by dust present along lines of sight to the Galactic Bulge, the highest signal to noise ratio for measurement of lightcurves will be obtained by means of a broad near infrared filter.

The considerations in the preceding paragraphs lead to the following observing requirements:

> **EML 2.3.1:** RST shall be capable of providing microlensing raw images in the archive for each detector exposure with each raw data record including a unique dataset identifier for each exposure, the exposure time, the time of exposure, all individual downlinked detector readouts used to make the exposure, the observatory pointing orientation and any additional engineering data the Science Center uses for subsequent processing.

> **EML 2.3.2:** RST shall be capable of observing a total 585.4 square degree-days over the course of the mission, with relative photometric measurements in the primary microlensing filter that have a statistical S/N of ≥100 per exposure for a HAB=21.4 star, if it is allocated 6 seasons of observing time.

Comment: This area corresponds to the 'Baseline' case described in Section 3.6.1. This corresponds to 7 fields * 0.281 sq-deg / field * 62 days / season * 6 seasons * 0.8.

EML 2.3.3: RST shall be capable of providing raw microlensing images with relative photometric measurements in the primary microlensing filter having a statistical S/N of ≥100 per exposure for a H_{AB}=21.4 star.

Comment: As described above, given our assumptions about the planet distribution, the microlensing event rate in the fields that we will be monitoring, and the prescribed observatory parameters, these are the most fundamental requirement that sets our total yield of planets, and thus is the primary requirement that determines our ability to meet our Level 2 science requirements.

EML 2.3.4: RST shall be capable of providing raw images of the microlensing fields with a wide filter spanning $\lambda \approx 1 - 2$ μm.

Comment: The width and central wavelength of the microlensing filter is required to achieve a sufficient number of photons to achieve a minimum SNR of 100 on our fiducial H_{AB}=21.4 magnitude star, which itself is required to detect a sufficient number of microlensing events and thus planetary perturbations.

EML 2.3.5: RST shall be capable of providing a photometric sampling cadence of ≤15 minutes for each microlensing field, while simultaneously achieving the S/N specified in EML 2.3.3.

Comment: The smallest timescale of perturbations to a microlensing event is given by the timescale to cross the source diameter. This is because perturbations from the lens that have features shorter than this duration will be 'smoothed' out by the finite size of the source. The typical source crossing time for the typical source is ~30 minutes, and thus in order to resolve the shortest features, we require cadences of less than ~30/2~15 minutes.

EML 2.3.6: RST shall be capable of providing microlensing raw images with an EE50 radius of the PSF in the wide filter <0.15".

Comment: In order to resolve out unrelated stars from the blended source and lens, which is required to isolate the lens flux and thus measure the lens mass, the PSF must have a full-width half-maximum less than the typical spacing between the stars in the crowded regions of the Bulge that will be monitored by the microlensing survey. Furthermore, if the PSF FWHM is significantly larger than ~0.15", the microlensed stars will be partially blended with nearby stars, incurring additional photon noise and systematic photometric uncertainties.

Many of the stars being monitored are bright enough to saturate the detector pixels during an exposure, hence the ability to downlink readouts obtained during each exposure is essential. In addition, due to the requirements on precise relative photometry and the need to obtain characterization data for a wide variety of detector performance parameters, RST should be capable of downlinking all the readouts from occasional samples of exposures.

EML 2.3.7: RST raw data records shall consist of at least 6 ground-configurable combinations of samples per microlensing exposure.

Comment: Onboard combinations of individual detector readouts include simple sums, differences, and/or averages of frames.

EML 2.3.8: Deleted

EML 2.3.9: RST shall be capable of performing microlensing observations over seasons of at least 60 days. At least 36 days of each season should be on the opposition side of quadrature (line of sight at greater than 90 degrees from the Sun vector).

Comment: A typical microlensing event lasts ~40 days. Therefore, in order to measure the baseline of typical events and thus robustly measure their timescale, seasons of at least 60 days are needed. Because ground-based observatories can only observe the Bulge for a limited window around opposition (depending on the latitude of the observatory), simultaneous observations from RST and the ground are enhanced if the RST observing season is weighted toward opposition.

EML 2.3.10: RST shall monitor the microlensing fields with a duty cycle of ≥90% per season.

Comment: Duty cycle here means the fraction of elapsed time devoted to microlensing observation activities; such activities include slewing between microlensing fields and target acquisitions and other observation-specific overheads, but not time devoted to momentum dumping, station keeping, non-microlensing observations, etc.

The planet yield is essentially proportional to the total amount of time spent monitoring the fields. Therefore, a reduction of 0.9 in the total amount of time surveying our fields will result in roughly a reduction in the precision of science goals of between 0.9 and $0.9^{0.5}$~0.95, which will still allow us to achieve our baseline level-2 science goals.

EML 2.3.11: RST shall be capable of periodically providing raw images of the microlensing fields in two R~4 filters; one with bandpass shortward of 1 μm and one with a bandpass longward of 1 μm. The cadence of these observations is defined in the Operations Concept document.

Comment: In order to measure the source color, and thus its angular radius, the source+host blended flux must be precisely measured in multiple filters when the microlensing event is significantly magnified, in order to separate the source flux and color from that of the lens.

EML 2.3.12: RST shall be capable of separating the first and last microlensing observing seasons by >4 years.

In addition, the first two and last two seasons should occur during the same 12-month period (i.e., one in the spring and one in the fall to provide parallax measurements).

Comment: The longer the separation between the first and last microlensing observing seasons, the more the lens and sources of the microlensing events that occur during (and before and after[3]) the RST mission will have separated. A larger lens-source separation improves the ability to measure the lens-source relative proper motion via direct resolution of the source and lens, via a measurement of the elongation of the PSF, and/or via a color-dependent centroid shift. Requiring that the first two and last two seasons occur during the same year maximizes ability to measure the source parallax.

Most of the higher-level calibration products will be derived internally from the microlensing survey datasets. This includes PSF size and shape, flat-fielding, detector characteristics, etc. However, in some cases the properties of the microlensing survey may not be ideal for characterizing all possible detector artifacts. In particular, the survey fields may be too crowded, and the dither strategy may not be able to calibrate large-scale astrometric offsets. Therefore, we will require the following calibration data.

> **EML 2.3.13:** RST shall be capable of providing stepped observations of a crowded field (but less crowded than the microlensing fields) with offsets that sample astrometric distortions on all scales. These fields should have stars with good Gaia parallaxes to set the absolute scale of the astrometric positions of the stars.

3.7 General Observer Science Programs

The General Observer programs may not impose driving requirements on the mission. It is anticipated that the requirements needed for implementation of the mandated cosmology and exoplanet programs will lead to mission capabilities sufficient for ground-breaking general observer programs. However, the requirements for representative GO programs are described in this section to inform mission development. If such programs benefit from performance capabilities not encompassed by the baseline science programs, the Project may choose to implement these capabilities if the concomitant costs and other impacts to the mission are minimal.

The requirements in this section are limited to the Wide-Field Instrument, as each of the WFI science programs described above has specialized requirements driven by specific scientific investigations that may not reflect the diverse scientific interests of the GO community. The CGI program described above, however, is in essence a GO program by construction.

Structure and Evolution of the Milky Way with resolved stellar populations.

This program investigates the observing programs needed to study stellar populations in the Milky Way for purposes of characterizing the structure and evolution of the Galaxy, its satellite galaxies and globular clusters, stellar evolution and chemical evolution.

The observing requirements for this program include point-source photometry in a wide range of filters, and astrometric measurements to study kinematics of stellar populations (complementing Gaia data and extending their temporal baseline). The RST data will extend into the NIR, complementing the Gaia data at visible wavelengths, but will also extend to fainter populations. Thus, RST data at wavelengths well below 1 micron will also be valuable.

In particular, determining ages and metallicity in stellar populations is facilitated by availability of imaging data at the shortest wavelengths for which the RST Wide-Field Instrument has significant effective area.

---

[3] Although microlensing events that occur before or after the RST mission will obviously not be detectable by RST itself, high-resolution precursor observations of the RST field taken before the mission launch, or observations taken after the mission is over, can still measure the relative lens-source proper motion, and thus enable the measurement of angular Einstein ring radius.

The Milky Way contains many bright, nearby stars that will saturate the RST detectors. Ideally, there will be observing modes that will enable observations of such stars. At a minimum, chance observations of such stars should not cause damage to RST detectors or degrade data over a wide region of the field of view surrounding such sources.

Assembly history and evolution of nearby galaxies.

This program investigates the observing programs needed to use resolved stellar populations in nearby galaxies to study the assembly history of these galaxies and the evolution of their stellar content.

The observing requirements for this program include point-source photometry in crowded fields, with a wide range of filters. The filter set must be sufficient for identifying source types, extinction, and redshifts, by their spectral energy distribution.

Performance requirements relevant to this program include having a narrow point-spread function that varies relatively little over the instrument field of view, and which has a well-understood shape. Characterization of the PSF will be done internally from the data, so long as spatial and temporal variations are not too large. This will require the capability of performing accurate sub-pixel dithers (typically half-pixel steps, with $1/10^{th}$ pixel precision). There is no requirement for accurate absolute pointing.

This program benefits from having a flexible detector readout scheme, such as supporting a variable number of detector readouts per exposure, and logarithmically-spaced readouts as well as linearly-spaced readouts.

Galaxy evolution at high redshift.

This program investigates use of RST deep imaging data to study galaxy formation and evolution, early active galactic nuclei and quasars, the epoch of reionization, and the growth of structure from early times up to redshifts of about 1.

While extragalactic discoveries will continue apace over the next decade, RST will conduct a rich portfolio of science programs that require wide-area, space-based infrared capabilities and therefore cannot be executed by precursor facilities. Over the last twelve years, since the installation of WFC3 on HST and MOSFIRE on Keck, much has been learned about the rest-frame optical and UV properties of thousands of galaxies at redshifts $z>1$. The CANDELS (Grogin et al. 2011; Koekemoer et al. 2011) and UDF12 surveys (Ellis et al. 2013; Illingworth et al. 2013) and the Frontier Fields survey have provided galaxy stellar mass functions to $z\sim5$, UV luminosity functions to $z\sim8$, and initial hints of $z>9$ populations. The MOSDEF survey (Kriek et al. 2015) has conducted the first detailed studies of rest-frame optical line emission in galaxies at $z\sim2$-3, yielding metallicities and clues to the character of stellar populations in the most distant galaxies yet reachable. These IR studies and other powerful programs conducted by groups around the world have made tangible progress in understanding the evolution of galaxies, but an important context has been missing — the connection between galaxy properties and environment at $z>1$, where sample sizes are still orders of magnitude less than what RST will provide (Durkalec et al. 2014). Precursor facilities have introduced new detector technologies limited to relatively small imaging arrays and, with additional constraints from the telescope optical designs, multi-band space- based IR surveys to date have been limited to <1000 $arcmin^2$

in total. Surveys from the ground including DES, HSC, and LSST will improve upon these areas, but will lack the unique combination of IR sensitivity, angular resolution, and slitless spectroscopy offered by RST. These features afford an opportunity to connect stellar mass, star formation rates, AGN activity, and morphology to environment through spatial clustering at z>1. The environmental context provided by RST is a qualitatively new feature for an IR survey, and transcends a simple improvement in number counting statistics.

Beyond the context of environment, the areal coverage provided by RST enables additional important capabilities. Rare objects, such as the highest-redshift quasars, massive early galaxy clusters, and bright primordial galaxies, test the limits of our structure formation models (e.g., Efstathiou and Rees 1988) and provide the ability to probe the intergalactic medium in the distant past (Fan et al. 2006, Mortlock et al. 2011). With an appropriate cadence, RST surveys can discover rare and exotic cosmic explosions such as pulsational-pair and pair instability supernovae in the distant universe, revealing clues to the stellar populations in early-forming galaxies. RST can sample a representative volume of the universe at z>6, enabling us to retire cosmic variance uncertainty in the determination of the roles of galaxies and quasars during reionization of the universe. Further, RST alone can map the spatial distribution of galaxies at z>6 with sufficient depth and over large sky regions for comparison with redshifted 21 cm surveys. To create a complete picture of cosmic reionization, the landmark event of the early history of galaxy formation, we will need to link the topology of the neutral and ionized IGM during reionization with a corresponding galaxy population. In conjunction with 21cm observations, RST provides the only foreseeable prospect for completing our picture of the way reionization unfolds, complementing the faint ionizing sources to be discovered with JWST.

Some specific observatory capabilities that may not be captured in prior sections are:

Medium and ultra-deep surveys of the reionization epoch require z-band imaging, to provide a Lyman break selection veto for redshift z>7 samples.

Lyman alpha emission and clustering measurements during the end of reionization require the grism wavelength range to extend to ~1.0 microns, corresponding to a Lyman alpha redshift of z~7.25.

While NII and H-alpha will not be separately resolved by the grism at most redshifts or for all galaxy sizes, the ability to infer OIII, H-alpha, H-beta, and NII from grism observations would provide the ability to measure the excitation diagram for millions of galaxies at z~2. A grism resolution floor of R ~ 1200 is required to estimate the NII contribution to the NII+H-alpha unresolved line for a galaxy with 0.3” half-light radius. (Note that this requirement, like the HLSS requirements, needs simulations that model the observed galaxy size distribution to evaluate, as that influences the effective resolution of the grism spectra).

The RST HLS provides a unique opportunity to find high-redshift galaxies over thousands of square degrees. By operating at 265K, RST will gain additional sensitivity to high-redshift galaxy stellar mass and photometric redshift measurements over unprecedented areas of the sky. Owing to the additional sensitivity in a fixed exposure time, a 265K RST will gain in source counts expected for the HLS imaging survey at redshifts $5 \leq z \leq 10$ relative to the previous nominal 284K operating temperature. Using redshift-dependent rest-frame ultraviolet luminosity function parameters determined by Bouwens et al. 2015 (ApJ, 803, 34), the estimated number of

sources in a HLS = 2227 deg^2 survey, assuming sources at high-redshift are nearly flat in their rest-UV Fν spectrum (e.g., Dunlop et al. 2013, MNRAS, 432, 3520), improve by ~ 8% at z ~ 5 to ~ 16% at z ~ 10 in H-band. For F184, the gains are more dramatic and increase from ~ 197% gains at z ~ 5 to ~ 759% gains at z ~ 10.

Beyond the question of available source counts, the fidelity with which high-redshift galaxies can be identified depends on the photometric redshift constraints achievable as a function of the observatory operating temperature and the corresponding sensitivities at a fixed exposure time. The photometric redshift accuracy with observatory temperature was evaluated by modeling a redshift z ~ 8 galaxy with H=26.62AB apparent magnitude. A realistic spectral energy distribution template was selected based on systems comparable to those found in the UDF12 observations, which are Y-band dropouts with roughly flat rest-frame ultraviolet spectra in Fν , and then expected Y, J, and F184 magnitudes computed using simple models for the RST filter response. Many realizations of the random noise in each band were simulated for the T = 260K, 284K, and 288K sensitivities, and then the simulated photometry results were fit in an attempt to recover the photometric redshift. The simulations show that for an operating temperature of T = 260K, fully 89% of realizations provide valid solutions (e.g., $7.5 \leq z \leq 8.5$) to the true redshift z ~ 8 of the object. This degrades to only 71% at an operating temperature of T = 288K. Importantly, the number of catastrophic errors with z ~ 2 solutions increases from 4% at T=260K to 18% at T=288K. A warmer operating temperature will lead to a factor of ~ 4× more catastrophic errors in photometric selections in high-redshift galaxies.

Another important application for the H- and F184-band photometry regards the stellar mass determination of galaxies at z ~ 3. The stellar mass inferred from the strength of the optical emission will be influenced by the precision of the near infrared photometry. The SED simulation was repeated for an H=26.62 galaxy at z ~ 3, with an extinction of $E(B - V) \approx 0.15$, stellar age of 500Myr, and a stellar mass of $M_\star \approx 109 M_\odot$ to probe the constraints on stellar mass given the HLS depths as a function of temperature. These constraints are challenging near the sensitivity limit of the survey, and correspondingly the simulations find that the fraction of realizations that provide acceptable stellar mass fits within the range $\log10\ M_\star/M_\odot = [8.5, 9.5]$ increases by ~ 18% from 57% at T=288K to 67% at T=260K. A lower operating temperature is therefore expected to substantially improve the stellar mass constraints on faint sources near the HLS detection limit.

Cosmic Dawn.

This program investigates use of deep wide-field grism spectroscopy to study the epoch of the formation of the first galaxies and quasars, and the consequent reionization of the universe. At present, the requirements for this program are a subset of those for the high-latitude spectroscopic survey program.

3.7.1 General Observer Program: Science Data Records

GO 2.1.1: RST shall be able to produce mosaic images of the General Observer (GO) imaging fields in each filter at each epoch of observation, using coordinates tied to the astrometric frame defined by the International Celestial Reference Frame (ICRF).

Mosaic here means coadded exposures of any given field, resampled as necessary to correct for geometric distortion in the data.

GO 2.1.2: RST shall be able to produce GO mosaics that include information on the flux uncertainty for each pixel, effective bandpass as a function of position, data quality flags, and additional data generated in producing the mosaics that characterize or support the mosaic generation process.

GO 2.1.3: RST shall be able to produce a catalog of each source in the GO imaging fields containing, at a minimum, positions, fluxes, and object classification information.

GO 2.1.4: RST shall be able to produce a catalog that includes statistical uncertainties for each quantity in the catalog determined from GO observations, as well as data quality flags where numeric uncertainties are not applicable.

GO 2.1.5: RST shall be able to produce a catalog of each source in GO grism or prism fields and associate spectra (or a range of spectral image pixels) with corresponding objects in the GO imaging catalog.

GO 2.1.6: RST shall be able to produce GO catalog grism or prism spectra that include information on uncertainties in the measured fluxes and wavelengths, effective LSF as a function of wavelength, data quality flags, and an estimate of contamination from the overlap of different spectra.

Comment: Information on the line-spread function may be in the form of model parameters.

3.7.2 General Observer Program: Calibrated Data Records

The nature of individual GO observing programs may be such that self-calibration techniques are not applicable. Likewise, due to variations over time or to nature of the sources being observed, the calibrations derived over the course of the big surveys may be less accurate for GO programs or not applicable. Hence, the calibration requirements in this section are less stringent than those of the cosmology or microlensing programs.

GO 2.2.1: RST shall be able to archive GO calibrated images with the PSF for each exposure specified as a function of position on the focal plane, the effective bandpass as a function of position and incorporate any World Coordinate System information needed for subsequent stages of processing.

Comment: The PSF can be provided in the form of model parameters and software that computes the PSF from the model.

GO 2.2.2: RST shall be able to provide GO calibrated data records with absolute photometry of point sources calibrated in one or more of the standard filters with a goal of better than 3% accuracy.

Comment: Goal for absolute photometric calibration is 3%.

GO 2.2.3: RST shall be able to provide GO calibrated data records with a goal of knowledge of the relative photometric zero-points of the filters better than 1%.

Comment: Goal for knowledge of the relative filter zero-points is <1%.

GO 2.2.4: RST shall be able to provide GO calibrated data records with the variation of the total system response known as a function of position within the field of view, such that the total flux of a point source with a known Spectral Energy Distribution (SED) can be corrected to a common filter system with a goal of better than 1% accuracy when imaged at any point on the focal plane.

Comment: Goal for accuracy of this correction is 1%.

GO 2.2.5: RST shall be able to provide GO calibrated data records with a relative photometric calibration in each filter that is spatially uniform over the WFI field of view, with a goal of systematic spatial variations being less than 1%.

Comment: Goal for calibration uniformity <1% RMS.

GO 2.2.6: RST shall be able to provide GO calibrated data records with a known systematic uncertainty in the astrometric accuracy, with a goal of 10 mas for absolute positions and 5mas for relative positions of objects within a given SCA.

Comment: Goal for relative uncertainty of the astrometric solution of multiple images of a given field is < 5mas.

GO 2.2.7: RST shall be able to archive GO calibrated spectra for each grism or prism exposure.

GO 2.2.8: RST shall be able to provide GO spectra with a goal for systematic wavelength uncertainty $\sigma\lambda$ of $\sigma\lambda/\lambda \leq 0.002$.

Comment: The goal for uncertainty of the wavelength measurement σ_λ of $\sigma_\lambda/\lambda \leq 0.002$.

GO 2.2.9: RST shall be able to provide calibrated GO grism or prism spectra with known uniformity of the relative spectrophotometric flux calibration, with a goal of <5% for systematic uncertainties in knowledge of the spatial variation.

Comment: The goal is to achieve uniformity of 5 percent or better over the area of the observing program.

GO 2.2.10: RST shall be able to provide calibrated GO spectra with a known relative wavelength-dependence of the spectrophotometric flux calibration, with a goal of <5% for systematic uncertainty in knowledge of the wavelength dependence.

Comment: The goal is to achieve knowledge of the wavelength dependence to 5 percent or better.

3.7.3 General Observer Program – Raw Data Records

GO 2.3.1: RST shall be able to provide GO raw images (direct images or grism or prism spectral images) in the archive for each detector exposure with each raw data record including a unique dataset identifier for each exposure, the exposure time, the time of exposure, all individual downlinked detector readouts used to make the exposure, the observatory pointing orientation and any additional engineering data the Science Center uses for subsequent processing.

GO 2.3.2: RST shall be capable of providing access to any field on the sky for GO observations during the prime mission lifetime.

Comment: This is intended to prevent the cosmology or microlensing programs from consuming all of the schedulable time for any given region on the sky.

GO 2.3.3: RST shall be capable of providing GO raw images at wavelengths 1.95 - 2.30 microns.

Comment: Extend survey capability over the full bandpass that is practical for the telescope and wide-field instrument.

3.8 Guest Investigator Program

The Guest Investigator (GI) program enables scientists to make use of RST data for research in any area of astrophysics. Access to RST data is provided by the archive, and will be done in the same manner for guest investigators as for the science teams selected to perform the projects described earlier in this document.

High-level descriptions of many of the data products to be included in the archive are provided among the requirements for the individual science programs earlier in this document and won't be repeated here. Requirements on archive capabilities not specific to any single science investigation are as follows.

AR 2.0.1: RST shall provide an archive containing all the science data from the mission, including raw and calibrated data, and high-level science products such as source catalogs derived from the science data.

AR 2.0.2: The RST archive shall include all the housekeeping data needed for processing or reprocessing the science data.

AR 2.0.3: RST science data products shall be publicly accessible.

Reserved

It is anticipated that it will be highly desirable for the RST archive to provide links to relevant data in other archives that were not produced by RST but which will be important for achieving RST scientific goals. The nature of such inter-archive exchanges is under investigation.

AR 2.0.5: The RST archive shall provide query tools that enable selection of sets of observations or sources that meet user-specified criteria. Examples include observation date, pointing, instrument configuration, or object-catalog entries.

AR 2.0.6: The RST archive shall allow users to download datasets identified in a user query. Downloads may be subject to practical limits on the size of the selected datasets and applicable policy restrictions.

AR 2.0.7: The RST archive shall be able to ingest user-supplied ("Level-5") data products. Ingestion of user-supplied data products may be subject to applicable policy restrictions on size, format, and documentation.

AR 2.0.8: The RST archive shall enable users to cross-match the RST source catalog with select non-RST datasets. [This can be made more specific at lower levels].

AR 2.0.9: The RST archive shall provide functionalities for extracting cutouts of images and spectra for any source in the catalog, or list of sources. Such user requests may be subject to applicable policy restrictions on the size of the list and the resulting data volume.

AR 2.0.10: The RST Archive shall provide tools for exploratory data visualization and analysis.

4 APPENDICES

4.1 Deriving the Microlensing Survey Yield and Associated Uncertainties

Quantitative predictions for the yields of a given realization of an exoplanet survey dataset require sophisticated simulations that incorporate models for the Galactic distribution of lenses and sources to simulate and evaluate the detectability of events with realistic photometric precision. In particular, the source star density and event rate are strong functions of Galactic coordinates, and the detection probability of a planet with a given set of properties depends sensitively on the detailed properties of the event (host star mass and distance, event duration, angular source size, photometric precision, cadence).

The basic input ingredients that are required for estimating the yield of a microlensing exoplanet survey are a (1) model for the spatial, kinematic, and luminosity distribution of source stars, (2) model for the spatial, mass, and kinematic distributions of the host lenses, which are then used to estimate microlensing event rates and event parameter distributions, and (3) a model for the probability distribution of planets as a function of planet mass and semi-major axis, and host mass and distance. Unfortunately, for the regimes of interest for RST, the properties of the populations of sources and host lenses are poorly constrained by empirical data, leading directly to relatively large uncertainties in the final yields. In particular, the magnitude distribution of source stars in the fields of interest has not been measured in the passbands and to the faint magnitudes that will be probed by RST. Similarly, the microlensing event rates for some of the fields of interest have not been measured, as these fields typically suffer high optical extinction, and to date all microlensing surveys have been performed in the far optical. These uncertainties are a direct result of the fact that WIFRST will probe regions of parameter space that have yet to be explored with current space and ground-based facilities. These uncertainties lead directly to uncertainties in the yield of planets that we can expect, but these uncertainties are dwarfed by the uncertainties in the planet populations themselves, which is precisely what we aim to determine.

The event rates and source stars densities adopted for RST were scaled to match published microlensing optical depth estimates (Popowski et al. 2005, Sumi et al. 2006, Hamadache et al. 2006, Alcock et al. 2000, Sumi et al. 2003) and source star luminosity function (Holtzman et al. 1998) from fields further from the plane than the preferred RST fields. The MOA team has recently performed a preliminary analysis of the 2006-2007 MOA-II data (Sumi et al. 2011) and used this to determine the optical depth and event rate toward each of the 22 MOA fields, each covering 2.2 deg^2. Four of these fields contain 45% of all the analyzed microlensing events and overlap with (or are very close to) some of the proposed RST fields. These results indicate a significantly higher optical depth than assumed in this report. Because they are based on preliminary, unpublished MOA-II data and analysis, we have chosen to be conservative and not use these for our baseline yields. However, we note that they have much higher statistical weight than the published results, and if they are correct, our planet yields are significantly underestimated. Nevertheless, these uncertainties in the planet populations themselves, which is precisely what we aim to determine, are dwarfed by the other uncertainties, and are therefore unlikely to affect our choice target fields substantially.

Another, somewhat subtler, source of uncertainty in the planet yields that may significantly impact the choice of target fields is the relative frequency of planets in the Galactic Bulge versus disk. The relative contribution of the Bulge and disk lenses to the event rate varies as a function

of Galactic latitude **b**, with Bulge lenses expected to dominate at low |**b**| (Gould 1995). If the Galactic Bulge happens to be devoid of planets, e.g., because of an extreme radiation environment during a starburst-like Bulge formation event (Thompson 2013), then it would likely be desirable to avoid such low latitude fields.

Finally, the yields for planets near the edge of the sensitivity of RST suffer from additional uncertainties beyond those arising the sources discussed above. This is due to the relatively strong dependence of number of detections on $\Delta\chi^2$ in these regimes, which includes planets with very small or very large separations, and very low mass planets. As a result of the strong scaling with $\Delta\chi^2$, small differences in the assumptions and approximations needed to make these predictions result in large changes in the estimates of the number of detected planets.

Predictions for the yield of habitable planets suffer from all of the uncertainties above, but are also sensitive to additional assumptions, such as the mass-bolometric luminosity relationship for stars in the Bulge and disk, the age and metallicity of the stars in the Bulge and disk, and the precise definitions for the mass and semi-major axes boundaries of the habitable zone. Therefore, the yields of habitable planets are particularly uncertain. Initial estimates indicate that RST will be sensitive to habitable planets, if the intrinsic frequency is large. However, substantially more work needs to be done to provide robust estimates of the habitable planet yield.

4.2 Threshold Requirements

Threshold performance requirements are not flowed down to lower levels, but it is instructive to define them at a top level for future reference.

4.2.1 Threshold Dark Energy Science Requirements for the HLSS

Threshold HLSS 2.0.1: RST shall be capable of executing a high-latitude spectroscopic survey that can, if allocated 0.64 years of total observing time, achieve BAO constraints that yield$FoM_{BAO} \geq FoM_{BAO,ref} / 4 = 2825$,

including statistical errors and observational systematic uncertainties, with FoM_{BAO} and $FoM_{BAO,ref}$ computed as described in Section 0.

Comment: A factor of 4 degradation in the FoM would correspond to a factor of two degradation in the errors on $D_A(z)$ and $H(z)$. We do not define a separate threshold requirement for RSD. If the HLSS cannot meet baseline requirements but does exceed the BAO threshold requirement, then RSD analyses will be carried out on a best-effort basis using the data set collected for BAO. We do not define individual threshold requirements for each of the more specific requirements below. Rather, the governing principle for thresholds is that the overall BAO performance forecast should still satisfy the above threshold requirement even if some individual requirements do not meet baseline.

4.2.2 Threshold Dark Energy Science Requirements for the HLIS

Threshold HLIS 2.0.1: RST shall be capable of executing a high-latitude imaging survey that can, in 1.07 years of total observing time, achieve WL constraints that yield

$FoM_{WL} \geq FoM_{WL,ref} / 4 = 143250$,

including statistical and systematic errors, with FoM_{WL} and $FoM_{WL,ref}$ computed as described above.

A factor of 4 degradation in the FoM would correspond to a factor of two degradation in the errors on $\sigma_m(z)$. This would still represent a factor of ≈ 20 improvement on current knowledge.

4.2.3 Threshold Dark Energy Requirements for the Supernova Survey

Threshold SN 2.0.1: RST shall be capable of executing a supernova Type Ia survey that can, if allocated 0.5 years of total observing time, achieve constraints that yield

$FoM_{SN} \geq FoM_{SN,Ref} / 4 = 162.5$.

A factor of 4 degradation in the FoM would still correspond to a factor of 5 improvement over current knowledge.

4.2.4 Threshold Level-2 Science Requirements for the Microlensing Survey

EML 1-T: RST shall measure the mass function of exoplanets with masses between 1 M_{Earth} and 30 $M_{Jupiter}$ and orbital semi-major axes ≥ 1 AU to better than 20% per decade in mass.

EML 2-T: RST shall measure the frequency of Mars-mass objects to 35%.

EML 3-T: RST shall determine the masses of, and distances to, host stars of 20% of the host stars of detected planets with a precision of 20% or better.

EML 4-T: RST shall measure the frequency of free floating planetary-mass objects in the Galaxy from Mars to 10 Jupiter masses in mass. If there is one M_{Earth} free-floating planet per star, measure this frequency to better than 35%.

EML 5-T: RST shall estimate η_{Earth} to a precision of 0.3 dex via extrapolation from larger and longer-period planets.

Comment: Our approach to setting our threshold requirements is to assume our yield will be half that of our baseline survey yield. A factor of two fewer detections leads to a Poisson uncertainty on the mass function, frequency of Mars mass planets, Earth mass free-floating planets, and our estimate of η_{Earth}, that is $0.5^{-1/2}$=1.41 times higher, and leads to a number of host stars with mass measurements with precisions of 20% that is 0.5 times lower.

5 TRACEABILITY MATRIX

The following tables list all of the requirements in the SRD. For each requirement the parent and child requirements are listed, and for data products the mission element responsible for meeting the requirement is listed in the column labeled ‘Recipient’. For data products designated as 'GND', the ground system is responsible for developing the data processing software and generating the data products, perhaps employing algorithms provided by SITs. For requirements on data products where the Recipient is labeled “GND+SIT”, GND will provide a basic data product satisfactory for many users, but data products meeting quantitative performance requirements are the responsibility of a SIT. The Ground System Requirements Document will specify which Ground Segment element (STScI, IPAC, or international partner) is responsible for each requirement labeled as 'GND'. For requirements on data products where the Responsible Element is labeled “SIT”, there is no counterpart provided by the ground system. The products are generated by the relevant Science Investigation Team (SIT) and delivered to the archive.

High Latitude Spectroscopic Survey - Survey Capability Requirements				
Reqmt	**SRD Requirement text**	**Parent (DOORS Out-links)**	**Child (DOORS In-links)**	**Recipient**
HLSS 2.0.1	RST shall be capable of executing a high-latitude spectroscopic survey that can, if allocated 0.64 years of total observing time, achieve BAO constraints that yield $FoM_{BAO} \geq FoM_{BAO,ref} / 1.5 = 7533$, including statistical errors and observational systematic uncertainties, with FoM_{BAO} and $FoM_{BAO,ref}$ computed as described in Section 3.3.1.	PLRA-12 **OBJ-2.1.1** PLRA-14 **OBJ-2.1.2** PLRA-16 **OBJ-2.1.3**	SRD-9 **HLSS 2.0.3** SRD-10 **HLSS 2.0.4** SRD-11 **HLSS 2.0.5**	
HLSS 2.0.2	RST shall be capable of executing a high-latitude spectroscopic survey that can, if allocated 0.64 years of total observing time, achieve RSD constraints that yield $FoM_{RSD} \geq FoM_{RSD,ref} / 1.5 = 4047$, including statistical errors and observational systematic uncertainties, with FoM_{RSD} and $FoM_{RSD,ref}$ computed as described in Section 3.3.1.	PLRA-12 **OBJ-2.1.1** PLRA-14 **OBJ-2.1.2** PLRA-16 **OBJ-2.1.3**	SRD-9 **HLSS 2.0.3** SRD-10 **HLSS 2.0.4** SRD-11 **HLSS 2.0.5**	
HLSS 2.0.3	RST shall be capable of executing a slitless spectroscopic survey covering the wavelength range $1.35\ \mu m \leq \lambda \leq 1.90\ \mu m$ with RMS redshift errors $\sigma_z \leq 0.001(1+z)$, reaching emission line flux sensitivity of 1.0×10^{-16} erg cm^{-2} s^{-1} for a point source at 1.8 μm with a net survey speed that is at least 0.34 deg^2/hr.	PLRA-84 **BSR1** PLRA-88 **BSR5** SRD-7 **HLSS 2.0.1** SRD-8 **HLSS 2.0.2**	MRD-11 MRD-32 MRD-152 MRD-340 MRD-432 MRD-433 MRD-434 MRD-475 MRD-477 SRD-16 **HLSS 2.1.5** SRD-17 **HLSS 2.1.6** SRD-18 **HLSS 2.1.7** SRD-19 **HLSS 2.1.8** SRD-20 **HLSS 2.1.9** SRD-21 **HLSS 2.1.10** SRD-22 **HLSS 2.1.11** SRD-28 **HLSS 2.3.2** SRD-29 **HLSS 2.3.3** SRD-30 **HLSS 2.3.4**	

High Latitude Spectroscopic Survey - Survey Capability Requirements				
Reqmt	**SRD Requirement text**	**Parent (DOORS Out-links)**	**Child (DOORS In-links)**	**Recipient**
HLSS 2.0.4	Roman shall be capable of conducting an HLSS with an average completeness ≥ 0.6.	SRD-7 **HLSS 2.0.1** SRD-8 **HLSS 2.0.2**	SRD-12 **HLSS 2.1.1** SRD-14 **HLSS 2.1.3** SRD-15 **HLSS 2.1.4** SRD-16 **HLSS 2.1.5** SRD-17 **HLSS 2.1.6** SRD-18 **HLSS 2.1.7** SRD-19 **HLSS 2.1.8** SRD-20 **HLSS 2.1.9** SRD-22 **HLSS 2.1.11** SRD-26 **HLSS 2.2.4** SRD-32 **HLSS 2.3.6**	SIT
HLSS 2.0.5	Galaxies counted towards meeting requirements HLSS 2.0.3-2.0.4, shall have RMS redshift errors $\sigma z \leq 0.001(1+z)$, after excluding galaxies larger than 0.54” in radius and excluding outliers, with a fraction of outliers less than 10% of the sample smaller than 0.54" in radius , and with outliers defined as $\lvert z_{obs}-z_{true}\rvert/(1+z_{true})>0.005$.	SRD-7 **HLSS 2.0.1** SRD-8 **HLSS 2.0.2**	SRD-13 **HLSS 2.1.2** SRD-14 **HLSS 2.1.3** SRD-15 **HLSS 2.1.4** SRD-16 **HLSS 2.1.5** SRD-17 **HLSS 2.1.6** SRD-18 **HLSS 2.1.7** SRD-19 **HLSS 2.1.8** SRD-20 **HLSS 2.1.9** SRD-22 **HLSS 2.1.11** SRD-24 **HLSS 2.2.2** SRD-28 **HLSS 2.3.2** SRD-30 **HLSS 2.3.4** SRD-31 **HLSS 2.3.5** SRD-32 **HLSS 2.3.6**	SIT

High Latitude Spectroscopic Survey Science Data Records				
Reqmt	**SRD Requirement text**	**Parent (DOORS Out-links)**	**Child (DOORS In-links)**	**Recipient**
HLSS 2.1.1	RST shall provide sufficient information to characterize completeness and survey depth as a function of sky position and redshift, with sufficient detail and accuracy that associated systematic uncertainties in galaxy clustering cause ≤ 20% degradation in the BAO and RSD figures of merit.	SRD-10 **HLSS 2.0.4**	MRD-330 SRD-14 **HLSS 2.1.3** SRD-15 **HLSS 2.1.4** SRD-16 **HLSS 2.1.5** SRD-17 **HLSS 2.1.6** SRD-18 **HLSS 2.1.7** SRD-19 **HLSS 2.1.8** SRD-20 **HLSS 2.1.9** SRD-22 **HLSS 2.1.11** SRD-25 **HLSS 2.2.3** SRD-26 **HLSS 2.2.4** SRD-32 **HLSS 2.3.6**	SIT
HLSS 2.1.2	RST shall provide sufficient information to enable determination of the incidence of outliers, to a fraction of 2.5×10-3 of the full galaxy sample over the entire survey redshift range.	SRD-11 **HLSS 2.0.5**	MRD-330 SRD-14 **HLSS 2.1.3** SRD-15 **HLSS 2.1.4** SRD-16 **HLSS 2.1.5** SRD-17 **HLSS 2.1.6** SRD-18 **HLSS 2.1.7** SRD-19 **HLSS 2.1.8** SRD-20 **HLSS 2.1.9** SRD-22 **HLSS 2.1.11** SRD-24 **HLSS 2.2.2** SRD-31 **HLSS 2.3.5** SRD-32 **HLSS 2.3.6**	SIT
HLSS 2.1.3	RST shall associate spectra (or a range of spectral image pixels) with the corresponding objects in the imaging catalog.	SRD-10 **HLSS 2.0.4** SRD-11 **HLSS 2.0.5** SRD-12 **HLSS 2.1.1** SRD-13 **HLSS 2.1.2**	MRD-337 SRD-22 **HLSS 2.1.11**	GND
HLSS 2.1.4	RST HLSS catalog spectra derived from individual exposures shall include information on flux uncertainty, effective line-spread function (LSF) as a function of position and wavelength, data quality flags, and an estimate of contamination from the overlap of different spectra.	SRD-10 **HLSS 2.0.4** SRD-11 **HLSS 2.0.5** SRD-12 **HLSS 2.1.1** SRD-13 **HLSS 2.1.2**	MRD-337	GND

High Latitude Spectroscopic Survey Science Data Records				
Reqmt	**SRD Requirement text**	**Parent (DOORS Out-links)**	**Child (DOORS In-links)**	**Recipient**
HLSS 2.1.5	RST shall produce a single net spectrum for each source by combining HLSS spectra from multiple roll angles.	SRD-9 **HLSS 2.0.3** SRD-10 **HLSS 2.0.4** SRD-11 **HLSS 2.0.5** SRD-12 **HLSS 2.1.1** SRD-13 **HLSS 2.1.2**	MRD-337	GND
HLSS 2.1.6	RST shall be capable of obtaining spectra at nearly opposing roll angles to account for possible offsets of the emitting region from the center of the broad-band image.	SRD-9 **HLSS 2.0.3** SRD-10 **HLSS 2.0.4** SRD-11 **HLSS 2.0.5** SRD-12 **HLSS 2.1.1** SRD-13 **HLSS 2.1.2**	SRD-31 **HLSS 2.3.5**	
HLSS 2.1.7	RST shall provide the following additional information for each net extracted spectrum (HLSS 2.1.5): uncertainties in the measured fluxes and wavelengths, effective line-spread function as a function of wavelength, data quality flags, and additional data generated in producing the spectra that characterize or support the spectra generation process.	SRD-9 **HLSS 2.0.3** SRD-10 **HLSS 2.0.4** SRD-11 **HLSS 2.0.5** SRD-12 **HLSS 2.1.1** SRD-13 **HLSS 2.1.2**	MRD-337 SRD-23 **HLSS 2.2.1** SRD-27 **HLSS 2.3.1**	GND
HLSS 2.1.8	RST shall provide HLSS science data records with redshifts as well as best fit spectral templates associated with that redshift.	SRD-9 **HLSS 2.0.3** SRD-10 **HLSS 2.0.4** SRD-11 **HLSS 2.0.5** SRD-12 **HLSS 2.1.1** SRD-13 **HLSS 2.1.2**	MRD-337	GND
HLSS 2.1.9	RST shall provide HLSS science data records with wavelengths and integrated fluxes of emission lines, as applicable.	SRD-9 **HLSS 2.0.3** SRD-10 **HLSS 2.0.4** SRD-11 **HLSS 2.0.5** SRD-12 **HLSS 2.1.1** SRD-13 **HLSS 2.1.2**	MRD-337	GND
HLSS 2.1.10	RST shall provide HLSS science data records with relative position measurement uncertainties less than 3.4” over the entire survey area.	SRD-9 **HLSS 2.0.3**	MRD-32 MRD-153 MRD-340	GND
HLSS 2.1.11	RST shall be capable of providing images and corresponding source catalogs of the HLSS fields that reach JAB=24.0, HAB=23.5, and F184AB=23.1 for an reff=0.3″ source at 10sigma to achieve a reference image position, in 3 filters.	SRD-9 **HLSS 2.0.3** SRD-10 **HLSS 2.0.4** SRD-11 **HLSS 2.0.5** SRD-12 **HLSS 2.1.1** SRD-13 **HLSS 2.1.2** SRD-14 **HLSS 2.1.3**	MRD-153 MRD-154 MRD-340 MRD-430	

High Latitude Spectropic Survey - Survery Capability Requirements				
Reqmt	**SRD Requirement text**	**Parent (DOORS Out-links)**	**Child (DOORS In-links)**	**Recipient**
HLSS 2.2.1	RST shall archive HLSS calibrated spectra for each grism exposure.	SRD-18 **HLSS 2.1.7**	MRD-329 MRD-337 SRD-27 **HLSS 2.3.1**	GND
HLSS 2.2.2	RST shall provide HLSS calibrated spectra with an uncertainty of the wavelength measurement σ_λ of $\sigma_\lambda/\lambda \leq 0.001$.	SRD-11 **HLSS 2.0.5** SRD-13 **HLSS 2.1.2**	MRD-340 MRD-444 SRD-28 **HLSS 2.3.2**	GND
HLSS 2.2.3	RST shall provide HLSS calibrated spectra with an uncertainty in the wavelength calibration that does not introduce biases to the wavelength measurement by amounts greater than $\sigma\lambda/\lambda \leq 10^{-4}$ on any angular scales exceeding 0.064 degrees within a field, and $\sigma\lambda/\lambda \leq 1\times10^{-4}$ from field to field.	SRD-12 **HLSS 2.1.1**	MRD-330 MRD-340	GND+SIT
HLSS 2.2.4	RST shall provide calibrated spectra with relative spectrophotometric flux calibration uniform to 2 percent (with the goal of 1%) over the area and wavelength range of the survey.	SRD-10 **HLSS 2.0.4** SRD-12 **HLSS 2.1.1**	MRD-330 MRD-340 MRD-384 SRD-32 **HLSS 2.3.6**	GND+SIT

High Latitude Spectroscopic Survey - Raw Data Record Requirements				
Reqmt	**SRD Requirement text**	**Parent (DOORS Out-links)**	**Child (DOORS In-links)**	**Recipient**
HLSS 2.3.1	RST shall provide raw spectral images in the archive for each downlinked detector readout with each raw data record including a unique dataset identifier for each exposure, the exposure time, the time of exposure, all individual downlinked detector readouts used to make the exposure, the observatory pointing orientation and any additional engineering data the Science Center uses for subsequent processing.	SRD-18 **HLSS 2.1.7** SRD-23 **HLSS 2.2.1**	MRD-329 MRD-337	GND
HLSS 2.3.2	RST shall provide HLSS raw spectral images with a spectral dispersion between 10 Å/pix and 12 Å/pix over the full bandpass and across the full field.	SRD-9 **HLSS 2.0.3** SRD-11 **HLSS 2.0.5** SRD-24 **HLSS 2.2.2**	MRD-161 MRD-430	
HLSS 2.3.3	RST shall provide raw spectral images for the HLSS with wavelength range of at least 1.32 to 1.93 µm.	SRD-9 **HLSS 2.0.3**	MRD-161 MRD-430	
HLSS 2.3.4	RST shall provide HLSS raw spectral images with 50% of the energy enclosed in a circle of radius <0.21" at 1.5 µm for a monochromatic point source, excluding diffraction spikes and non-first order light and including the effects of pointing jitter, for at least 95% of the exposures and over 95% of the FOV.	SRD-9 **HLSS 2.0.3** SRD-11 **HLSS 2.0.5**	MRD-355 MRD-394 MRD-395 MRD-430	
HLSS 2.3.5	RST shall be capable of providing HLSS raw spectral images of each field with a minimum of 3 dispersion directions, with two being 180 +/- 30 degrees opposed.	SRD-11 **HLSS 2.0.5** SRD-13 **HLSS 2.1.2** SRD-17 **HLSS 2.1.6**	MRD-44 MRD-340 MRD-430	
HLSS 2.3.6	RST shall be capable of obtaining 20 spectroscopic observations in the HLSS deep fields with dispersion directions of the observations roughly evenly distributed between 0 and 360 degrees.	SRD-10 **HLSS 2.0.4** SRD-11 **HLSS 2.0.5** SRD-12 **HLSS 2.1.1** SRD-13 **HLSS 2.1.2** SRD-26 **HLSS 2.2.4**	MRD-340 MRD-430	

High Latitude Imaging Survey - Survey Capability Requirements				
Reqmt	**SRD Requirement text**	**Parent (DOORS Out-links)**	**Child (DOORS In-links)**	**Recipient**
HLIS 2.0.1	RST shall be capable of executing a high-latitude imaging survey that can, in 1.07 years of total observing time, achieve WL constraints that yield $FoM_{WL} \geq FoM_{WL,ref} / 1.75 = 327400$, including statistical and systematic errors, with FoM_{WL} and $FoM_{WL,ref}$ computed as described above.	PLRA-12 **OBJ-2.1.1** PLRA-14 **OBJ-2.1.2** PLRA-16 **OBJ-2.1.3**	SRD-34 **HLIS 2.0.2** SRD-37 **HLIS 2.0.5**	
HLIS 2.0.2	RST shall be capable of executing a High Latitude Imaging Survey to measure galaxy shapes with a total effective galaxy density of at least $n_{eff} = 27$ per arcmin^2 in at least two bands, and three bands for at least half of these galaxies, and photometry in 4 NIR bands to support photometric redshift determination, with a net survey speed that is at least 0.20 deg^2/hr.	PLRA-88 **BSR5** SRD-33 **HLIS 2.0.1**	MRD-11 MRD-32 MRD-152 MRD-340 MRD-414 MRD-432 MRD-433 MRD-434 MRD-475 MRD-477 SRD-35 **HLIS 2.0.3** SRD-36 **HLIS 2.0.4** SRD-38 **HLIS 2.1.1** SRD-39 **HLIS 2.1.2** SRD-40 **HLIS 2.1.3** SRD-41 **HLIS 2.1.4** SRD-42 **HLIS 2.1.5** SRD-44 **HLIS 2.1.7** SRD-46 **HLIS 2.1.9** SRD-47 **HLIS 2.1.10** SRD-48 **HLIS 2.1.11** SRD-53 **HLIS 2.2.2** SRD-60 **HLIS 2.2.9** SRD-61 **HLIS 2.2.10** SRD-62 **HLIS 2.2.11** SRD-64 **HLIS 2.3.2**	

High Latitude Imaging Survey - Survey Capability Requirements				
Reqmt	**SRD Requirement text**	**Parent (DOORS Out-links)**	**Child (DOORS In-links)**	**Recipient**
HLIS 2.0.3	RST shall enable shear measurements with additive shear errors A limited in RMS per component over the range of angular multipoles $1.5 < \log_{10}\ell < 3.5$ as specified below: $\sqrt{\sum A^2 S} < 7.0 \times 10^{-5}$ for $1.5 < \log_{10}\ell < 2.0$ $\sqrt{\sum A^2 S} < 9.9 \times 10^{-5}$ for $2.0 < \log_{10}\ell < 2.5$ $\sqrt{\sum A^2 S} < 1.4 \times 10^{-4}$ for $2.5 < \log_{10}\ell < 3.0$ $\sqrt{\sum A^2 S} < 1.9 \times 10^{-4}$ for $3.0 < \log_{10}\ell < 3.5$ where the sum is over independent terms in the additive systematic budget. The total additive systematic budget, obtained via RSS of the scale bins, is 2.7×10^{-4}.	SRD-34 **HLIS 2.0.2**	SRD-50 **HLIS 2.1.13** SRD-51 **HLIS 2.1.14** SRD-54 **HLIS 2.2.3** SRD-56 **HLIS 2.2.5** SRD-57 **HLIS 2.2.6**	
HLIS 2.0.4	RST shall enable shear measurements with multiplicative shear errors M shall be known to $\sqrt{\sum M^2 S} < 3.2 \times 10^{-4}$ where the sum is over independent terms in the multiplicative systematic budget.	SRD-34 **HLIS 2.0.2**	SRD-50 **HLIS 2.1.13** SRD-51 **HLIS 2.1.14** SRD-55 **HLIS 2.2.4**	
HLIS 2.0.5	RST shall be capable of observing a deep field of at least 6 deg^2 within the HLIS with a depth five times greater (in inverse variance) than the main survey in each of the HLIS filters, and with at least twice the number of dither and roll positions as the broader HLIS.	SRD-33 **HLIS 2.0.1**	MRD-340 SRD-67 **HLIS 2.3.5**	

High Latitude Imaging Survey - Science Data Records				
Reqmt	**SRD Requirement text**	**Parent (DOORS Out-links)**	**Child (DOORS In-links)**	**Recipient**
HLIS 2.1.1	RST shall be capable of producing mosaic images of the HLIS fields using data in each filter, and using coordinates tied to the astrometric frame defined by the ICRF.	SRD-34 **HLIS 2.0.2**	MRD-329 MRD-337 SRD-52 **HLIS 2.2.1** SRD-63 **HLIS 2.3.1**	GND
HLIS 2.1.2	RST shall be capable of producing HLIS mosaics that include information on the flux uncertainty or effective depth as a function of position, data quality flags, and additional data generated in producing the mosaics that characterize or support the mosaic generation process.	SRD-34 **HLIS 2.0.2**	MRD-329 MRD-337 SRD-52 **HLIS 2.2.1** SRD-63 **HLIS 2.3.1**	GND
HLIS 2.1.3	RST shall be capable of producing a catalog containing information for each detected source in the HLIS field, including positions, classifications, photometry (e.g. aperture photometry, model fits, adaptive moment photometry), and limited time domain information for variable sources.	SRD-34 **HLIS 2.0.2**	MRD-330 MRD-337 SRD-52 **HLIS 2.2.1** SRD-60 **HLIS 2.2.9** SRD-61 **HLIS 2.2.10** SRD-62 **HLIS 2.2.11** SRD-63 **HLIS 2.3.1**	GND+SIT
HLIS 2.1.4	RST shall be capable of producing a catalog containing information for each detected source in the HLIS field, image moments (through at least 2nd order) in each filter at each epoch, and object-appropriate derived data. Examples of object-appropriate derived data include photometric redshifts and morphological parameters for galaxies, parallaxes and proper motions for stars.	SRD-34 **HLIS 2.0.2**	MRD-330 MRD-337 SRD-52 **HLIS 2.2.1** SRD-60 **HLIS 2.2.9** SRD-61 **HLIS 2.2.10** SRD-62 **HLIS 2.2.11** SRD-63 **HLIS 2.3.1**	GND+SIT
HLIS 2.1.5	The RST shall be capable of including in the HLIS catalog information on the statistical uncertainties for each quantity in the catalog as well as data quality flags where numeric uncertainties are not applicable.	SRD-34 **HLIS 2.0.2**	MRD-330 MRD-337 SRD-52 **HLIS 2.2.1** SRD-63 **HLIS 2.3.1**	GND+SIT
HLIS 2.1.6	Deleted			
HLIS 2.1.7	RST shall be capable of providing HLIS science data products with the angular mask and noise map of the lensing sample.	SRD-34 **HLIS 2.0.2**	MRD-330 MRD-337	SIT
HLIS 2.1.8	RST shall provide a means for users to determine a redshift probability distribution for an arbitrary sample of objects that reflects a true N(z) with an error on that estimate.	SRD-47 **HLIS 2.1.10**	MRD-330	SIT

High Latitude Imaging Survey - Science Data Records				
Reqmt	**SRD Requirement text**	**Parent (DOORS Out-links)**	**Child (DOORS In-links)**	**Recipient**
HLIS 2.1.9	RST shall enable users to determine redshift probability distributions p(z) for galaxies in each tomographic bin of the HLIS lensing sample per the table below on the fraction of probability within $\lvert z_{phot}-z_{spec}\rvert/(1+z)$ of the true redshift.	SRD-34 **HLIS 2.0.2**	MRD-33 MRD-330 SRD-49 **HLIS 2.1.12** SRD-51 **HLIS 2.1.14** SRD-53 **HLIS 2.2.2** SRD-59 **HLIS 2.2.8** SRD-60 **HLIS 2.2.9** SRD-61 **HLIS 2.2.10** SRD-62 **HLIS 2.2.11** SRD-64 **HLIS 2.3.2** SRD-67 **HLIS 2.3.5** SRD-68 **HLIS 2.3.6**	SIT
HLIS 2.1.10	RST shall enable users to determine the N(z) of each tomographic bin of Δz_{phot}=0.05 such that the systematic uncertainty in the mean redshift of the bin, Δz, is given by $\Delta z/(1+z)<0.002$.	SRD-34 **HLIS 2.0.2**	MRD-330 SRD-45 **HLIS 2.1.8** SRD-49 **HLIS 2.1.12** SRD-51 **HLIS 2.1.14** SRD-53 **HLIS 2.2.2** SRD-64 **HLIS 2.3.2** SRD-67 **HLIS 2.3.5** SRD-68 **HLIS 2.3.6**	SIT
HLIS 2.1.11	RST shall be capable of providing HLIS science data record with S/N ≥ 18 (matched filter detection significance, combining all exposures) per shape/color filter for a galaxy with an exponential disk profile and r_{eff} = 180 mas and mag AB = 24.4/24.3/23.7 (J/H/F184).	PLRA-85 **BSR2** SRD-34 **HLIS 2.0.2**	MRD-340 SRD-64 **HLIS 2.3.2**	SIT
HLIS 2.1.12	RST shall be capable of providing a sample of spectroscopic redshifts over the entire HLIS footprint, covering $0<z\leq2.5$ and with a known selection function.	SRD-46 **HLIS 2.1.9** SRD-47 **HLIS 2.1.10**	MRD-340	
HLIS 2.1.13	RST shall provide simulation packages that can "observe" simulated fields (e.g. from a catalog of galaxies, with an x-y-λ data cube of each) and feed the results into the data reduction pipeline, all the way through to simulated catalogs.	SRD-35 **HLIS 2.0.3** SRD-36 **HLIS 2.0.4**	MRD-330	SIT

High Latitude Imaging Survey - Science Data Records				
Reqmt	**SRD Requirement text**	**Parent (DOORS Out-links)**	**Child (DOORS In-links)**	**Recipient**
HLIS 2.1.14	RST shall provide a simulation package that can inject simulated galaxies (e.g. from x-y-λ data cubes) or stars into the real images and re-run (portions of) the data processing. This is needed to assess completeness/selection effects, the impact of blending on objects of known properties, and the impact of nearby stars on the measurement of galaxy photometric properties. In principle, much of this could be done from observing simulated skies, but these hybrid simulations are useful because they have the correct instrument noise properties and level of crowding by construction.	SRD-35 **HLIS 2.0.3** SRD-36 **HLIS 2.0.4** SRD-46 **HLIS 2.1.9** SRD-47 **HLIS 2.1.10**	MRD-330	SIT

High Latitude Imaging Survey - Calibrated Data Records				
Reqmt	**SRD Requirement text**	**Parent (DOORS Out-links)**	**Child (DOORS In-links)**	**Recipient**
HLIS 2.2.1	RST shall be capable of archiving HLIS calibrated images with the PSF for each exposure specified as a function of position on the focal plane and incorporate any World Coordinate System information needed for subsequent stages of processing.	SRD-38 **HLIS 2.1.1** SRD-39 **HLIS 2.1.2** SRD-40 **HLIS 2.1.3** SRD-41 **HLIS 2.1.4** SRD-42 **HLIS 2.1.5**	MRD-329 MRD-337 SRD-63 **HLIS 2.3.1**	GND
HLIS 2.2.2	RST shall be capable of providing HLIS calibrated data records with the relative photometric calibration in each HLIS filter spatially uniform on angular scales l<3200 to better than 10 millimag RMS.	SRD-34 **HLIS 2.0.2** SRD-46 **HLIS 2.1.9** SRD-47 **HLIS 2.1.10**	MRD-330 MRD-340 MRD-384 MRD-390 MRD-391 MRD-509 MRD-510 SRD-69 **HLIS 2.3.7**	GND+SIT
HLIS 2.2.3	RST shall be capable of providing HLIS science data records with the PSF ellipticity, defined by the moment ratios e1=(Ixx-Iyy)/(Ixx+Iyy) and e2=2Ixy/(Ixx+Iyy), determined to an error of $\leq 5.7\times10^{-4}$ RMS per component on angular multipole scales $32 < l < 3200$.	SRD-35 **HLIS 2.0.3**	MRD-3 MRD-33 MRD-114 MRD-153 MRD-187 MRD-330 MRD-353 MRD-428 SRD-58 **HLIS 2.2.7** SRD-65 **HLIS 2.3.3** SRD-66 **HLIS 2.3.4**	SIT
HLIS 2.2.4	RST shall be capable of providing HLIS science data records with the PSF size, defined by the second moment Ixx+Iyy, determined to a relative error of $\leq 7.2\times10^{-4}$ RMS on angular multipole scales $l < 3200$.	SRD-36 **HLIS 2.0.4**	MRD-3 MRD-33 MRD-114 MRD-187 MRD-330 MRD-353 SRD-58 **HLIS 2.2.7** SRD-65 **HLIS 2.3.3** SRD-66 **HLIS 2.3.4**	SIT

High Latitude Imaging Survey - Calibrated Data Records				
Reqmt	**SRD Requirement text**	**Parent (DOORS Out-links)**	**Child (DOORS In-links)**	**Recipient**
HLIS 2.2.5	RST shall be capable of providing HLIS calibrated data records with the astrometric solution in the WFI images having a relative error (offset between two images of the same galaxy or star, possibly taken at different times during the survey) of < 1.3mas.	SRD-35 **HLIS 2.0.3**	MRD-30 MRD-330 SRD-58 **HLIS 2.2.7**	GND+SIT
HLIS 2.2.6	RST shall be capable of providing HLIS calibrated data records with the astrometric solution in the WFI images having an absolute error, relative to the astrometric frame defined by the ICRF of: <26 mas RMS per component for $\log_{10} l = 1.5$—2.0 <11 mas RMS per component for $\log_{10} l = 2.0$—2.5 <5.1 mas RMS per component for $\log_{10} l = 2.5$—3.0 <2.2 mas RMS per component for $\log_{10} l = 3.0$—3.5.	SRD-35 **HLIS 2.0.3**	MRD-330 SRD-58 **HLIS 2.2.7**	GND+SIT
HLIS 2.2.7	RST shall be capable of providing a map of the pixel-to-pixel variations in the pixel response functions. For a postage stamp image of a star containing a total count of 87,000 electrons in an HLIS exposure, the individual pixel response function map shall introduce an error of no more than 0.5σ in the 0th, 1st, or 2nd moments. Here "σ" represents the RMS statistical error, including Poisson and read noise.	SRD-54 **HLIS 2.2.3** SRD-55 **HLIS 2.2.4** SRD-56 **HLIS 2.2.5** SRD-57 **HLIS 2.2.6**	MRD-330	SIT
HLIS 2.2.8	RST shall be capable of providing HLIS calibrated data records with the variation of the total system response known as a function of position within the field of view, such that the total flux of a source with a known Spectral Energy Distribution (SED) can be corrected to a common filter system at the ~0.5% level when imaged at any point on the focal plane.	SRD-46 **HLIS 2.1.9**	MRD-330 MRD-340 MRD-384 MRD-390 MRD-391 MRD-509 MRD-510	GND+SIT
HLIS 2.2.9	RST shall be capable of providing calibrated data records with absolute photometry of point sources calibrated in one or more of the standard filters to <2%, with a goal of 1%.	SRD-34 **HLIS 2.0.2** SRD-40 **HLIS 2.1.3** SRD-41 **HLIS 2.1.4** SRD-46 **HLIS 2.1.9**	MRD-181 MRD-330 MRD-340 MRD-384 MRD-390 MRD-391 MRD-509 MRD-510 SRD-63 **HLIS 2.3.1** SRD-66 **HLIS 2.3.4**	SIT

High Latitude Imaging Survey - Calibrated Data Records				
Reqmt	**SRD Requirement text**	**Parent (DOORS Out-links)**	**Child (DOORS In-links)**	**Recipient**
HLIS 2.2.10	RST shall be capable of providing calibrated data records with photometric zeropoints varying by less than 0.5% over the duration of the high latitude imaging survey program.	SRD-34 **HLIS 2.0.2** SRD-40 **HLIS 2.1.3** SRD-41 **HLIS 2.1.4** SRD-46 **HLIS 2.1.9**	MRD-181 MRD-187 MRD-330 MRD-340 MRD-384 MRD-390 MRD-391 SRD-63 **HLIS 2.3.1** SRD-66 **HLIS 2.3.4**	SIT
HLIS 2.2.11	RST shall be capable of providing calibrated data records with relative photometric zero-points of the filters known to <0.5%, relative to a standard star.	SRD-34 **HLIS 2.0.2** SRD-40 **HLIS 2.1.3** SRD-41 **HLIS 2.1.4** SRD-46 **HLIS 2.1.9**	MRD-181 MRD-330 MRD-340 MRD-384 MRD-390 MRD-391 MRD-509 MRD-510 SRD-63 **HLIS 2.3.1** SRD-66 **HLIS 2.3.4**	SIT

High Latitude Imaging Survey – Raw Data Records				
Reqmt	**SRD Requirement text**	**Parent (DOORS Out-links)**	**Child (DOORS In-links)**	**Recipient**
HLIS 2.3.1	RST shall be capable of providing HLIS raw images in the archive for each detector exposure with each raw data record including a unique dataset identifier for each exposure, the exposure time, the time of exposure, all individual downlinked detector readouts used to make the exposure, the observatory pointing orientation and any additional engineering data the Science Center uses for subsequent processing.	SRD-38 **HLIS 2.1.1** SRD-39 **HLIS 2.1.2** SRD-40 **HLIS 2.1.3** SRD-41 **HLIS 2.1.4** SRD-42 **HLIS 2.1.5** SRD-52 **HLIS 2.2.1** SRD-60 **HLIS 2.2.9** SRD-61 **HLIS 2.2.10** SRD-62 **HLIS 2.2.11**	MRD-329 MRD-337	GND
HLIS 2.3.2	RST shall have the capability of providing HLIS raw images of galaxies in 4 filters (Y, J, H, and F184).	SRD-34 **HLIS 2.0.2** SRD-46 **HLIS 2.1.9** SRD-47 **HLIS 2.1.10** SRD-48 **HLIS 2.1.11**	MRD-154 MRD-340 MRD-430	
HLIS 2.3.3	RST shall be capable of providing HLIS raw images with a system PSF EE50 radius ≤ 0.12 (Y band), 0.12 (J), 0.14 (H), or 0.14 (F184) arcsec, excluding diffraction spikes and non-first order light and including the effects of pointing jitter, for at least 95% of the exposures and over 95% of the FOV.	SRD-54 **HLIS 2.2.3** SRD-55 **HLIS 2.2.4**	MRD-38 MRD-39 MRD-352 MRD-353 MRD-430 MRD-469	
HLIS 2.3.4	RST shall be capable of providing HLIS raw images in at least 2 passes at different roll angles, and dithered so that >90% of the survey area receives 5 exposures (J and H bands) or 4 exposures (Y and F184 bands) of the survey area, in the survey mode defined by HLIS 2.0.2.	SRD-54 **HLIS 2.2.3** SRD-55 **HLIS 2.2.4** SRD-60 **HLIS 2.2.9** SRD-61 **HLIS 2.2.10** SRD-62 **HLIS 2.2.11**	MRD-44 MRD-153 MRD-340 MRD-430	
HLIS 2.3.5	RST shall be capable of acquiring at least 15,000 spectroscopic redshifts in the HLIS deep field (see HLIS 2.0.5), representing the full extent of color space for detected galaxies. (Spectra could be from RST observations or from ground-based observatories).	SRD-37 **HLIS 2.0.5** SRD-46 **HLIS 2.1.9** SRD-47 **HLIS 2.1.10**	MRD-340 MRD-430	
HLIS 2.3.6	RST shall be capable of periodic acquisition of HLIS deep field imaging observations throughout the HLIS observing program.	SRD-46 **HLIS 2.1.9** SRD-47 **HLIS 2.1.10**	MRD-340 MRD-430	
HLIS 2.3.7	RST raw data records shall consist of at least 6 ground-configurable combinations of samples per microlensing exposure.	SRD-53 **HLIS 2.2.2**	MRD-18 MRD-186 MRD-340	
HLIS 2.3.8	Deleted			

High Latitude Imaging Survey – Raw Data Records				
Reqmt	**SRD Requirement text**	**Parent (DOORS Out-links)**	**Child (DOORS In-links)**	**Recipient**
HLIS 2.3.9	Deleted			
HLIS 2.3.10	Deleted			
HLIS 2.3.11	Deleted			
HLIS 2.3.12	Deleted			
HLIS 2.3.13	Deleted			

Supernova Survey – Science Requirements				
Reqmt	**SRD Requirement text**	**Parent (DOORS Out-links)**	**Child (DOORS In-links)**	**Recipient**
SN 2.0.1	RST shall be capable of executing a supernova Type Ia survey that can, if allocated 0.5 years of total observing time, achieve constraints that yield $FoM_{SN} \geq FoM_{SN,Ref} / 2 = 325$,	PLRA-12 **OBJ-2.1.1** PLRA-14 **OBJ-2.1.2**	SRD-77 **SN 2.0.2**	
SN 2.0.2	RST shall enable a supernova survey that can measure the distance modulus $\mu(z)$ over the redshift range $0.2 \leq z \leq 1.7$, with observational noise contributions to the uncertainty $\sigma\mu \leq 0.02$ per $\Delta z=0.1$ bin.	SRD-76 **SN 2.0.1**	MRD-33 MRD-390 SRD-78 **SN 2.0.3** SRD-79 **SN 2.0.4** SRD-80 **SN 2.1.1** SRD-81 **SN 2.1.2** SRD-82 **SN 2.1.3** SRD-83 **SN 2.1.4** SRD-84 **SN 2.1.5** SRD-85 **SN 2.1.6** SRD-87 **SN 2.2.2** SRD-88 **SN 2.2.3** SRD-90 **SN 2.2.5** SRD-91 **SN 2.2.6** SRD-96 **SN 2.3.2** SRD-98 **SN 2.3.4** SRD-99 **SN 2.3.5** SRD-100 **SN 2.3.6** SRD-101 **SN 2.3.7** SRD-102 **SN 2.3.8**	

Supernova Survey – Science Requirements				
Reqmt	**SRD Requirement text**	**Parent (DOORS Out-links)**	**Child (DOORS In-links)**	**Recipient**
SN 2.0.3	RST shall enable a SN survey to observe more than 100 SNe-Ia per Δz=0.1 bin.	SRD-77 **SN 2.0.2**	MRD-11 MRD-152 MRD-340 MRD-432 MRD-433 MRD-434 MRD-475 MRD-477 SRD-80 **SN 2.1.1** SRD-81 **SN 2.1.2** SRD-82 **SN 2.1.3** SRD-83 **SN 2.1.4** SRD-84 **SN 2.1.5** SRD-85 **SN 2.1.6** SRD-97 **SN 2.3.3** SRD-98 **SN 2.3.4** SRD-99 **SN 2.3.5**	
SN 2.0.4	RST shall enable a SN survey with the systematic bias in redshift, $\sigma_z/(1 + z)$, less than the values in the following table:	SRD-77 **SN 2.0.2**	SRD-89 **SN 2.2.4** SRD-96 **SN 2.3.2** SRD-100 **SN 2.3.6** SRD-101 **SN 2.3.7** SRD-102 **SN 2.3.8**	

Supernova Survery – Science Data Records				
Reqmt	**SRD Requirement text**	**Parent (DOORS Out-links)**	**Child (DOORS In-links)**	**Recipient**
SN 2.1.1	RST shall be capable of producing mosaic images of the SN fields in each filter at each epoch of observation, using coordinates tied to the astrometric frame defined by the International Celestial Reference Frame (ICRF).	SRD-77 **SN 2.0.2** SRD-78 **SN 2.0.3**	MRD-329 MRD-337 SRD-86 **SN 2.2.1** SRD-95 **SN 2.3.1**	GND
SN 2.1.2	RST shall be capable of including information in the SN mosaics on the flux uncertainty for each pixel, data quality flags, and additional data generated in producing the mosaics that characterize or support the mosaic generation process.	SRD-77 **SN 2.0.2** SRD-78 **SN 2.0.3**	MRD-329 MRD-337 SRD-86 **SN 2.2.1** SRD-95 **SN 2.3.1**	GND
SN 2.1.3	RST shall be capable of producing, quarterly throughout the survey and at the end of the survey, a mosaic image of the SN fields that combines data from individual epochs to form a deep “static sky” image. Producing this "static sky" image on approximately quarterly time frame supports GI deep field science.	SRD-77 **SN 2.0.2** SRD-78 **SN 2.0.3**	MRD-330 MRD-337	SIT
SN 2.1.4	RST shall be capable of producing a catalog containing information for each detected source in the SN fields, including positions, classifications, photometry (e.g. aperture photometry, model fits, adaptive moment photometry), and limited time domain information for variable sources.	SRD-77 **SN 2.0.2** SRD-78 **SN 2.0.3**	MRD-330 MRD-337 SRD-86 **SN 2.2.1** SRD-92 **SN 2.2.7** SRD-93 **SN 2.2.8** SRD-95 **SN 2.3.1**	GND+SIT
SN 2.1.5	RST shall be capable of producing a catalog of each source in the SN fields containing object-appropriate derived data. Examples of object-appropriate derived data include photometric and spectroscopic redshifts and morphological parameters for galaxies, parallaxes and proper motions for stars, and light curves for variable sources.	SRD-77 **SN 2.0.2** SRD-78 **SN 2.0.3**	MRD-330 MRD-337 SRD-86 **SN 2.2.1** SRD-92 **SN 2.2.7** SRD-93 **SN 2.2.8** SRD-95 **SN 2.3.1**	GND+SIT
SN 2.1.6	RST shall be capable of including in the SN catalog information on the statistical uncertainties for each quantity in the catalog as well as data quality flags where numeric uncertainties are not applicable.	SRD-77 **SN 2.0.2** SRD-78 **SN 2.0.3**	MRD-330 MRD-337 SRD-86 **SN 2.2.1** SRD-92 **SN 2.2.7** SRD-93 **SN 2.2.8** SRD-95 **SN 2.3.1**	GND+SIT

Supernova Survey – Calibrated Data Records				
Reqmt	**SRD Requirement text**	**Parent (DOORS Out-links)**	**Child (DOORS In-links)**	**Recipient**
SN 2.2.1	RST shall be capable of archiving SN calibrated images with the PSF for each exposure specified as a function of position on the focal plane, the effective bandpass as a function of position and incorporate any World Coordinate System information needed for subsequent stages of processing.	SRD-80 **SN 2.1.1** SRD-81 **SN 2.1.2** SRD-83 **SN 2.1.4** SRD-84 **SN 2.1.5** SRD-85 **SN 2.1.6**	MRD-329 MRD-337 SRD-95 **SN 2.3.1**	GND
SN 2.2.2	RST shall be capable of providing knowledge of the relative instrumental bias on the photometric calibration (defined as (Ftrue(λ) – Fmeas(λ)) / Ftrue(λ), where F(λ) is the flux calibration) that must be <0.005 between any two filter bands in the instrument.	PLRA-86 **BSR3** SRD-77 **SN 2.0.2**	MRD-33 MRD-181 MRD-330 MRD-340 MRD-384 MRD-509 MRD-510	SIT
SN 2.2.3	RST shall be capable of providing photometric calibration accuracy such that the reported flux from a source of AB 26th mag is 25,119±75 times fainter than an AB 15th mag source, after calibration.	SRD-77 **SN 2.0.2**	MRD-33 MRD-181 MRD-186 MRD-330 MRD-340 MRD-384 MRD-506	GND+SIT
SN 2.2.4	RST shall be capable of providing calibrated spectra with a wavelength accuracy of $\sigma_\lambda/\lambda <$ 0.001 for spectra used to determine redshifts.	SRD-79 **SN 2.0.4**	MRD-330 MRD-340 MRD-444 SRD-100 **SN 2.3.6**	SIT
SN 2.2.5	RST shall be capable of providing calibrated data records with absolute photometry of point sources calibrated (against standard stars) in one or more of the standard filters to <2%, with a goal of 1%.	SRD-77 **SN 2.0.2**	MRD-181 MRD-330 MRD-340 MRD-384 MRD-390 MRD-391 MRD-509 MRD-510 SRD-95 **SN 2.3.1**	GND+SIT

Supernova Survey – Calibrated Data Records				
Reqmt	**SRD Requirement text**	**Parent (DOORS Out-links)**	**Child (DOORS In-links)**	**Recipient**
SN 2.2.6	RST shall be capable of providing calibrated data records with photometric zeropoints varying by less than 0.5% over the duration of the supernova program.	SRD-77 **SN 2.0.2**	MRD-181 MRD-330 MRD-340 MRD-384 MRD-390 MRD-391 SRD-95 **SN 2.3.1**	GND+SIT
SN 2.2.7	RST shall archive SN program calibrated spectra for each prism exposure.	SRD-83 **SN 2.1.4** SRD-84 **SN 2.1.5** SRD-85 **SN 2.1.6**	MRD-329 MRD-337 SRD-95 **SN 2.3.1**	GND
SN 2.2.8	RST shall provide spectra with relative spectrophotometric flux calibration as a function of wavelength accurate to 3%, when calibrated against standard stars.	SRD-83 **SN 2.1.4** SRD-84 **SN 2.1.5** SRD-85 **SN 2.1.6**	MRD-329 MRD-337 SRD-95 **SN 2.3.1** RPRI-104	GND
SN 2.2.9	Deleted			

Supernova Survey – Raw Data Records				
Reqmt	**SRD Requirement text**	**Parent (DOORS Out-links)**	**Child (DOORS In-links)**	**Recipient**
SN 2.3.1	RST shall be capable of providing raw images in the archive for each detector exposure with each raw data record including a unique dataset identifier for each exposure, the exposure time, the time of exposure, all individual downlinked detector readouts used to make the exposure, the observatory pointing orientation and any additional engineering data the Science Center uses for subsequent processing.	SRD-80 **SN 2.1.1** SRD-81 **SN 2.1.2** SRD-83 **SN 2.1.4** SRD-84 **SN 2.1.5** SRD-85 **SN 2.1.6** SRD-86 **SN 2.2.1** SRD-90 **SN 2.2.5** SRD-91 **SN 2.2.6** SRD-92 **SN 2.2.7** SRD-93 **SN 2.2.8**	MRD-329 MRD-337	GND
SN 2.3.2	RST shall be able to observe supernovae in fields with low Galactic extinction, such that E(B-V) ≤ 0.02 over 90% of the area, and low zodiacal light background. Here, Galactic extinction is that defined by Schlafly & Finkbeiner 2011 (ApJ 737, 103).	SRD-77 **SN 2.0.2** SRD-79 **SN 2.0.4**	MRD-42 MRD-340 MRD-430	
SN 2.3.3	The RST field of regard shall be large enough to provide a continuous viewing zone (CVZ) that encompasses regions of the sky suitable for observing supernovae.	PLRA-86 **BSR3** SRD-78 **SN 2.0.3**	MRD-42 MRD-340 MRD-430	
SN 2.3.4	RST shall enable a SN survey that monitors the SN fields with an uninterrupted sampling cadence ≤ 5 days.	PLRA-86 **BSR3** SRD-77 **SN 2.0.2** SRD-78 **SN 2.0.3**	MRD-42 MRD-44 MRD-340 MRD-430	
SN 2.3.5	RST shall have the capability of providing raw images of SN fields in up to six filters that span roughly 0.5 – 2.0 µm.	PLRA-86 **BSR3** PLRA-87 **BSR4** SRD-77 **SN 2.0.2** SRD-78 **SN 2.0.3**	MRD-154 MRD-340 MRD-430	
SN 2.3.6	RST shall be capable of obtaining spectra over the bandpass 0.75-1.8 microns, with spectral dispersion lambda/delta_lambda>70 per two-pixel resolution element at all wavelengths, and <170 per two-pixel resolution element at wavelengths longer than 0.8 microns.	PLRA-87 **BSR4** SRD-77 **SN 2.0.2** SRD-79 **SN 2.0.4** SRD-89 **SN 2.2.4**	MRD-479 MRD-480 MRD-481 MRD-482	
SN 2.3.7	RST shall provide raw spectral images with 50% of the energy enclosed in a circle of radius < 0.17" at 1.2 microns for a monochromatic point source, excluding diffraction spikes and including the effects of pointing jitter, for at least 95% of exposures and over 90% of the field of view.	PLRA-86 **BSR3** SRD-77 **SN 2.0.2** SRD-79 **SN 2.0.4**	MRD-479 MRD-480 MRD-481	

Supernova Survey – Raw Data Records				
Reqmt	**SRD Requirement text**	**Parent (DOORS Out-links)**	**Child (DOORS In-links)**	**Recipient**
SN 2.3.8	RST shall be able to obtain a prism spectrum of a flat-spectrum source with a signal to noise of 10 per 2-pixel resolution element in 600 seconds for a source magnitude of AB=22.3 at 1.2 microns.	SRD-77 **SN 2.0.2** SRD-79 **SN 2.0.4**	MRD-432 MRD-433 MRD-479 MRD-480 MRD-481	
SN 2.3.9	Deleted			
SN 2.3.10	Deleted			
SN 2.3.11	Deleted			
SN 2.3.12	Deleted			
SN 2.3.13	Deleted			

Exoplanet Microlensing Survey – Science Requirements				
Reqmt	**SRD Requirement text**	**Parent (DOORS Out-links)**	**Child (DOORS In-links)**	**Recipient**
EML 2.0.1	RST shall be capable of measuring the mass function of exoplanets with masses in the range 1 $M_{Earth} < m < 30\ M_{Jupiter}$ and orbital semi-major axes ≥ 1 AU to better than 15% per decade in mass.	PLRA-18 **OBJ-2.1.4**	SRD-115 **EML 2.1.3** SRD-116 **EML 2.1.4** SRD-117 **EML 2.1.5** SRD-118 **EML 2.1.6** SRD-121 **EML 2.2.3** SRD-122 **EML 2.2.4** SRD-123 **EML 2.2.5** SRD-124 **EML 2.2.6** SRD-125 **EML 2.2.7** SRD-129 **EML 2.3.2** SRD-130 **EML 2.3.3** SRD-131 **EML 2.3.4** SRD-132 **EML 2.3.5** SRD-133 **EML 2.3.6** SRD-134 **EML 2.3.7** SRD-136 **EML 2.3.9** SRD-137 **EML 2.3.10**	
EML 2.0.2	RST shall be capable of measuring the frequency of bound exoplanets with masses in the range 0.1 $M_{Earth} < m < 0.3M_{Earth}$ to better than 25%.	PLRA-18 **OBJ-2.1.4**	SRD-115 **EML 2.1.3** SRD-116 **EML 2.1.4** SRD-117 **EML 2.1.5** SRD-118 **EML 2.1.6** SRD-121 **EML 2.2.3** SRD-122 **EML 2.2.4** SRD-123 **EML 2.2.5** SRD-124 **EML 2.2.6** SRD-125 **EML 2.2.7** SRD-129 **EML 2.3.2** SRD-130 **EML 2.3.3** SRD-131 **EML 2.3.4** SRD-132 **EML 2.3.5** SRD-133 **EML 2.3.6** SRD-134 **EML 2.3.7** SRD-136 **EML 2.3.9** SRD-137 **EML 2.3.10**	

Exoplanet Microlensing Survey – Science Requirements				
Reqmt	**SRD Requirement text**	**Parent (DOORS Out-links)**	**Child (DOORS In-links)**	**Recipient**
EML 2.0.3	RST shall be capable of determining the masses of, and distances to, host stars of 40% of the detected planets with a precision of 20% or better.	PLRA-18 **OBJ-2.1.4**	MRD-61 SRD-115 **EML 2.1.3** SRD-116 **EML 2.1.4** SRD-117 **EML 2.1.5** SRD-118 **EML 2.1.6** SRD-121 **EML 2.2.3** SRD-122 **EML 2.2.4** SRD-123 **EML 2.2.5** SRD-126 **EML 2.2.8** SRD-127 **EML 2.2.9** SRD-131 **EML 2.3.4** SRD-132 **EML 2.3.5** SRD-133 **EML 2.3.6** SRD-136 **EML 2.3.9** SRD-137 **EML 2.3.10** SRD-138 **EML 2.3.11** SRD-139 **EML 2.3.12**	
EML 2.0.4	RST shall be capable of measuring the frequency of free floating planetary-mass objects in the Galaxy from Mars to 10 Jupiter masses. If there is one M_{Earth} free-floating planet per star, measure this frequency to better than 25%.	PLRA-18 **OBJ-2.1.4**	SRD-115 **EML 2.1.3** SRD-116 **EML 2.1.4** SRD-117 **EML 2.1.5** SRD-118 **EML 2.1.6** SRD-121 **EML 2.2.3** SRD-122 **EML 2.2.4** SRD-123 **EML 2.2.5** SRD-124 **EML 2.2.6** SRD-125 **EML 2.2.7** SRD-129 **EML 2.3.2** SRD-130 **EML 2.3.3** SRD-131 **EML 2.3.4** SRD-132 **EML 2.3.5** SRD-133 **EML 2.3.6** SRD-134 **EML 2.3.7**	

Exoplanet Microlensing Survey – Science Requirements				
Reqmt	**SRD Requirement text**	**Parent (DOORS Out-links)**	**Child (DOORS In-links)**	**Recipient**
EML 2.0.5	RST shall be capable of estimating η_{Earth} (defined as the frequency of planets orbiting FGK stars with mass ratio and estimated projected semimajor axis within 20% of the Earth-Sun system) to a precision of 0.2 dex via extrapolation from larger and longer-period planets.	PLRA-18 **OBJ-2.1.4**	SRD-118 **EML 2.1.6** SRD-121 **EML 2.2.3** SRD-122 **EML 2.2.4** SRD-123 **EML 2.2.5** SRD-124 **EML 2.2.6** SRD-125 **EML 2.2.7** SRD-129 **EML 2.3.2** SRD-130 **EML 2.3.3** SRD-131 **EML 2.3.4** SRD-132 **EML 2.3.5** SRD-133 **EML 2.3.6** SRD-134 **EML 2.3.7** SRD-136 **EML 2.3.9** SRD-137 **EML 2.3.10**	

Exoplanet Microlensing Survey – Science Data Records				
Reqmt	**SRD Requirement text**	**Parent (DOORS Out-links)**	**Child (DOORS In-links)**	**Recipient**
EML 2.1.1	RST shall be capable of providing supersampled stacked images of the microlensing fields after every microlensing season.	SRD-114 **EML 2.1.2** SRD-115 **EML 2.1.3** SRD-116 **EML 2.1.4** SRD-117 **EML 2.1.5**	MRD-329	GND
EML 2.1.2	RST shall be capable of producing a catalog of each source in the microlensing fields containing positions, fluxes, with object-appropriate derived data. Examples of object-appropriate derived data include object classification, parallaxes and proper motions for stars and limited time domain information for variable sources.	SRD-115 **EML 2.1.3**	MRD-329 MRD-337 SRD-113 **EML 2.1.1** SRD-118 **EML 2.1.6** SRD-119 **EML 2.2.1** SRD-125 **EML 2.2.7** SRD-126 **EML 2.2.8** SRD-127 **EML 2.2.9** SRD-128 **EML 2.3.1**	GND
EML 2.1.3	RST shall be capable of producing a catalog of each microlensing event in the microlensing fields containing positions, fluxes, object classification information with event-appropriate derived data. Examples of event-appropriate derived data include links to the corresponding source catalog entries and moment curves.	SRD-108 **EML 2.0.1** SRD-109 **EML 2.0.2** SRD-110 **EML 2.0.3** SRD-111 **EML 2.0.4**	MRD-329 MRD-337 SRD-113 **EML 2.1.1** SRD-114 **EML 2.1.2** SRD-118 **EML 2.1.6** SRD-119 **EML 2.2.1** SRD-124 **EML 2.2.6** SRD-125 **EML 2.2.7** SRD-126 **EML 2.2.8** SRD-127 **EML 2.2.9** SRD-128 **EML 2.3.1**	GND
EML 2.1.4	RST shall be capable of including information in the microlensing catalog on statistical and systematic uncertainties for each quantity in the catalog and/or data quality flags, as applicable.	SRD-108 **EML 2.0.1** SRD-109 **EML 2.0.2** SRD-110 **EML 2.0.3** SRD-111 **EML 2.0.4**	MRD-329 MRD-337 SRD-113 **EML 2.1.1** SRD-118 **EML 2.1.6** SRD-119 **EML 2.2.1** SRD-124 **EML 2.2.6** SRD-125 **EML 2.2.7** SRD-126 **EML 2.2.8** SRD-127 **EML 2.2.9** SRD-128 **EML 2.3.1**	GND

Exoplanet Microlensing Survey – Science Data Records				
Reqmt	**SRD Requirement text**	**Parent (DOORS Out-links)**	**Child (DOORS In-links)**	**Recipient**
EML 2.1.5	RST shall be capable of providing calibrated photometry and position measurements for each microlensing event on a daily basis, and ellipticity measurements every 8th day.	SRD-108 **EML 2.0.1** SRD-109 **EML 2.0.2** SRD-110 **EML 2.0.3** SRD-111 **EML 2.0.4**	MRD-329 MRD-337 SRD-113 **EML 2.1.1** SRD-118 **EML 2.1.6** SRD-120 **EML 2.2.2** SRD-124 **EML 2.2.6** SRD-125 **EML 2.2.7** SRD-126 **EML 2.2.8** SRD-127 **EML 2.2.9**	GND
EML 2.1.6	RST shall be capable of providing science data records with relative astrometric measurements having a systematic precision of ≤100 μas over each microlensing season, for sources imaged on the same detector in at least two passbands.	SRD-108 **EML 2.0.1** SRD-109 **EML 2.0.2** SRD-110 **EML 2.0.3** SRD-111 **EML 2.0.4** SRD-112 **EML 2.0.5** SRD-114 **EML 2.1.2** SRD-115 **EML 2.1.3** SRD-116 **EML 2.1.4** SRD-117 **EML 2.1.5**	MRD-187 MRD-329 MRD-337 SRD-121 **EML 2.2.3**	GND

Exoplanet Microlensing Survey – Calibrated Data Records				
Reqmt	**SRD Requirement text**	**Parent (DOORS Out-links)**	**Child (DOORS In-links)**	**Recipient**
EML 2.2.1	RST shall be capable of archiving microlensing calibrated images and incorporate any World Coordinate System information needed for subsequent stages of processing.	SRD-114 **EML 2.1.2** SRD-115 **EML 2.1.3** SRD-116 **EML 2.1.4**	MRD-329 MRD-337	GND
EML 2.2.2	RST shall be capable of providing calibrated data records for photometry and position of microlensing events on a daily basis, and every 8th day for ellipticity.	SRD-117 **EML 2.1.5** SRD-122 **EML 2.2.4**	MRD-329	GND
EML 2.2.3	RST shall be capable of providing calibrated data records with relative astrometric measurements having a statistical precision of ≤1 mas per measurement for a star of H_{AB}=21.4 in at least two passbands.	SRD-108 **EML 2.0.1** SRD-109 **EML 2.0.2** SRD-110 **EML 2.0.3** SRD-111 **EML 2.0.4** SRD-112 **EML 2.0.5** SRD-118 **EML 2.1.6**	MRD-329 MRD-406 SRD-140 **EML 2.3.13**	GND
EML 2.2.4	RST shall be capable of providing calibrated data records with the FWHM for 99% of stars brighter than H(AB)=21.4 with a precision ≤1% in both axes after every 8 consecutive day interval.	SRD-108 **EML 2.0.1** SRD-109 **EML 2.0.2** SRD-110 **EML 2.0.3** SRD-111 **EML 2.0.4** SRD-112 **EML 2.0.5** SRD-123 **EML 2.2.5**	MRD-329 SRD-120 **EML 2.2.2**	GND
EML 2.2.5	RST shall be capable of providing calibrated data records with the FWHM of each source measured in both axes of a H_{AB}=21.4 star to ≤0.2% for each observing season of the microlensing survey.	SRD-108 **EML 2.0.1** SRD-109 **EML 2.0.2** SRD-110 **EML 2.0.3** SRD-111 **EML 2.0.4** SRD-112 **EML 2.0.5**	MRD-329 SRD-122 **EML 2.2.4**	GND
EML 2.2.6	RST shall be capable of providing calibrated data records with relative photometric measurements in the primary microlensing filter having a systematic precision of ≤0.1% over a season.	SRD-108 **EML 2.0.1** SRD-109 **EML 2.0.2** SRD-111 **EML 2.0.4** SRD-112 **EML 2.0.5** SRD-115 **EML 2.1.3** SRD-116 **EML 2.1.4** SRD-117 **EML 2.1.5**	MRD-33 MRD-187 MRD-384 MRD-406 MRD-509 MRD-510	

Exoplanet Microlensing Survey – Calibrated Data Records				
Reqmt	**SRD Requirement text**	**Parent (DOORS Out-links)**	**Child (DOORS In-links)**	**Recipient**
EML 2.2.7	RST shall be capable of providing calibrated data records with relative photometric measurements from separate seasons tied to ≤0.1% for any individual star.	SRD-108 **EML 2.0.1** SRD-109 **EML 2.0.2** SRD-111 **EML 2.0.4** SRD-112 **EML 2.0.5** SRD-114 **EML 2.1.2** SRD-115 **EML 2.1.3** SRD-116 **EML 2.1.4** SRD-117 **EML 2.1.5**	MRD-33 MRD-340 MRD-384 MRD-406 MRD-509 MRD-510	
EML 2.2.8	RST shall be capable of providing calibrated data records with absolute photometry of point sources calibrated in one or more of the standard filters to <3%.	SRD-110 **EML 2.0.3** SRD-114 **EML 2.1.2** SRD-115 **EML 2.1.3** SRD-116 **EML 2.1.4** SRD-117 **EML 2.1.5**	MRD-33 MRD-340 MRD-384 MRD-406 MRD-509 MRD-510	GND
EML 2.2.9	RST shall be capable of providing calibrated data records with relative zero-points of the filter photometry known to <1.4%.	SRD-110 **EML 2.0.3** SRD-114 **EML 2.1.2** SRD-115 **EML 2.1.3** SRD-116 **EML 2.1.4** SRD-117 **EML 2.1.5**	MRD-33 MRD-340 MRD-384 MRD-406 MRD-509 MRD-510	

Exoplanet Microlensing Survey – Raw Data Records				
Reqmt	**SRD Requirement text**	**Parent (DOORS Out-links)**	**Child (DOORS In-links)**	**Recipient**
EML 2.3.1	RST shall be capable of providing microlensing raw images in the archive for each detector exposure with each raw data record including a unique dataset identifier for each exposure, the exposure time, the time of exposure, all individual downlinked detector readouts used to make the exposure, the observatory pointing orientation and any additional engineering data the Science Center uses for subsequent processing.	SRD-114 **EML 2.1.2** SRD-115 **EML 2.1.3** SRD-116 **EML 2.1.4**	MRD-329 MRD-337	GND
EML 2.3.2	RST shall be capable of observing a total 585.4 square degree-days over the course of the mission, with relative photometric measurements in the primary microlensing filter that have a statistical S/N of ≥100 per exposure for a HAB=21.4 star, if it is allocated 6 seasons of observing time.	SRD-108 **EML 2.0.1** SRD-109 **EML 2.0.2** SRD-111 **EML 2.0.4** SRD-112 **EML 2.0.5**	MRD-11 MRD-152 MRD-340 MRD-430 MRD-432 MRD-433 MRD-434 MRD-475 MRD-477	
EML 2.3.3	RST shall be capable of providing raw microlensing images with relative photometric measurements in the primary microlensing filter having a statistical S/N of ≥100 per exposure for a H_{AB}=21.4 star.	PLRA-87 **BSR4** SRD-108 **EML 2.0.1** SRD-109 **EML 2.0.2** SRD-111 **EML 2.0.4** SRD-112 **EML 2.0.5**	MRD-340 MRD-430 MRD-432 MRD-433 MRD-434 MRD-475 MRD-477	
EML 2.3.4	RST shall be capable of providing raw images of the microlensing fields with a wide filter spanning $\lambda \approx 1 - 2$ μm.	PLRA-87 **BSR4** SRD-108 **EML 2.0.1** SRD-109 **EML 2.0.2** SRD-110 **EML 2.0.3** SRD-111 **EML 2.0.4** SRD-112 **EML 2.0.5**	MRD-154 MRD-340 MRD-430	
EML 2.3.5	RST shall be capable of providing a photometric sampling cadence of ≤15 minutes for each microlensing field, while simultaneously achieving the S/N specified in EML 2.3.3.	SRD-108 **EML 2.0.1** SRD-109 **EML 2.0.2** SRD-110 **EML 2.0.3** SRD-111 **EML 2.0.4** SRD-112 **EML 2.0.5**	MRD-340 MRD-415 MRD-416 MRD-417 MRD-430	

Exoplanet Microlensing Survey – Raw Data Records				
Reqmt	**SRD Requirement text**	**Parent (DOORS Out-links)**	**Child (DOORS In-links)**	**Recipient**
EML 2.3.6	RST shall be capable of providing microlensing raw images with an EE50 radius of the PSF in the wide filter <0.15”.	SRD-108 **EML 2.0.1** SRD-109 **EML 2.0.2** SRD-110 **EML 2.0.3** SRD-111 **EML 2.0.4** SRD-112 **EML 2.0.5**	MRD-38 MRD-39 MRD-352	
EML 2.3.7	RST raw data records shall consist of at least 6 ground-configurable combinations of samples per microlensing exposure.	SRD-108 **EML 2.0.1** SRD-109 **EML 2.0.2** SRD-111 **EML 2.0.4** SRD-112 **EML 2.0.5**	MRD-18 MRD-186 MRD-340	
EML 2.3.8	Deleted			
EML 2.3.9	RST shall be capable of performing microlensing observations over seasons of at least 60 days. At least 36 days of each season should be on the opposition side of quadrature (line of sight at greater than 90 degrees from the Sun vector).	SRD-108 **EML 2.0.1** SRD-109 **EML 2.0.2** SRD-110 **EML 2.0.3** SRD-112 **EML 2.0.5**	MRD-3 MRD-42 MRD-340	
EML 2.3.10	RST shall monitor the microlensing fields with a duty cycle of ≥90% per season.	SRD-108 **EML 2.0.1** SRD-109 **EML 2.0.2** SRD-110 **EML 2.0.3** SRD-112 **EML 2.0.5**	MRD-3 MRD-340	
EML 2.3.11	RST shall be capable of periodically providing raw images of the microlensing fields in two R~4 filters; one with bandpass shortward of 1 µm and one with a bandpass longward of 1 µm. The cadence of these observations is defined in the Operations Concept document.	SRD-110 **EML 2.0.3**	MRD-154 MRD-340	
EML 2.3.12	RST shall be capable of separating the first and last microlensing observing seasons by >4 years. In addition, the first two and last two seasons should occur during the same 12-month period (i.e., one in the spring and one in the fall to provide parallax measurements).	SRD-110 **EML 2.0.3**	MRD-340	
EML 2.3.13	RST shall be capable of providing stepped observations of a crowded field (but less crowded than the microlensing fields) with offsets that sample astrometric distortions on all scales. These fields should have stars with good Gaia parallaxes to set the absolute scale of the astrometric positions of the stars.	SRD-121 **EML 2.2.3**	MRD-340	

General Observer Program – Science Data Records				
Reqmt	**SRD Requirement text**	**Parent (DOORS Out-links)**	**Child (DOORS In-links)**	**Recipient**
GO 2.1.1	RST shall be able to produce mosaic images of the General Observer (GO) imaging fields in each filter at each epoch of observation, using coordinates tied to the astrometric frame defined by the International Celestial Reference Frame (ICRF).	PLRA-20 **OBJ-2.1.5**	MRD-329 MRD-337 SRD-147 **GO 2.2.1** SRD-152 **GO 2.2.6**	GND
GO 2.1.2	RST shall be able to produce GO mosaics that include information on the flux uncertainty for each pixel, effective bandpass as a function of position, data quality flags, and additional data generated in producing the mosaics that characterize or support the mosaic generation process.	PLRA-20 **OBJ-2.1.5**	MRD-329 MRD-337 SRD-147 **GO 2.2.1**	GND
GO 2.1.3	RST shall be able to produce a catalog of each source in the GO imaging fields containing, at a minimum, positions, fluxes, and object classification information.	PLRA-20 **OBJ-2.1.5**	MRD-329 MRD-337 SRD-147 **GO 2.2.1** SRD-152 **GO 2.2.6**	GND
GO 2.1.4	RST shall be able to produce a catalog that includes statistical uncertainties for each quantity in the catalog determined from GO observations, as well as data quality flags where numeric uncertainties are not applicable.	PLRA-20 **OBJ-2.1.5**	MRD-329 MRD-337 SRD-147 **GO 2.2.1**	GND
GO 2.1.5	RST shall be able to produce a catalog of each source in GO grism or prism fields and associate spectra (or a range of spectral image pixels) with corresponding objects in the GO imaging catalog.	PLRA-20 **OBJ-2.1.5**	MRD-329 MRD-337 SRD-147 **GO 2.2.1** SRD-152 **GO 2.2.6** SRD-153 **GO 2.2.7**	GND
GO 2.1.6	RST shall be able to produce GO catalog grism or prism spectra that include information on uncertainties in the measured fluxes and wavelengths, effective LSF as a function of wavelength, data quality flags, and an estimate of contamination from the overlap of different spectra.	PLRA-20 **OBJ-2.1.5**	MRD-329 MRD-337 SRD-147 **GO 2.2.1** SRD-153 **GO 2.2.7**	GND

General Observer Program – Calibrated Data Records				
Reqmt	**SRD Requirement text**	**Parent (DOORS Out-links)**	**Child (DOORS In-links)**	**Recipient**
GO 2.2.1	RST shall be able to archive GO calibrated images with the PSF for each exposure specified as a function of position on the focal plane, the effective bandpass as a function of position and incorporate any World Coordinate System information needed for subsequent stages of processing.	SRD-141 **GO 2.1.1** SRD-142 **GO 2.1.2** SRD-143 **GO 2.1.3** SRD-144 **GO 2.1.4** SRD-145 **GO 2.1.5** SRD-146 **GO 2.1.6**	MRD-329 MRD-337 SRD-148 **GO 2.2.2** SRD-149 **GO 2.2.3** SRD-150 **GO 2.2.4** SRD-151 **GO 2.2.5** SRD-152 **GO 2.2.6** SRD-157 **GO 2.3.1**	GND
GO 2.2.2	RST shall be able to provide GO calibrated data records with absolute photometry of point sources calibrated in one or more of the standard filters with a goal of better than 3% accuracy.	SRD-147 **GO 2.2.1**	MRD-181 MRD-329 MRD-337 MRD-340 MRD-384 MRD-390 MRD-391 SRD-157 **GO 2.3.1**	GND
GO 2.2.3	RST shall be able to provide GO calibrated data records with a goal of knowledge of the relative photometric zero-points of the filters better than 1%.	SRD-147 **GO 2.2.1**	MRD-181 MRD-329 MRD-337 MRD-340 MRD-384 MRD-390 MRD-391 SRD-157 **GO 2.3.1**	GND
GO 2.2.4	RST shall be able to provide GO calibrated data records with the variation of the total system response known as a function of position within the field of view, such that the total flux of a point source with a known Spectral Energy Distribution (SED) can be corrected to a common filter system with a goal of better than 1% accuracy when imaged at any point on the focal plane.	SRD-147 **GO 2.2.1**	MRD-181 MRD-329 MRD-337 MRD-340 MRD-384 MRD-390 MRD-391 SRD-157 **GO 2.3.1**	GND

General Observer Program – Calibrated Data Records				
Reqmt	**SRD Requirement text**	**Parent (DOORS Out-links)**	**Child (DOORS In-links)**	**Recipient**
GO 2.2.5	RST shall be able to provide GO calibrated data records with a relative photometric calibration in each filter that is spatially uniform over the WFI field of view, with a goal of systematic spatial variations being less than 1%.	SRD-147 **GO 2.2.1**	MRD-181 MRD-329 MRD-337 MRD-340 MRD-384 MRD-390 MRD-391 SRD-157 **GO 2.3.1**	GND
GO 2.2.6	RST shall be able to provide GO calibrated data records with a known systematic uncertainty in the astrometric accuracy, with a goal of 10 mas for absolute positions and 5mas for relative positions of objects within a given SCA.	SRD-141 **GO 2.1.1** SRD-143 **GO 2.1.3** SRD-145 **GO 2.1.5** SRD-147 **GO 2.2.1**	MRD-181 MRD-329 MRD-337 MRD-340 MRD-384 MRD-390 MRD-391 SRD-157 **GO 2.3.1**	GND
GO 2.2.7	RST shall be able to archive GO calibrated spectra for each grism or prism exposure.	SRD-145 **GO 2.1.5** SRD-146 **GO 2.1.6**	MRD-329 MRD-337 SRD-154 **GO 2.2.8** SRD-155 **GO 2.2.9** SRD-156 **GO 2.2.10** SRD-157 **GO 2.3.1**	GND
GO 2.2.8	RST shall be able to provide GO spectra with a goal for systematic wavelength uncertainty $\sigma\lambda$ of $\sigma\lambda/\lambda \leq 0.002$.	SRD-153 **GO 2.2.7**	MRD-181 MRD-329 MRD-337 MRD-340 MRD-384 MRD-390 MRD-391 SRD-157 **GO 2.3.1**	GND

General Observer Program – Calibrated Data Records				
Reqmt	**SRD Requirement text**	**Parent (DOORS Out-links)**	**Child (DOORS In-links)**	**Recipient**
GO 2.2.9	RST shall be able to provide calibrated GO grism or prism spectra with known uniformity of the relative spectrophotometric flux calibration, with a goal of <5% for systematic uncertainties in knowledge of the spatial variation.	SRD-153 **GO 2.2.7**	MRD-181 MRD-329 MRD-337 MRD-340 MRD-384 MRD-390 MRD-391 SRD-157 **GO 2.3.1**	GND
GO 2.2.10	RST shall be able to provide calibrated GO spectra with a known relative wavelength-dependence of the spectrophotometric flux calibration, with a goal of <5% for systematic uncertainty in knowledge of the wavelength dependence.	SRD-153 **GO 2.2.7**	MRD-181 MRD-329 MRD-337 MRD-340 MRD-384 MRD-390 MRD-391 SRD-157 **GO 2.3.1**	GND

General Observer Program – Raw Data Records				
Reqmt	**SRD Requirement text**	**Parent (DOORS Out-links)**	**Child (DOORS In-links)**	**Recipient**
GO 2.3.1	RST shall be able to provide GO raw images (direct images or grism or prism spectral images) in the archive for each detector exposure with each raw data record including a unique dataset identifier for each exposure, the exposure time, the time of exposure, all individual downlinked detector readouts used to make the exposure, the observatory pointing orientation and any additional engineering data the Science Center uses for subsequent processing.	SRD-147 **GO 2.2.1** SRD-148 **GO 2.2.2** SRD-149 **GO 2.2.3** SRD-150 **GO 2.2.4** SRD-151 **GO 2.2.5** SRD-152 **GO 2.2.6** SRD-153 **GO 2.2.7** SRD-154 **GO 2.2.8** SRD-155 **GO 2.2.9** SRD-156 **GO 2.2.10**	MRD-329 MRD-337	GND
GO 2.3.2	RST shall be capable of providing access to any field on the sky for GO observations during the prime mission lifetime.	PLRA-20 **OBJ-2.1.5**	MRD-341	

Guest Investigator / Archival Research Program				
Reqmt	**SRD Requirement text**	**Parent (DOORS Out-links)**	**Child (DOORS In Links)**	**Recipient**
AR 2.0.1	RST shall provide an archive containing all the science data from the mission, including raw and calibrated data, and high-level science products such as source catalogs derived from the science data.	PLRA-22 **OBJ-2.1.6**	MRD-337	GND
AR 2.0.2	The RST archive shall include all the housekeeping data needed for processing or reprocessing the science data.	PLRA-22 **OBJ-2.1.6**	MRD-337	GND
AR 2.0.3	RST science data products shall be publicly accessible.	PLRA-22 **OBJ-2.1.6**	MRD-337	GND
AR 2.0.4	Reserved			
AR 2.0.5	The RST archive shall provide query tools that enable selection of sets of observations or sources that meet user-specified criteria. Examples include observation date, pointing, instrument configuration, or object-catalog entries.	PLRA-22 **OBJ-2.1.6**	MRD-337	GND
AR 2.0.6	The RST archive shall allow users to download datasets identified in a user query. Downloads may be subject to practical limits on the size of the selected datasets and applicable policy restrictions.	PLRA-22 **OBJ-2.1.6**	MRD-337	GND
AR 2.0.7	The RST archive shall be able to ingest user-supplied ("Level-5") data products. Ingestion of user-supplied data products may be subject to applicable policy restrictions on size, format, and documentation.	PLRA-22 **OBJ-2.1.6**	MRD-337	GND
AR 2.0.8	The RST archive shall enable users to cross-match the RST source catalog with select non-RST datasets. [This can be made more specific at lower levels].	PLRA-22 **OBJ-2.1.6**	MRD-337	GND
AR 2.0.9	The RST archive shall provide functionalities for extracting cutouts of images and spectra for any source in the catalog, or list of sources. Such user requests may be subject to applicable policy restrictions on the size of the list and the resulting data volume.	PLRA-22 **OBJ-2.1.6**	MRD-337	GND
AR 2.0.10	The RST Archive shall provide tools for exploratory data visualization and analysis.	PLRA-22 **OBJ-2.1.6**	MRD-337	GND

6 APPENDIX A ABBREVIATIONS AND ACRONYMS

Abbreviation/ Acronym	DEFINITION
ACS	Attitude Control System
AGB	Asymptotic Giant Branch
AR	Archival Research
AU	Astronomical Unit
BAO	Baryon Acoustic Oscillations
BOSS	Baryon Oscillation Spectroscopic Survey
BSR	Baseline Science Requirement
CANDELS	Cosmic Assembly Near-IR Deep Extragalactic Legacy Survey
CCB	Change Control Board
CCR	Configuration Change Request
CGI	Coronagraph Instrument
CM	Configuration Management
CMB	Cosmic Microwave Background
CVZ	Continuous Viewing Zone
DES	Dark Energy Survey
DESI	Dark Energy Spectroscopic Instrument
DETF	Dark Energy Task Force
ELG	Emission Line Galaxy
EML	Exoplanet Microlensing
EXPO	Extra-galactic Potential Observations
FoM	Figure of Merit
FOV	Field of View
FSWG	Formulation Science Working Group
FWHM	Full-Width at Half-Maximum
GI	Guest Investigator
GO	General Observer
GND	Ground
GR	General Relativity
GRS	Galaxy Redshift Survey
GSFC	Goddard Space Flight Center
HGA	High Gain Antenna
HLIS	High Latitude Imaging Survey
HLS	High Latitude Survey
HLSS	High Latitude Spectroscopic Survey
HSC	Hyper-Suprime Cam
HST	Hubble Space Telescope
ICRF	International Celestial Reference Frame
IMCOM	IMage COMbination

Abbreviation/ Acronym	DEFINITION
IPC	Inter-pixel capacitance
IR	Infrared
IRAS	Infrared Astronomy Satellite
I&T	Integration and Test
IPAC	Infrared Processing and Analysis Center
JDEM	Joint Dark Energy Mission
JPL	Jet Propulsion Laboratory
JWST	James Webb Space Telescope
KBO	Kuiper Belt Object
ΛCDM	Lambda Cold Dark Matter
LCS	Light Curve Shape
LSST	Large Synoptic Survey Telescope
MNRAS	Monthly Notices of the Royal Astronomical Society
MOA	Microlensing Observations in Astrophysics
MOSDEF	MOSFIRE Deep Evolution Field
MOSFIRE	Multi-Object Spectrograph For InfraRed Exploration
4MOST	4-meter Multi-Object Spectroscopic Telescope
Mpc	Megaparsec
MRD	Mission Requirements Document
MW	Milky Way
NASA	National Aeronautics and Space Administration
NEO	Near-Earth Object
NIR	Near Infrared
NWNH	New Worlds, New Horizons
OGLE	Optical Gravitational Lensing Experiment
PHAT	Panchromatic Hubble Andromeda Treasury
PLRA	Program-Level Requirements Appendix
PSF	Point Spread Function
PZC	Photometric Redshift Calibration
QE	Quantum Efficiency
RCS	Relative Calibration System
RMS	Root Mean Square
RSD	Redshift Space Distortions
RST	Roman Space Telescope
S/C	Spacecraft
SDSS	Sloan Digital Sky Survey
SED	Spectral Energy Distribution
SIT	Science Investigation Team
SN	Supernova
SNe	Supernovae

Abbreviation/ Acronym	DEFINITION
SNR	Signal to Noise Ratio
SOC	Science Operations Center
SRD	Science Requirement Document
STScI	Space Telescope Science Institute
S/W	Software
TBD	To Be Determined
TBR	To Be Revised
TBS	To Be Scheduled
TNO	Trans-Neptunian Object
UDF	Ultra-Deep Field
UV	Ultraviolet
WFC3	Wide-Field Camera 3
WFI	Wide Field Instrument
WIM	Wide-Field Imaging Mode
WISP	WFC3 Infrared Spectroscopic Parallel
WSM	Wide-Field Spectroscopic Mode
WL	Weak Lensing